The Characterization of the Dynamic Interaction between Highway Bridges and Long, Multi-Trailer Heavy Vehicles

by

Markus Meyer

Dissertation for the degree of Doctor of Philosophy,

Department of Civil Engineering,

University of Stellenbosch

Supervisor: Prof. Roman Lenner
Co-supervisor: Prof. Nico de Koker

April 2022

DECLARATION

By submitting this thesis/dissertation electronically, I declare that the entirety of the work contained therein is my own, original work, that I am the sole author thereof (save to the extent explicitly otherwise stated), that reproduction and publication thereof by Stellenbosch University will not infringe any third party rights and that I have not previously submitted it, in its entirety or in part, to obtain any qualification.

April 2022

ABSTRACT

Around the world, many countries are experiencing an increase in demand for freight to be transported by road. One solution is to introduce larger heavy vehicles, which are capable of transporting more freight. These vehicles have more trailers, more axles and are longer and heavier than existing heavy vehicle traffic. All these factors have an important influence on the dynamic amplification between the vehicle and bridge. This contribution investigates the dynamic behaviour of long, multi-trailer vehicles, specifically the B-Double vehicles, when crossing short to medium span bridges.

The dynamic behaviour of these larger vehicles is compared to the well-known single articulated vehicles which are currently operating in many countries around the world. The effect of axle groups and their spacing on dynamic amplification is explored in depth to support the finding that the time of entry of axle groups on an excited bridge is key to the explanation of dynamic response. The relationship between midspan accelerations and dynamic amplification is introduced and explored extensively for further validation of the findings presented.

There is an indication that the commonly accepted inverse relationship between the high static load and observed low dynamic amplification is not generally true when comparing vehicles of different axle configurations. The number of axles, along with inter-axle spacing matching the natural frequency of the bridge, is of substantial relevance to the dynamic response, yielding in some cases higher dynamic amplification of high static loads. It is shown that due to the latter, the significantly heavier vehicles can induce higher dynamic amplification on medium span bridges than some lighter vehicles with different axle configurations.

Furthermore, a dynamic load signature is developed which defines the typical dynamic loads induced by B-Double vehicles at midspan for short to medium span bridges. It is shown that the dynamic loads can be defined as a function of the first natural frequency of the bridge and the midspan accelerations.

Ultimately, a new method of estimating dynamic amplification factors by implementing a dynamic load signature function in addition to strain and acceleration measurements, is proposed.

OORSIG

Regoor die wêreld ervaar lande 'n toename in die vraag om goedere padlangs te vervoer. Een oplossing is om groter swaarvoertuie bekend te stel met 'n hoër vragkapasiteit. Hierdie voertuie het meer sleepwaens, meer asse en is langer en swaarder as bestaande swaarvoertuigverkeer. Al hierdie faktore het 'n belangrike invloed op die dinamiese versterking tussen die voertuig en die brug. Hierdie bydrae ondersoek die dinamiese gedrag van lang, veelsleepwa-voertuie, spesifiek die "B-Double" voertuie wanneer hulle kort- tot mediumspan-brûe oorsteek.

Die dinamiese gedrag van hierdie voertuie word vergelyk met die bekende enkel-geartikuleerde voertuie wat tans in baie lande regoor die wêreld werk. Die effek van asgroepe en hul spasiëring op dinamiese versterking word in diepte ondersoek om die bevinding te ondersteun dat die tyd van toetrede van asgroepe die sleutel is tot die verduideliking van die dinamiese reaksie. Die verband tussen middelspanversnellings en dinamiese versterking word bekendgestel en omvattend ondersoek vir verdere bevestiging van die voorgestelde bevindinge.

Daar is 'n aanduiding dat die algemeen aanvaarde omgekeerde verband tussen die hoë statiese las en waargenome lae dinamiese versterking nie oor die algemeen waar is wanneer voertuie met verskillende askonfigurasies vergelyk word nie. Die aantal asse, tesame met tussenaspasiëring wat ooreenstem met die natuurlike frekwensie van die brug is van wesenlike relevansie vir die dinamiese reaksie, wat in sommige gevalle hoër dinamiese versterking van hoë statiese ladings lewer. Daar word getoon dat as gevolg van laasgenoemde, die aansienlik swaarder voertuie hoër dinamiese versterking op mediumspan-brûe kan induseer as sommige ligter voertuie met verskillende as-konfigurasie.

Verder word 'n dinamiese laskenmerk ontwikkel wat die tipiese dinamiese vragte definieer wat deur B-Double-voertuie by middelspan vir kort tot mediumspan-brûe veroorsaak word. Daar word getoon dat die dinamiese ladings definieer kan word as 'n funksie van die eerste natuurlike frekwensie van die brug en die middelspanversnellings. Ten slotte word 'n nuwe metode voorgestel om dinamiese

versterkingsfaktore te skat deur die dinamiese laskenmerkfunksie bykomend tot vervormings- en versnellingsmetings te implementeer.

ACKNOWLEDGEMENTS

Firstly, I would like to thank the Structures Division of Stellenbosch University for providing me with the opportunity to further my studies in this interesting field. My special thanks go to my supervisors, Prof. Roman Lenner and Prof. Nico de Koker, who have guided me throughout this project. Furthermore, I want to express my deepest gratitude to Prof. Daniel Cantero for his insightful contributions and inputs over the last two years – all the way from Norway.

Finally and most importantly, to my parents, thank you for your love and support throughout this journey. Without you none of this would have been possible.

TABLE OF CONTENTS

LIST OF FIGURES

LIST OF TABLES

xiv

CHAPTER 1:   INTRODUCTION

The majority of countries across the globe are experiencing an ongoing increase in road freight traffic. There are concerns that the current capacity of infrastructure will not be sufficient to accommodate the anticipated freight traffic levels. One solution is to introduce larger vehicles capable of transporting more freight with minimal or no structural alterations to existing infrastructure needed. A recent report from the International Transport Forum (ITF), of which 59 countries are members, examined the experience of the countries that had already introduced larger freight vehicles. The ITF report found that the implementation of these vehicles improves transport efficiency, reduces traffic volumes, lowers carbon emissions and improves road safety (Sjögren, 2019). Based on these results the ITF report recommends the incorporation of these larger vehicles to accommodate the increase in road freight around the world.

There are some countries, such as South Africa, which have already implemented these types of heavy vehicles but use dynamic design loads complying with foreign specifications which do not account for these types of heavy vehicles. These vehicles can have various trailer and axle configurations, but one of the most common is the 7-axle B-Double (BD7) heavy vehicle as seen in Figure 1.1.
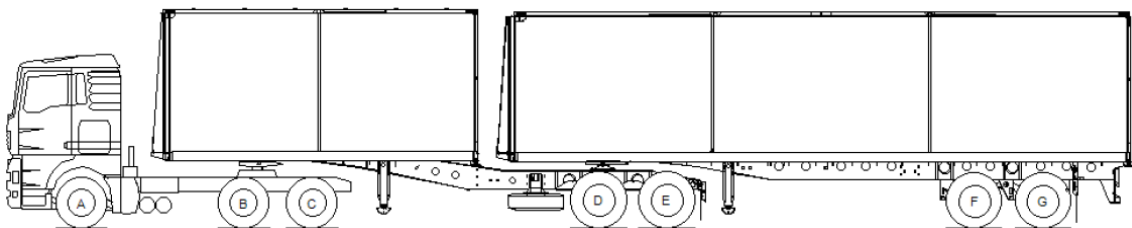
Figure 1.1: Typical B-Double heavy vehicle (Thorogood et al., 2009).

The tractor and trailer units of B-Doubles are connected by load transferring hinges, resulting in a different dynamic system compared to other common types of heavy vehicles, such as the 5- and 6-axle single articulated (SA5 and SA6) vehicles.

A highway bridge is designed to carry traffic loads and must fulfil its role with adequate safety over its lifetime. As the heavy vehicle traverses a bridge, there is a dynamic interaction between the two which induces an additional dynamic load within the bridge (Meyer, *et al.*, 2019). B-Double vehicles frequently weigh more than 50 tons, so any additional dynamic load induced may have a significant influence on the final design loads. These loads are normally quantified by a Dynamic Amplification Factor (DAF), defined by the ratio of total load effect (bending moment in this case) to the static load effect. The DAF can be calculated by:

$$DAF = \frac{M_t}{M_s} \qquad\qquad\qquad (1.1)$$

where M_t is the maximum total bending moment experienced at midspan and M_s is the static bending moment experienced at the same instant. A review by Van Der Spuy, *et al*, (2019), found that great variations exist amongst the international codes of practice with regards to the specification of the DAF. The 1981 bridge loading code of South Africa, Technical Methods for Highways 7 (TMH-7), adopted the so-called "Swiss Formula" to define the dynamic amplification for local conditions as a function of the equivalent span length; however, no clear reference exists to the derivation of the formula (Committee of State Road Authorities, 1981). It is clear that the Swiss Formula was not derived based on typical South African traffic, but rather on European traffic.

Substantial differences exist between the standards governing European and South African heavy vehicles, such as gross vehicle weights, axle loads, number of trailers and the number of axles per vehicle. For example, South African vehicles have a higher allowable gross vehicle weight of 56 ton compared to the 40-44 ton range in most European countries (Lenner, 2018). Freight vehicles in South Africa have more axles with a lower allowable weight per axle and are longer, up to 22 m, compared to the 18.5 m in Europe (States, 1996). According to Žnidarič (2015) the typical heavy vehicle on European roads is the 5-axle single articulated vehicle while on South African roads it is the 7-axle B-Double vehicle. These vehicles have completely different trailer and axle configurations which result

Stellenbosch University https://scholar.sun.ac.za

The Characterization of the Dynamic Interaction between Highway Bridges and Long, Multi-Trailer Heavy Vehicles
_____

in unique dynamic loads that would be induced by these vehicles when interacting with highway bridges.

The future incorporation of the B-Double heavy vehicles by countries with an increasing demand on road transport along with outdated dynamic loading specifications of some countries where these vehicles have already been implemented, emphasizes the need for a thorough dynamic interaction investigation of the B-Double vehicle. This contribution is the first of its kind which aims to gain insight into the dynamic behaviour of B-Double vehicles traversing short to medium span bridges.

1.1 Objectives

The research aims to specifically address the following topics:

- The development of a new vehicle-bridge interaction (VBI) model to cater for long, multi-trailer BD7 heavy vehicles, which provides the capability of investigating the dynamic interaction of a large range of highway bridges. Such a model could be adopted in countries with similar traffic conditions.

- The investigation and comparison of the differences and relationships in vehicle-bridge dynamics between single articulated and long, multi-trailer (BD7) heavy vehicles. This is to ensure an understanding of the different dynamic behaviour of the two and to quantify the difference in the amplification due to long multi-trailer BD7 vehicles.

- The in-depth investigation of the main influencing factors that cause the unique dynamic amplification results of the BD7 vehicle, such as the axle configurations and how the latter are linked to bridge accelerations.

- The exploration of the unique relationship between the dynamic components (DAF and dynamic loads) and the corresponding bridge accelerations.

Stellenbosch University https://scholar.sun.ac.za

The Characterization of the Dynamic Interaction between Highway Bridges and Long, Multi-Trailer Heavy Vehicles
_____

- The development of a Dynamic Load Signature (DLS) for BD7 vehicles traversing simply supported bridges to be used in comparative bridge assessment studies. Furthermore, to develop a new method to estimate the DAF induced by BD7 vehicles on a bridge by implementing the DLS along with infield strain and acceleration measurements which could easily be implemented by foreign countries which share similar dynamic amplification investigations.

1.2 Scope

The scope of this research is confined to a range of beam and slab simply supported bridges interacting with three heavy vehicle configurations: the 5-axle single articulated (SA5), the 6-axle single articulated (SA6) and the 7-axle B-Double (BD7) vehicles. The input parameters of the vehicles are from a WIM station which recorded the velocity, number of axles, axle spacing and axle loads in the slow lane of a national route in South Africa. A VBI solution is developed to determine the total load induced at midspan per loading event. The bridges are modelled with a series Euler-Bernoulli finite element while the vehicles are modelled by in plane dynamic models. The dynamic amplification factors are calculated using the midspan sagging bending moments as load effects. The DAFs presented in this work are not intended for the design of bridges, but rather serve as a comparison of the results achieved and indicate the actual magnitude of the dynamics experienced.

1.3 Dissertation Structure

The research project consists of several of investigations and developments in order to achieve the objectives outlined.

Chapter 2 provides an in-depth literature review of the work that has been done over the past decades with regards to the different methods available to investigate and quantify the dynamic loads experienced by bridges due to their interaction with moving vehicles.

Stellenbosch University https://scholar.sun.ac.za

The Characterization of the Dynamic Interaction between Highway Bridges and Long, Multi-Trailer Heavy Vehicles
_____

Chapter 3 derives the vehicle-bridge interaction solutions for the considered heavy vehicles interacting with a range of short to medium bridge spans.

Chapter 4 demonstrates the verification process of the derived VBI solution against infield measurements taken from a study of a simply supported bridge in Vransko, Slovenia.

Chapter 5 presents the input parameters for the three vehicle types gathered from WIM as well as the bridge properties utilized to model the stock of bridges investigated in this research.

Chapter 6 presents the first dynamic interaction comparison of the three vehicle types where the significance of the amplification capabilities of the BD7 vehicles is presented. Furthermore, the effect of axle configurations and the link between amplification and bridge accelerations is explored.

Chapter 7 discusses the results of an extensive simulation in which the entire BD7 vehicle population is simulated interacting with a range of short to medium span bridges. The influence of velocity and GVM is also presented.

Chapter 8 develops a Dynamic Load Signature (DLS) for the BD7 vehicles interacting with simply supported bridges. Furthermore, a novel method to estimate the DAF induced by BD7 vehicles on a bridge by utilizing the DLS, strain and acceleration measurements is presented.

Stellenbosch University https://scholar.sun.ac.za

The Characterization of the Dynamic Interaction between Highway Bridges and Long, Multi-Trailer Heavy Vehicles
_____

CHAPTER 2:   BACKGROUND

The phenomenon of vehicle-bridge interaction has been a topic of interest for more than a century due its significance to bridge loading. The intricate dynamic system of a moving mass connected to a set of stiffness and damping mechanisms introduce loads on structures which vary within space and time, significantly increasing the degree of difficulty of solving and quantifying these loads. As heavy vehicles cross a highway bridge, the bridge will experience varying loads in addition to the static loads which are induced by the dynamic components of the vehicle-bridge interaction system.

Theoretically, the vehicle and bridge can be simulated as two elastic subsystems which interact with one another, each with a unique set of frequency vibrations. The interactions are made possible through the contact forces which occur between the points of contact between the two subsystem, i.e., the wheels of the vehicle and the road surface of the bridge. The two subsystems experience relative movement which causes the contact forces to vary with time as the vehicle crosses the bridge. Due to the time dependency of the contact forces, the problem is nonlinear. The level of dynamic amplification experienced is mainly determined by the fundamental frequencies of the two systems and the driving frequency of the vehicle.

The resonance phenomenon can cause significant bridge amplification and more severe dynamic loads on the bridge when frequency matching occurs between the vehicle frequencies and the natural frequencies of the bridge. Vehicle-bridge interaction models have the ability to accurately determine the extent of dynamic amplification and dynamic loads during loading events where frequency matching is prominent.

The first form of the vehicle-bridge interaction problem was addressed in the early 1900s by rail engineers studying the interaction between rail traffic and railway bridges (Gonzalez, 2010). The equations of motion were derived based on a moving mass travelling at a constant velocity over a

Stellenbosch University https://scholar.sun.ac.za

The Characterization of the Dynamic Interaction between Highway Bridges and Long, Multi-Trailer Heavy Vehicles
_____

massless bridge which were first solved using series expansion undertaken by Stokes (1896). The first 50 years of the 1900s saw the fundamental developments made by Stephen Timoshenko with regards to the dynamics of simply supported beams. Timoshenko (1908) studied the dynamic behaviour of a simply supported beam subjected to a constant moving point load by implementing eigenfunction expansion which was later extended by Timoshenko (1922) in which the constant moving point load was replaced by a harmonic force traversing the beam. In this period significant research had been done on the dynamics of railway bridges, of which an in depth revision was done by Timoshenko (1953).

The VBI problem quickly extended to the road network, specifically to highway bridges, to accommodate the increase in heavier vehicles travelling at higher speeds. The ASCE committee laid the basis for VBI research in 1931 by field testing which was extended in the 1950's by the Ontario test program (Csagoly & Dorton, 1975). Field tests provide the best representation of the real-world situation; however, they are limited in terms of the amount of variability that can be captured which is where the VBI models have the advantage. Frýba (1972) did an extensive study on the solution of the differential equations of motion of the planar beam VBI problems incorporating constant, periodic force and spring-mass models. This work laid the foundation for many modern day bridge dynamic studies.

The introduction of the finite element method to analyze structures along with the improvement of computerized technology at the turn of the century reduced the difficulty of solving differential equations analytically. The use of the finite element method enabled more intricate dynamic interaction problems to be solved with improved efficiency. It was now possible to model vehicles with multi degrees of freedom and bridges as 2D and 3D models while incorporating the influence of surface roughness on the dynamic system (Li 2005).

2.1 Modelling the Vehicle

Moving load models ignore the inertia effects of the vehicle and consider the vehicle as a series of constant loads traversing the bridge. Timoshenko (1922) developed a great number of approximate

solutions for a simply supported bridge subjected to constant moving loads. In the past century numerous investigations where vehicles were simulated as constant moving loads on bridges have been published (Chen & Li, 2000; L Frýba & Yau, 2009; Khadri et al., 2009; Rao, 2000; Zheng et al., 1998). To model vehicles as constant moving loads is the simplest form of studying vehicle-bridge interaction. Such studies are generally focused on capturing the bridge characteristics induced by the movement of loads which can be done with an adequate degree of accuracy when the moving mass of the vehicle is small in relation to that of the bridge.

Heavier vehicles, of which the inertial effects cannot be ignored, can be modelled using the moving mass model which is shown in Figure 2.1. The first moving mass investigation of significance was done by Jeffcott (1929) which studied the inertial effects of both the bridge and the moving vehicle. Since then, various studies have implemented the moving mass model to investigate bridge behaviour. Frýba (1972) reviewed the development and application of the moving mass model with specific focus on simple supported beams. A literature review by Yang, *et al*., (2004) compared the various applications of the moving mass model and emphasized the lack thereof to accurately capture the full vehicle-bridge interaction due to the exclusion of vehicle suspension and the effect of surface roughness.
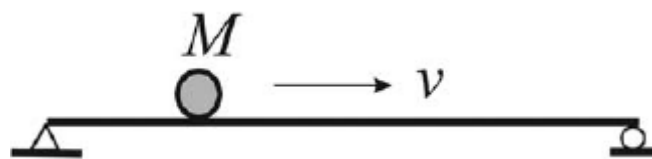
Figure 2.1: Moving mass model (Yang, et al., 2004).

The influence of vehicle suspension and road roughness can be incorporated by modelling the vehicle as a sprung mass model as shown in Figure 2.2, also referred to as a quarter-car model. The vehicle body and the axle is simulated by a single mass, m_s and m_u, the suspension of the vehicle is modelled using a spring and damper system, k_s and c_s and the tyre stiffness is simulated by k_t. The road roughness height, $r(x)$, is a function of the distance along the bridge. The displacement of the contact point between

the wheel and the bridge surface is defined by $y_b(x, t)$ while the independent vehicle body and axle displacements are defined by $y_s(t)$ and $y_u(t)$. In recent years "Drive-by bridge health monitoring" has become a field of great interest. This is based on the concept that a instrumented vehicle can act as moving sensor to identify damaged bridges through vehicle-bridge studies. Malekjafarian, *et al.*, (2015) simulated this concept by implementing a quarter-car model to detect bridge deterioration. The quarter-car model can simulate the suspension system of the vehicle to some extent while incorporating the effect of road roughness, which is a significant advance compared to the moving mass model.
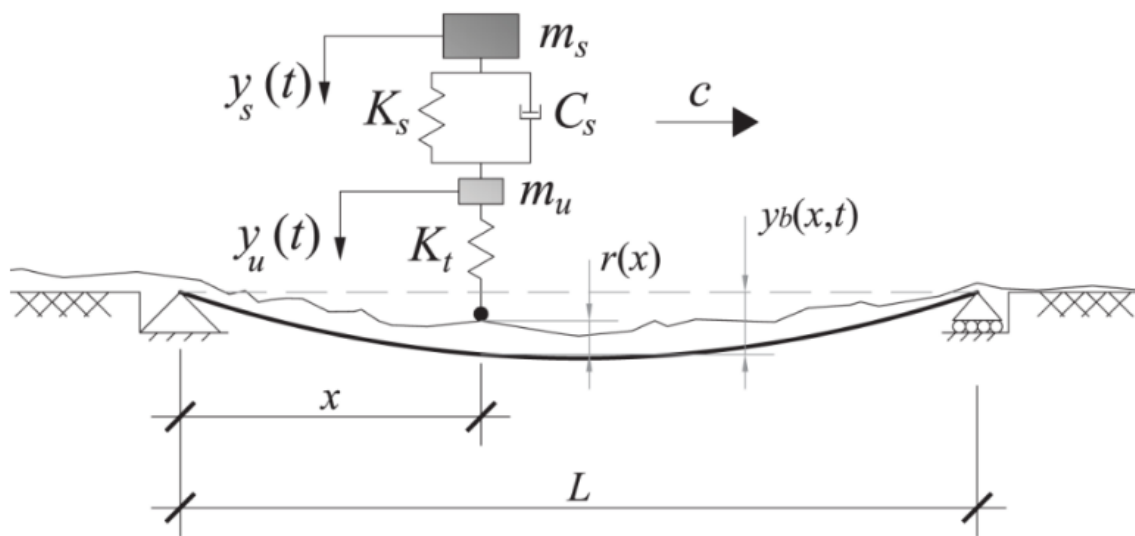
Figure 2.2: Quarter-car model (Malekjafarian, et al., 2015).

The advance in computational and computerized technologies, allowed the development of more accurate vehicle models which are able to simulate the dynamic properties of a greater number of dynamic vehicle components. Yang, *et al.*, (1999) considered vehicle pitching effect by simulating a railroad car as a rigid beam supported by a double set of spring and dampers connect to the wheel mass. Green and Cebon (1997) and Henchi *et al.*, (1998) studied the dynamic response of a bridge subjected to a set of vehicle axle loads by solving the convolution integral for the vehicle-bridge interaction problem. The 2-axle vehicles were modelled as a system of sprung masses simulating the vehicle body and axles.

Stellenbosch University https://scholar.sun.ac.za

The Characterization of the Dynamic Interaction between Highway Bridges and Long, Multi-Trailer Heavy Vehicles
_____

The first decade of the 2000s saw an increase in VBI studies which investigated the dynamic loads associated with critical bridge loading vehicles such as the 5-axle single articulated heavy vehicles. These vehicles required a more extensive dynamic model due to the intricate dynamic system which exists due to the tractor-trailer configurations and the significant number of axles, as shown in Figure 2.3. These vehicles can also be modelled in three dimensions to incorporate the effect of vehicle body roll. Cantero, *et al.*, (2010) derived the equations of motion for single articulated vehicles with a variable number of axles for the planar and three-dimensional cases by applying equilibrium of forces and moments acting on the vehicle.
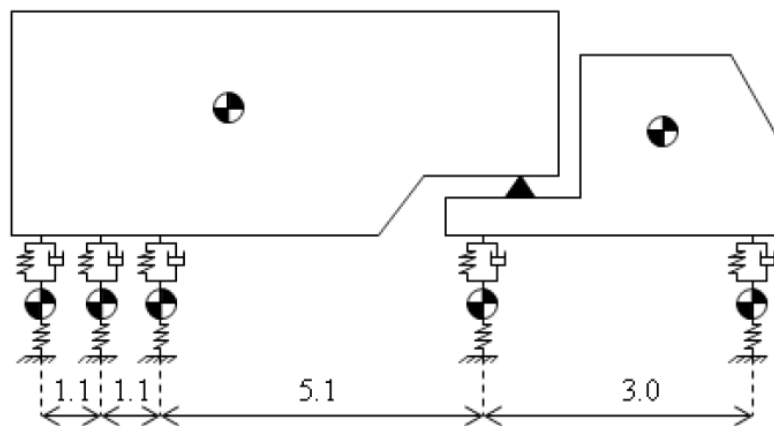
Figure 2.3: 5-axle single articulated vehicle model (González, *et al.*, 2011).

The 5-axle single articulated vehicle has been frequently implemented in comparative studies to investigate bridge dynamic amplification. The dynamic loads induced by critical loading vehicles (multi-axle cranes) which weigh more than 100 ton were investigated by Cantero, *et al.*, (2009) and compared to the loads induced by the typical 5-axle single articulated heavy vehicles. Mohammed, *et al.*, (2018) investigated the dynamic loads induced by permit vehicles which have a number of equally spaced axles and found that a series of equally spaced axles can cause resonance effects at low speeds. The recurrence of the equally spaced axles synchronizes with the natural period of vibration of the bridge which results in considerable dynamic amplification of the dynamic response.

Stellenbosch University https://scholar.sun.ac.za

The Characterization of the Dynamic Interaction between Highway Bridges and Long, Multi-Trailer Heavy Vehicles
_____

Gonzalez (2010) did a review on the development of VBI models using finite element methods by modelling single articulated vehicle by a combination of mass, spring, rigid and bar elements. One such study by Rattigan, *et al.*, (2005) investigated the dynamic amplification of critical loads induced by 5-axle single articulated vehicles by modelling the bridge and vehicle using finite elements on MSC Nastran.

The mathematical models for vehicles can range from less complex to highly complex depending on the level of accuracy required and the research purpose. The sprung-mass vehicle model accounts for the necessary dynamic components such as the tyres and suspension system and is an effective model to be used for VBI studies which require a large number of bridge loading events due to its computational efficiency compared to detailed three-dimensional vehicle models (Y. B. Yang & Lin, 2005).

2.2 Modelling the Bridge

In the field of vehicle-bridge interaction, the simply supported beam configuration has been widely used for numerous applications to study dynamically induced bridge loads. Due to the effectiveness of these models to capture the fundamental dynamic bridge behaviour, while being computationally very efficient, has led to the models being implemented since the early 1900s to the present day. The book by Frýba (1972) explores the various simply supported beam dynamic problems and the corresponding solution approaches available.

One of the most popular approaches is to apply the modal superposition method (MSM) to the Euler-Bernoulli beam theory for flexural vibrations (Meyer, *et al., 2019*; Yang and Duan, 2013; Frýba 1972; Harris, *et al.*, 2007; Yang and Lin, 2005; Koç *et al.*, 2016; Youcef *et al.*, 2013). The main characteristic of the modal superposition method is the ability to capture the dynamic response of the bridge in terms of a set of mode shapes with various amplitudes by decomposing the system's equations of motion. The equations of motion are transformed from being partial differential to ordinary differential which can

be solved by numerical methods. The concept of modal decomposition can easily be illustrated by considering the interaction of the fundamental Euler-Bernoulli beam with a moving vehicle with j axles.

To illustrate, the Euler-Bernoulli beam theory for flexural vibrations of a beam with a span length of L can be defined by:

$$EI\frac{\partial^4 y_b(x,t)}{\partial x^4} + \rho\frac{\partial^2 y_b(x,t)}{\partial t^2} + \mu\frac{\partial y_b(x,t)}{\partial t} = -\sum_{i=1}^{j} F_i(x_i,t)\delta(x_i)$$

(2.1)

where EI is the modulus of rigidity of the beam, ρ the constant mass per unit length, μ the damping per unit length and $y_b(x,t)$ the beam displacement induced by the coupled axle forces $F_i(x_i,t)$ which are activated and deactivated by the Dirac delta function $\delta(x_i)$ for each axle x_i. The displacement of the bridge, given in Equation 2.2 can be defined in terms of the modal coordinates $z_n(t)$ and modes of vibration $\varphi_n(x)$. The vibration of the beam is governed by a low number of N modes.

$$y_b(x,t) = \sum_{n=1}^{N} \varphi_n(x_i)z_n(t)$$

(2.2)

The nth normalized mode of vibration is described as a function of the position x along the length of the bridge by:

$$\varphi_n(x) = \sqrt{\frac{2}{\rho L}}\sin(\frac{n\pi x}{L})$$

(2.3)

The modal equation of motion for the bridge can be derived with the substitution of Equations 2.2 and 2.3 into Equation 2.1 for a chosen number of modes and can be defined as:

_____

$$\ddot{z}_n + 2\xi\omega_n\dot{z}_n + \omega_n^2 z_n = -\sum_{i=1}^{j} F_i(x_i, t)\delta(x_i)\varphi_n(x_i)$$

(2.4)

where ξ the percentage of bridge damping, ω_n is the natural frequency of the nth mode of vibration defines as:

$$\omega_n^2 = \frac{EI}{\rho}\frac{n^4\pi^4}{L^4}$$ (2.5)

The simply supported bridge can alternatively be modelled using discretized finite beam elements for vehicle-bridge interaction studies as done by Meyer, *et al.*, (2021), O'Brien, *et al.*, (2014) and Cantero *et al.*, (2019). The use of a sufficient number of discretized finite elements to model the bridge structure ensures the ability to adequately represent the dynamic characteristics of these bridges throughout the length of the bridge. These models have also played an integral role in bridge health monitoring investigations due to the ability to change the bridge properties at localized sections to simulate bridge deterioration (O'Brien, *et al.*, 2014).

The finite element method has the ability to accommodate complex bridge structures with intricate boundary conditions which may be problematic when using the modal superposition method due to the difficulty of obtaining the mode shapes of such complex structures (Frangopol, 2011). Bridges can be modelled by two dimensional plate and grillage elements and as three-dimensional solid elements or as a combination of the above (Gonzalez, 2010). The general formula defining the dynamic response of a discretized finite element bridge model subjected to a number of time dependent loads can be defined by:

$$[M_b]\{\ddot{q}_b\} + [C_b]\{\dot{q}_b\} + [K_b]\{q_b\} = \{f_b\}$$ (2.6)

where $[K_b]$, $[C_b]$ and $[M_b]$ are global stiffness, damping and mass matrices with $\{q_b\}$, $\{\dot{q}_b\}$ and $\{\ddot{q}_b\}$ the nodal displacement, velocity and acceleration vectors of the bridge, while $\{f_b\}$ is the global force vector which contains the interaction forces between the bridge and the vehicle. The values and size of

_____

the mass, stiffness and damping matrices are determined by which finite elements are used to model the bridge. An in-depth literature review, done by Gonzalez (2010) on vehicle-bridge interaction modelling using the finite element method, classified the determination of the coefficients of these matrices into two categories:

1. The application of the principal of virtual displacement to derive the mass, stiffness and damping matrices per element and assembling the elementary matrices into the global matrices, done manually.

2. The use of finite element packages which incorporates the principles mentioned in point 1 to construct the bridge models as done by Kwasniewski, *et al.*, (2006), González *et al.*, (2008), Kirkegaard, *et al.*, (1997) and Deng and Cai (2010).

The past two decades have seen numerous vehicle-bridge interaction investigations ranging from specialty cases where one specific bridge is modelled using a great number of complex finite elements to generic investigations considering a range of bridges modelled by simpler finite element models. The type of finite element to be used in VBI studies depends solely on the purpose of the investigation.

2.3 VBI Algorithms

There are two main algorithm categories into which all VBI models can be classified: a) the coupled algorithm and b) the uncoupled algorithm. The purpose of both algorithms is to solve the two subsystems of equations (vehicle and the bridge), while ensuring perfect compatibility between the contact points of the vehicle wheels and the bridge. Both the coupled and the uncoupled algorithms use numerical methods to solve the system of equations in time steps. In a review done by Gonzalez (2010) the two algorithm categories and their application are explored. These are revisited in the following sections.

2.3.1 Uncoupled Algorithms

The uncoupled algorithm, follows a direct integration scheme to solve the equations of motion of the bridge and the vehicle separately while ensuring compatibility and equilibrium between both sets of equations. Essentially, the sprung mass model is simulated to cross a road roughness to generate initial displacements for the contact points which are substituted into the vehicle equations of motion to generate the interaction forces. The bridge displacements can then be determined by substituting the interaction forces of the contact points into the equations of motion of the bridge which represents improved estimates of the initial displacements of the contact points. The procedure continues until the difference between successive iterations is insignificant (Gonzalez 2010; Green and Cebon 1992,1997; Henchi *et al*., 1998; Yang & Duan, 2013). Implicit integration schemes such as the Wilson-θ or the Newmark-β are used to solve each system of equations after several iterations to achieve convergence.

2.3.2 Coupled Algorithms

The coupled algorithm is characterized by the formation of a unique system matrix, which is updated at each time step, and which includes the equations of the vehicle and of the bridge while the interaction forces are eliminated. The equations of motion of the bridge and vehicle are not solved separately but rather simultaneously. The position of the contact points constantly changes as the vehicle crosses the bridge, which results in the coupled system of differential equations being time dependent. Thus, for each time step, a unique set of differential equations exists with no closed-form solution. For this reason, a stable integration scheme, such as the Newmark-β method, is generally used to approximate the solution (Kim, *et al.*, 2005; Gonzalez 2010). The Newmark-β integration method, derived from Taylor's series, assumes the acceleration between two-time steps to be linear (Gonzalez 2010). This research implements the coupled approach while solving the intricate system of differential equations using the Newmark-β method.

Stellenbosch University https://scholar.sun.ac.za

The Characterization of the Dynamic Interaction between Highway Bridges and Long, Multi-Trailer Heavy Vehicles
_____

2.4 Variables Influencing Dynamic Interaction

The extent of vehicle-bridge interaction can be influenced by several variables which can cause large dynamic loads due to significant bridge amplification. The influence of these variables has been investigated by Deng *et al.*, (2015), Caprani, (2017) and Van Der Spuy, *et al.*, (2019). The effect of these variables is discussed in the following sections.

2.4.1 Gross Vehicle Mass

Multiple studies have concluded that there is a definite relationship between GVM and dynamic amplification. Broquet *et al.*, (2004), Ashebo, *et al.*, (2007), Cantero *et al.*, (2009) and Caprani, (2017) state that if the GVM increases, the dynamic amplification of the bridge decreases as the added vehicle mass reduces the amplitude and frequency of the bridge response. Newpher, *et al.*, (2014) do not agree with this and suggest that the GVM parameter does not correlate with bridge frequency and is therefore not significant. Most authors do support the idea that there is an inverse relationship between the GVM and the dynamic amplification. However, a problem arises when combining the dynamic effects with the governing static load effects because the vehicle causing the largest static load effect also experiences the smallest dynamic amplification in comparison to light vehicles which governs the dynamic response (Kwasniewski, Wekezer, *et al*., 2006).

2.4.2 Road Roughness

There exists a significant correlation between the magnitude of dynamic amplification and the road quality. Various studies have concluded that there is a direct correlation between the severity of road roughness and the dynamic amplification. Yang and Chang (2014) found that a decrease in pavement quality increases the dynamic amplitude of the crossing vehicle which finally increases the dynamic amplitude of the bridge. Along with the latter, Brady, *et al.*, (2010) specified that for any dynamic simulation, the vehicle has to have a 100 m approach with the same class of road roughness as the bridge, to ensure that the vehicle has reached a steady state of vibration before it enters the bridge deck area.

2.4.3 Number of Axles

Ashebo, *et al.*, (2007) and Schwarts and Laman (2001) found that there is almost zero statistical relationship between the number of axles and dynamic bridge response; however, some design specifications define dynamic amplification as a function of the number of axles. This highlights the uncertainty across the globe with regards to how the axle configuration influences bridge dynamics.

2.4.4 Span Length

The norm that an increase in span length causes a decrease in dynamic amplification is supported by various studies but explicitly discussed by Li (2005). However, it must be noted that there can be an exception to this. The dynamic amplification can significantly increase when there is a resonance excitation between the vehicle and the bridge. This is illustrated by Figure 2.4, comparing span lengths to dynamic amplification, where the spike at 30 m is due to resonant excitation between the vehicle and the bridge (Li, 2005).
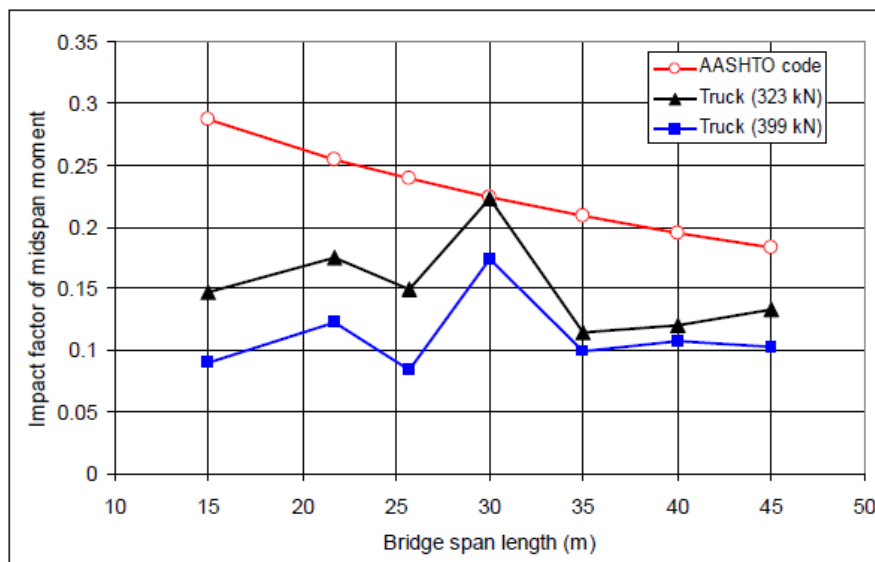
Figure 2.4: Dynamic amplification vs. span length (Li, 2005).

2.4.5 Vehicle Velocity

The majority of studies, such as Chang and Lee (1994), Cantero *et al.*, (2009) and Mohammed *et al.*, (2018) found that the general trend, shown in Figure 2.5, is that the dynamic amplification increases

with an increase of vehicle speed with the peaks representing critical bridge velocities at which there is a degree of resonance between the vehicle and bridge. Yang, *et al.*, (1995) found that at midspan of simply supported and continuous beams a clear correlation exists between the dynamic amplification and the velocity.
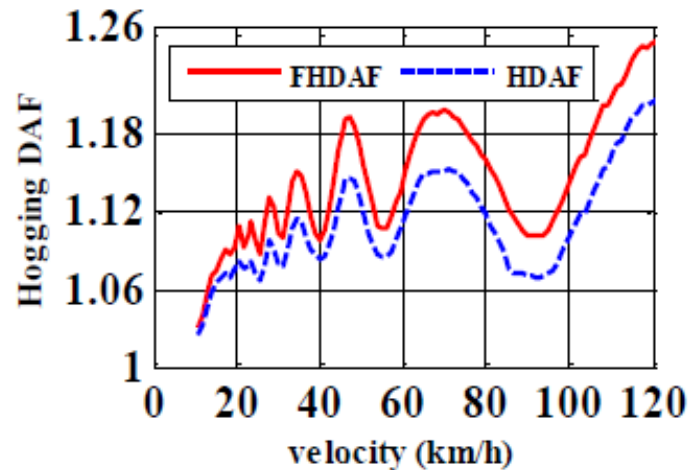
Figure 2.5: Dynamic Amplification vs. velocity (Cantero *et al.*, 2009).

However, Newpher, *et al.*, (2014) do not agree with the above and suggest that there is no definite relationship between vehicle velocity and the dynamic amplification of bridges. Most researchers in the field accept that there exists a direct correlation between vehicle velocity and the DAF. Whatever the case may be, velocity is a major influencing factor in the field of dynamic bridge amplification.

2.4.6 Suspension Parameters

The undercarriage of heavy vehicles consists of sets of dampers (shocks, air suspension etc.) and springs which work together to form the suspension. Kwasniewski *et al.*, (2006) found by running field tests that a high suspension stiffness causes an increase in the dynamic amplification. This is confirmed by the findings of Kirkegaard, *et al.*, (1997) showing that a lower suspension stiffness reduces the dynamic amplification. This was also confirmed by an investigation by the Iowa State University (Y. Deng & Phares, 2016).

Stellenbosch University https://scholar.sun.ac.za

The Characterization of the Dynamic Interaction between Highway Bridges and Long, Multi-Trailer Heavy Vehicles
_____

2.5 *Standardized Dynamic Amplification*

The dynamic loads induced by vehicle-bridge interaction have been incorporated in bridge design specifications around the world by various measures such as: dynamic load allowance (DLA), impact factor (IM) and predominantly by the dynamic amplification factor (DAF). These measures of quantifying dynamic amplification are essentially defining the dynamic loads by a factor to be multiplied with the static bridge loads to reach the final design loads. This section reviews how dynamic amplification is accounted for by various bridge design specifications around the world. While the purpose of this research project is not to develop new DAFs for design purposes, the notable differences amongst these codes are an indication that grey areas exist within the field, especially within the light of the introduction larger heavy vehicles.

The current bridge design code in South Africa TMH-7 accounts for dynamic effects by using the Swiss formula which is a function of the effective bridge length, L_s, given by Equation 2.7 and is incorporated in the NA and NB loading (Committee of State Road Authorities, 1981).

$$DAF = 0.05 \frac{(100+L_s)}{(10+Ls)}$$
(2.7)

The scarcity of references and background documents to support the Swiss formula leads to the conservative assumption that the formula was not developed based on the vehicles which represent South African traffic.

In 1992 the American Association of State Highway and Transportation Officials (AASHTO) defined the dynamic loading effects with a dynamic impact factor (IM) as a function of the span length (Cary et al., 2000). This impact factor was however replaced in 1994 with the dynamic load allowance (DLA), independent of the span length but dependent on limit states and components. The Australian Standard (AS5100) defines DAFs as a function of load configurations being 1.3 for moving loads (M1600) and 0 for static loads (S1600) (Van Der Spuy, *et al.* , 2019).

Stellenbosch University https://scholar.sun.ac.za

The Characterization of the Dynamic Interaction between Highway Bridges and Long, Multi-Trailer Heavy Vehicles
_____

The Canadian design code defines a dynamic load allowance (DLA) based on an idealized five axle heavy vehicle, known as a CL-W. The dynamic allowance is thus a function of the number of vehicle's axles. The DLA defines the dynamic load as the percentage of the static load to be added to the static load to reach the final design load. These percentages are 40%, 30% and 25% for single, double and more than double axle loadings.

The Eurocode 1991-2 ("Eurocode 1: Actions on structures - Part 2: Traffic loads on bridges," 2011) does not account for dynamic loading by a separate calculated factor, but rather incorporate it in the overall load model. The Eurocode defines the DAF as a function of the load effect, number of loaded lanes and the span length along with a pneumatic suspension vehicle and a medium quality road roughness. Eurocode 1991-2 specifies DAFs for three separate cases; single lane, double lane and four lane bridges. DAFs for single lane bridges are defined for bending as 1.7 for spans shorter than 5 m and reduce to 1.4 for spans longer than 15 m. The DAFs for double lane bridges, with no distinction between shear and bending, reduce linearly from 1.3 to 1.1 for spans from 0 m to 50 m with the DAF kept constant after 50 m. The DAFs for four lane bridges are defined as 1.1 with no distinction between the shear and the bending moments (EN 1991-2 (2003)).

The ARCHES report introduces a dynamic load allowance as a function of the road roughness of the bridge surface according to the ISO 8608 road class spectrum. Figure 2.6 presents the findings of the ARCHES report compared to the DAFs specified by the Eurocode. For ISO road Class A, a DAF of 1.3 is prescribed for a span length of 5 m and reduces linearly to 1.15 for a 15 m bridge. For ISO road class B, the DAF is given as 1.4 for a span length of 5 m reducing to 1.2 at 15 m. Beyond 15 m the DAFs remain constant (González, A., *et al.*, 2009; Van Der Spuy, 2019).
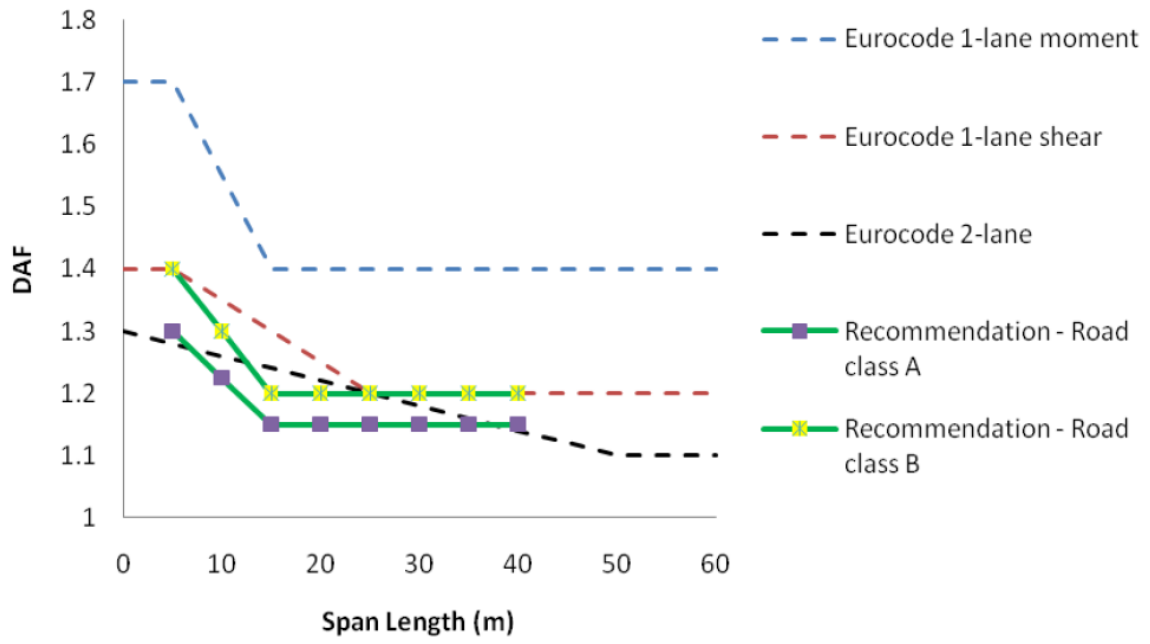
Figure 2.6: Recommended DAFs of ARCHES report versus Eurocode.

CHAPTER 3: DEVELOPMENT OF VEHICLE-BRIDGE INTERACTION MODELS

3.1 Introduction

The vehicle-bridge interaction models used to simulate the interaction of the single articulated and B-Double vehicles are developed. A planar VBI model is implemented for this research due to its inherent computational efficiency and accuracy to simulate the fundamental dynamic bridge properties during vehicle-bridge interaction. In this chapter, specific attention is given to the derivation of the equation of motions of the BD7 heavy vehicles which consist of two semi-trailers hooked in series which exhibit different dynamic behaviour than the well-studied single articulated vehicles.

An earlier version of the work to has been documented in (Meyer, *et al*., 2019).

3.2 Bridge Models

The superstructure of a bridge is simulated using Euler-Bernoulli finite beam elements, each with two nodes and two degrees of freedom per node: rotation and vertical translation. The bridges are modelled as simply supported finite element beam models which are traversed by a series of time dependent interaction forces. The equation of motion for this system is defined by:

$$[M_b]\{\ddot{q}_b\} + [C_b]\{\dot{q}_b\} + [K_b]\{q_b\} = [H]\{W_i + f_i\} \tag{3.1}$$

where $[K_b]$, $[C_b]$ and $[M_b]$ are global stiffness, damping and mass matrices with $\{q_b\}$, $\{\dot{q}_b\}$ and $\{\ddot{q}_b\}$ the nodal displacement, velocity and acceleration vectors of the bridge. $[H]$ is the distribution matrix which distributes the dynamic interaction forces, $\{W_i + f_i\}$, to equivalent nodal forces, refer to Appendix A. W_i and f_i is the ith static wheel force and dynamic contact force. Viscous Rayleigh damping is implemented to simulate the inherent damping of the bridge as documented by O'Brien, *et al.*, (2014) and Gonzalez, (2010). The damping matrix of the bridge is defined by:

Stellenbosch University https://scholar.sun.ac.za

The Characterization of the Dynamic Interaction between Highway Bridges and Long, Multi-Trailer Heavy Vehicles
_____

$$[C_b] = \alpha[M_b] + \beta[K_b] \tag{3.2}$$

where β and α are the damping proportion constants. These constants are defined by the first two natural bridge frequencies, ω_1 and ω_2, along with the damping ratio of the bridge, ζ, and are given in Equations 3.3 and 3.4.

$$\alpha = \frac{2\zeta\omega_1\omega_2}{(\omega_1+\omega_2)} \tag{3.3}$$

$$\beta = \frac{2\zeta}{(\omega_1+\omega_2)} \tag{3.4}$$

A range of generic bridges to study the dynamic behaviour of these vehicles is considered. The structural properties of these bridges are given in Chapter 4.

3.3 Vehicle Models

In this investigation three types of heavy vehicles are considered. First, the typical truck configuration on European highways, the 5-axle Single Articulated (SA5) vehicle (Žnidarič, 2015). Then, two longer vehicles are introduced – the 6-axle Single Articulated (SA6) and the 7-axle B-Double (BD7) vehicles.

The tractor, trailers and axles of the vehicles are simulated as lumped masses. The suspension system, which connects the tractor and trailer masses to that of the axle, is simulated with a spring and dashpot and similarly for the tyres of the vehicles connecting the vehicle to the road. The DOF for a two-dimensional, 5-axle articulated vehicle model (two tractor axles and three trailer axles) will be as follows; the tractor and trailer bodies will both have two DOF, a vertical displacement as well as a rotational DOF capturing the pitching motion of the vehicle and the five axles will each have one DOF capturing the vertical displacement of the axle. The equations of motion of the single articulated vehicles are derived according to principles outlined by Cantero, *et al*., (2010) which presents the detailed derivations for the equations of motion for the single articulated heavy vehicles.

_____

The larger BD7 vehicle consists of two double-axle semi-trailers and a 3-axle tractor. The configuration has two 5th wheels, one mounted on the tractor connecting the tractor with the 1st trailer and the other mounted on the back of the 1st trailer connecting the 2nd trailer seen in Figure 3.1a. The suspension system connects the lumped masses of the two trailers and the tractor to the wheel masses which are connected to the bridge surface by the tyres. Both the suspension and the tyres are dynamic in nature and simulated by a dashpot-spring system, shown in Figure 3.1b.
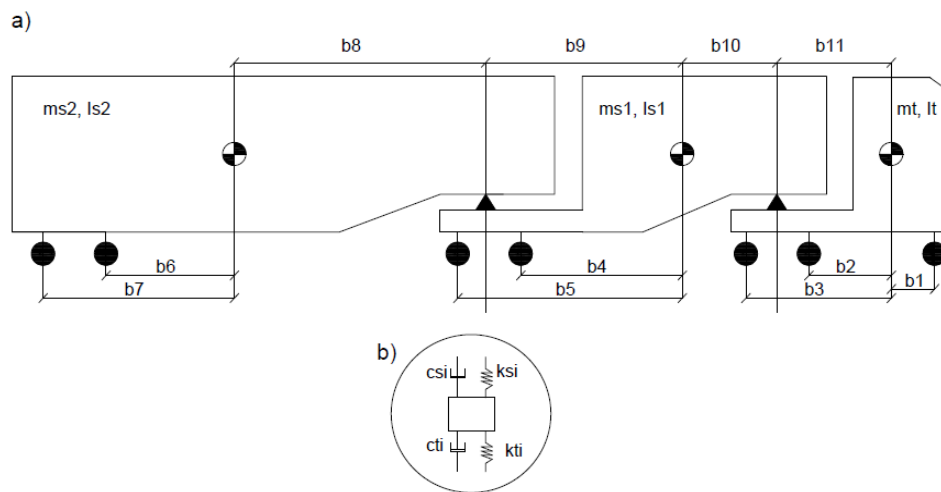
Figure 3.1: a) B-Double schematic, b) Suspension system.

The equations of motion for the BD7 vehicle are described by second-order differential equations and solved using a time-stepping algorithm. It is assumed that the wheels of the vehicle are always in contact with the bridge surface and that the vehicle is moving in a straight line across the bridge. The equations of motion of the BD7 vehicle are determined by enforcing equilibrium of the moment and forces which act on the vehicle.

The equations of motion are described in terms of the degrees of freedom of the vehicle and are expressed by:

$$[M_v]\{\ddot{q}_v\} + [C_v]\{\dot{q}_v\} + [K_v]\{q_v\} = \{F_v\} \tag{3.5}$$

where $[K_v]$, $[C_v]$ and $[M_v]$ are global stiffness, damping and mass matrices with $\{q_v\}$, $\{\dot{q}_v\}$ and $\{\ddot{q}_v\}$ the displacement, velocity and acceleration vectors of the vehicle with $\{F_v\}$ the global force vector containing the vehicle contact forces. The global force vector will contain zeros at the degrees of freedom associated with the tractor and trailer bodies. The force vector is defined by:

$$\{F_v\} = \{0\ 0\ 0\ 0\ f_1\ \cdots\ f_7\} \tag{3.6}$$

where f_i is the contact force applied by the ith wheel of the vehicle and is defined by:

$$f_i = k_{ti}r_i + c_{ti}\dot{r}_i \tag{3.7}$$

with r_i being the road profile, k_{ti} the tyre stiffness and c_{ti} the damping of the tyre. Section 3.3.1 presents the detailed derivation for the equations of motion of the BD7 vehicle.

3.3.1 Equations of Motion of the B-Double

The schematization of the BD7 vehicle model is presented in Figure 3.1. The vehicle model consists of three body masses, the tractor and the two trailer masses (m_t, m_{s1} and m_{s2}). Again, the spring-dashpot system portraying the suspension and the tyres of the vehicle is illustrated in Figure 3.1(b), both connected to a mass simulating the combined mass of the axle, the wheels on the axle and the mass of the suspension system per axle.

The degrees of freedom (DOF) of the vehicle are described by the vertical tractor displacement y_t, tractor pitch θ_t, vertical trailer displacemensts y_{s1} and y_{s2}, trailer 1 pitch θ_{s1}, trailer 2 pitch θ_{s2} and vertical axle displacements y_i. By modelling the tractor and trailers as rigid beams, the total number of degrees of freedom can be reduced to 11 by using the geometric relationships given in Equations 3.8 and 3.9.

$$y_{s1} = y_t + b_{11}\theta_t + b_{10}\theta_{s1} \tag{3.8}$$

Stellenbosch University https://scholar.sun.ac.za

The Characterization of the Dynamic Interaction between Highway Bridges and Long, Multi-Trailer Heavy Vehicles
_____

$$y_{s2} = y_t + (b_{10}+b_9)\theta_t + b_8\theta_{s2} \tag{3.9}$$

By applying force and moment equilibrium to each body mass along with Equations 3.8 and 3.9, the equations of motion are derived and given in Equations 3.10 to 3.13. The displacement DOF of the system are:

$$y_v^T = \{y_t \ \theta_t \ \theta_{s1} \ \theta_{s2} \ y_1 \ y_2 \ y_3 \ y_4 \ y_5 \ y_6 \ y_7\} \tag{3.10}$$

The vertical vibrations of the tractor and trailers can be described by applying Newton's second law of motion in Equation 3.11.

$$m_t\ddot{y}_t + m_{s1}\ddot{y}_{s1} + m_{s2}\ddot{y}_{s2}$$

$$+ \sum_{i=1}^{3}\left[k_{si}(y_t - y_i + b_i\theta_t) + c_{si}(\dot{y}_t - \dot{y}_i + b_i\dot{\theta}_t)\right]$$

$$+ \sum_{i=4}^{5}\left[k_{si}(y_{s1} - y_i + b_i\theta_{s1}) + c_{si}(\dot{y}_{s1} - \dot{y}_i + b_i\dot{\theta}_{s1})\right]$$

$$+ \sum_{i=6}^{7}\left[k_{si}(y_{s2} - y_i + b_i\theta_{s2}) + c_{si}(\dot{y}_{s2} - \dot{y}_i + b_i\dot{\theta}_{s2})\right] = 0$$

$$\tag{3.11}$$

The law of the conservation of angular momentum is applied to the tractor and given in Equation 3.12.

$$(m_{s1}b_{11})\ddot{y}_{s1} + I_t\ddot{\theta}_t + (m_{s2}b_{11})\ddot{y}_{s2}$$

$$+ \sum_{i=1}^{3} b_i[k_{si}(y_t - y_i + b_i\theta_t) + c_{si}(\dot{y}_t - \dot{y}_i + b_i\dot{\theta}_t)] + \sum_{i=4}^{5} b_{11}[k_{si}(y_{s1} - y_i$$

$$+ b_i\theta_{s1}) + c_{si}(\dot{y}_{s1} - \dot{y}_i + b_i\dot{\theta}_{s1})]$$

$$+ \sum_{i=6}^{7} b_{11}[k_{si}(y_{s2} - y_i + b_i\theta_{s2}) + c_{si}(\dot{y}_{s2} - \dot{y}_i + b_i\dot{\theta}_{s2})] = 0$$

$$\tag{3.12}$$

Stellenbosch University https://scholar.sun.ac.za

The Characterization of the Dynamic Interaction between Highway Bridges and Long, Multi-Trailer Heavy Vehicles
_____

The law of the conservation of angular momentum is applied to the first trailer and given in Equation 3.13.

$$(m_{s1}b_{10})\ddot{y}_{s1} + m_{s2}(b_{10} + b_9)\ddot{y}_{s2} + I_{s1}\ddot{\theta}_{s1}$$

$$+ \sum_{i=1}^{3} b_i[k_{si}(y_t - y_i + b_i\theta_t) + c_{si}(\dot{y}_t - \dot{y}_i + b_i\dot{\theta}_{s1})] + \sum_{i=4}^{5} b_i[k_{si}(y_{s1} - y_i$$

$$+ b_i\theta_{s1}) + c_{si}(\dot{y}_{s1} - \dot{y}_i + b_i\dot{\theta}_{s1})]$$

$$+ \sum_{i=6}^{7} (b_{10} + b_9)[k_{si}(y_{s2} - y_i + b_i\theta_{s2}) + c_{si}(\dot{y}_{s2} - \dot{y}_i + b_i\dot{\theta}_{s2})]$$

$$+ \sum_{i=5}^{5} b_{10}[k_{si}(y_{s1} - y_i + b_i\theta_{s1}) + c_{si}(\dot{y}_{s1} - \dot{y}_i + b_i\dot{\theta}_{s1}) = 0$$

(3.13)

The conservation of angular momentum is applied to the second trailer and given in Equation 3.14.

$$(m_{s2}b_8)\ddot{y}_{s2} + I_{s2}\ddot{\theta}_{s2} + \sum_{i=6}^{7} (b_8 + b_i)[k_{si}(y_{s2} - y_i + b_i\theta_{s2}) + c_{si}(\dot{y}_{s2} - \dot{y}_i + b_i\dot{\theta}_{s2})] = 0$$

(3.14)

Applying Newton's second law to the vertical vibrations of the axles, Equations 3.15, 3.16 and 3.17 are used to determine the equations of motion for axles one to three, axles four and five and axles six and seven.

$$m_i\ddot{y}_i - k_{si}(y_t - y_i + b_i\theta_t) - c_{si}(\dot{y}_t - \dot{y}_i + b_i\dot{\theta}_t) + k_{ti}y_i + c_{ti}\dot{y}_i = k_{ti}y_{ci} + c_{ti}\dot{y}_{ci}$$

(3.15)

$$m_i\ddot{y}_i - k_{si}(y_{s1} - y_i + b_i\theta_{s1}) - c_{si}(\dot{y}_{s1} - \dot{y}_i + b_i\dot{\theta}_{s1}) + k_{ti}y_i + c_{ti}\dot{y}_i = k_{ti}y_{ci} + c_{ti}\dot{y}_{ci}$$

(3.16)

$$m_i\ddot{y}_i - k_{si}(y_{s2} - y_i + b_i\theta_{s2}) - c_{si}(\dot{y}_{s2} - \dot{y}_i + b_i\dot{\theta}_{s2}) + k_{ti}y_i + c_{ti}\dot{y}_i = k_{ti}y_{ci} + c_{ti}\dot{y}_{ci}$$

(3.17)

_____

The total mass matrix is defined in Equation 3.18 with Equations 3.19 and 3.20 defining the mass matrices for the vehicle bodies and the wheels.

$$M_v = \begin{pmatrix} M_{v11} & 0 \\ 0 & M_{v22} \end{pmatrix}$$

(3.18)

$$M_{v11} = \begin{pmatrix} m_{11} & m_{12} & m_{13} & m_{14} \\ & m_{22} & m_{23} & m_{24} \\ & & m_{33} & m_{34} \\ Sym. & & & m_{44} \end{pmatrix}$$

(3.19)

where,

$m_{11} = m_t + m_{s1} + m_{s2}$

$m_{12} = (m_{s1} + m_{s2})b_{11}$

$m_{13} = m_{s1}b_{10} + m_{s2}(b_{10} + b_9)$

$m_{14} = m_{s2}b_8$

$m_{22} = (m_{s1} + m_{s2})b_{11}^2 + I_t$

$m_{23} = (m_{s1}b_{10} + m_{s2}(b_{10} + b_9))b_{11}$

$m_{24} = m_{s2}b_8b_{11}$

$m_{33} = m_{s1}b_{10}^2 + m_{s2}(b_{10} + b_9)^2 + I_{s1}$

$m_{34} = m_{s2}b_8(b_{10} + b_9)$

$m_{44} = m_{s2}b_8^2 + I_{s2}$

$$M_{v22} = \begin{pmatrix} m_1 & \cdots & 0 & \cdots & 0 \\ & \ddots & \vdots & & \vdots \\ & & m_i & & 0 \\ & & & \ddots & \vdots \\ Sym. & & & & m_7 \end{pmatrix}$$

(3.20)

_____

The stiffness matrix is defined in Equation 3.21 which consists of submatrices 3.22 to 3.24 simulating the stiffness of the vehicle bodies and the wheels.

$$K_v = \begin{pmatrix} K_{v11} & K_{v12} \\ Sym. & K_{v22} \end{pmatrix}$$

(3.21)

$$K_{v11} = \begin{pmatrix} k_{11} & k_{12} & k_{13} & k_{14} \\ & k_{22} & k_{23} & k_{24} \\ & & k_{33} & k_{34} \\ Sym. & & & k_{44} \end{pmatrix}$$

(3.22)

where,

$$k_{11} = \sum_{i=1}^{7} k_{si}$$

$$k_{12} = (-b_1 k_{s1} + b_2 k_{s2} + b_3 k_{s3} + \sum_{i=4}^{7} b_{11} k_{si})$$

$$k_{13} = \sum_{i=4}^{5} k_{si}(b_{10} + b_i) + (k_{s6} + k_{s7})(b_{10} + b_9)$$

$$k_{14} = \sum_{i=6}^{7} k_{si}(b_8 + b_i)$$

$$k_{22} = \sum_{i=1}^{3} b_i^2 k_{si} + \sum_{i=4}^{7} b_{11}^2 k_{si}$$

$$k_{23} = b_{11}[(k_{s6} + k_{s7})(b_{10} + b_9) + \sum_{i=4}^{5} k_{si}(b_{10} + b_i)]$$

$$k_{24} = \sum_{i=6}^{7} b_{11} k_{si}(b_8 + b_i)$$

$$k_{33} = \sum_{i=4}^{5} k_{si}(b_{10} + b_i)^2 + \sum_{i=6}^{7} k_{si}(b_{10} + b_9)^2$$

$$k_{34} = (b_{10} + b_9) \sum_{i=6}^{7} k_{si}(b_8 + b_i)$$

$$k_{44} = \sum_{i=6}^{7} k_{si}(b_8 + b_i)^2$$

$$K_{v12} = \begin{pmatrix} -k_{s1} & -k_{s2} & -k_{s3} & -k_{s4} & -k_{s5} & -k_{s6} & -k_{s7} \\ -k_{21} & k_{22} & k_{23} & k_{24} & k_{25} & k_{26} & k_{27} \\ 0 & 0 & 0 & k_{34} & k_{35} & k_{36} & k_{37} \\ 0 & 0 & 0 & 0 & 0 & k_{46} & k_{47} \end{pmatrix}$$

(3.23)

where,

$$k_{2(i=1\rightarrow 3)} = -b_i k_{si}$$

$$k_{2(i=4\rightarrow 7)} = -b_{11} k_{si}$$

$$k_{3(i=4\rightarrow 7)} = -k_{si}(b_{10} + b_i)$$

$$k_{4(i=6\rightarrow 7)} = -k_{si}(b_8 + b_i)$$

$$K_{v22} = \begin{pmatrix} k_{s1} + k_{t1} & \cdots & 0 \\ \vdots & \ddots & \vdots \\ 0 & \cdots & k_{s7} + k_{t7} \end{pmatrix}$$

(3.24)

The structure of the damping matrix, C_v, is identical to that of the stiffness matrix with only the entries changed from stiffness constants to damping constants, $k_{s1} \rightarrow c_{s1}$. Refer to Appendix A for the detailed expansion of vehicle matrices.

_____

3.4 Coupled Interaction

The equations of motion of the vehicle and the bridge are combined to form a global system of equations. This is done by coupling the bridge and vehicle at the points of contact using the dynamic interaction forces defined in Equation 3.7. The coupled equation of motion is given by:

$$[M_g]\{\ddot{q}_g\} + [C_g]\{\dot{q}_g\} + [K_g]\{q_g\} = \{F_g\} \tag{3.25}$$

where $[M_g]$ and $[C_g]$ is the coupled mass and damping matrices. $[K_g]$ is the time dependent stiffness matrix, see Appendix A. $\{F_g\}$ is the coupled force vector defined by:

$$\{F_g\} = \begin{Bmatrix} \{F_v\} \\ [H]\{W_i + f_i\} \end{Bmatrix}_{(n+11) \times 1} \tag{3.27}$$

where $\{F_v\}$ is the contact force vector defined in Equation 3.6 and $[H]\{W_i + f_i\}$ the equivalent nodal dynamic interaction forces defined in Equation 3.1. The coupled equations of motion are then solved using iteration and the Newmark-Beta numerical integration scheme (Gonzalez 2010; Paultre 2003). The VBI solution produces the total (static plus dynamic) deflection, velocity and acceleration responses at each node of the beam elements. By using Hermitian shape functions, the strains at the mid-span node can be determined and used to calculate the maximum total bending moment response. The static finite element solution is used to determine the static bending moment at the instant at which the maximum dynamic moment occurs. Equation 1.1 can then be used to calculate the DAF of the considered crossing event.

3.5 Road Roughness

The roughness of the road surfaces of the bridges are randomly generated as power spectral density functions according to the ISO 8608 (1995) road roughness spectrum. The PSD function $G_d(n)$, is calculated by:

$$G_d(n) = G_d(n_0)\left(\frac{n}{n_0}\right)^{-2} \tag{3.28}$$

_____

where n is the spatial frequency per meter, $n_0 = 0.1$ cycles per meter and $G_d(n_0)$ is specified in ISO 8608 (1995) per road roughness class. $G_d(n)$ can be substituted into Equation 3.29, the road roughness function, to generate the different roughness profiles within the bounds of the specific road classes as a function of the transverse positions of the bridge x_i per time step.

$$R(x_i) = \sum_{i=1}^{N} \sqrt{4G_d(n)\Delta n} \, \cos(n_{si}x_i + \theta_i) \tag{3.29}$$

where Δn is the spatial frequency interval, n_{si} is the considered frequency and θ_i in the cosine function is the random phase angle. ISO defines eight road classes sorted in descending order from Class A being the best quality surface to Class H being the worst. Table 3.1 presents the values for $G_d(n_0)$ for the first three road classes according to the ISO spectrum. In this investigation, the focus is on Class A due to the national routes being generally well maintained by authorities. Figure 3.2 presents an example of the comparison of the generated roughness profiles of the first three road classes. The total distance includes a 100 m approach length, the full vehicle length and 10 m bridge span.

Table 3.1: Values for $G_d(n_0)$ according to ISO 8608 (1995).

Road Class	$G_d(n_0)$ Range
A	$G_d < 32 \times 10^6$
B	$32 \times 10^6 \leq G_d < 128 \times 10^6$
C	$128 \times 10^6 \leq G_d < 512 \times 10^6$
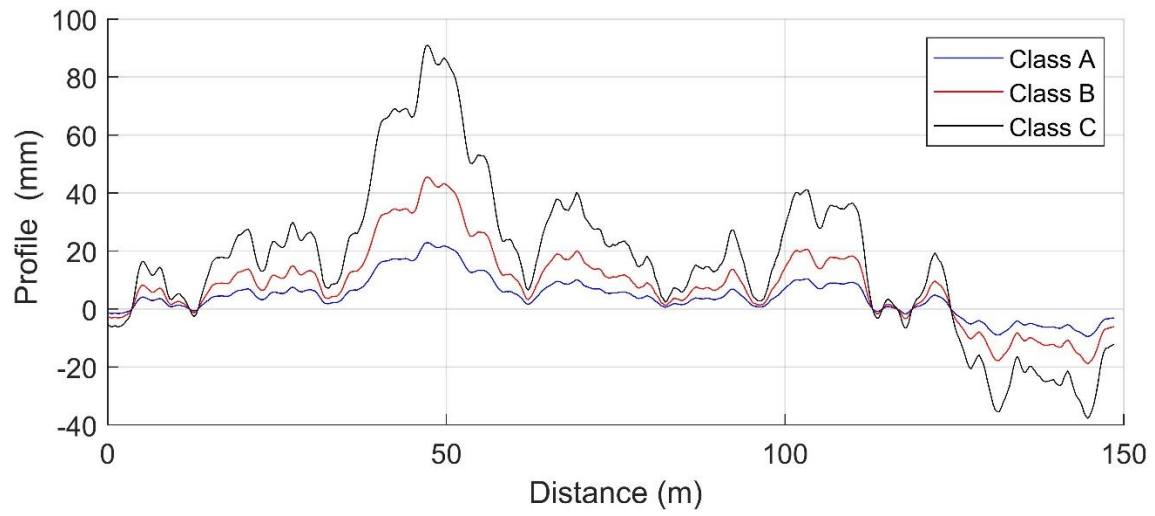
Figure 3.2: Road profiles for the first three road classes.

CHAPTER 4:   VERIFICATION OF VEHICLE-BRIDGE INTERACTION MODEL

4.1 Introduction

The basic VBI solution theory has been studied and implemented by numerous researchers within the field of bridge dynamics. However, the development of an intricate numerical solution which is dependent on a wide range of variables should be verified with infield test results gathered from instrumented bridge studies. One such bridge is the Vransko bridge located in Slovenia which has been instrumented to capture strain history induced by the passage of traffic. The study formed part of the ARCHES project which measured the strains for approximately two months in 2006 after which a Bridge Weigh-in-Motion (BWIM) algorithm was implemented to calculate the DAFs induced on the bridge (Gonzalez *et al*., 2010). The BWIM algorithm utilizes a low pass filter to determine the maximum static strain by removing the dynamic component of the measured strain. The difference between the maximum recorded strain and the calculated static strain is used to calculate the final DAF. The dynamic amplification results from the Vransko bridge experiment are used to test the accuracy of the VBI solution developed for this research project.

4.2 Field Experiment Details

The experiment to determine the DAFs induced on the Vransko bridge consisted of two groups of 2-axle vehicles categorized by two vehicle groups; light and heavy. A total of 7603 light vehicles and 8913 heavy vehicles were recorded, of which their number of axles, axle weights, axle spacing and velocity were determined using WIM sensors (Gonzalez *et al.*, 2010). The mean and standard deviations of the axle spacing and axle weights of both vehicle groups are given in Table 4.1 while the dispersion of vehicle velocities for the two groups is shown in Figure 4.1.

The bridge is a simply supported double lane beam and slab bridge with a span length of 24.8 m and a first natural frequency of 5.1 Hz. The bridge consists out of five precast beams with a depth of 1.4 m tied by 0.24 m concrete slab. The total width of the bridge 12.07 m with a depth of 1.64 m. Figure 4.2 presents the cross-section of the Vransko bridge. The road profile of the bridge is classified as a Class A road surface condition (Gonzalez *et al*., 2010). The strain measurements are taken under the right wheel path in both of the bridge lanes.

Table 4.1: WIM data of recorded 2-axle vehicle traversing Vransko Bridge (Gonzalez *et al*., 2010).

Group	Gross vehicle weight (kN)		Axle spacing (m)		1st Axle weight (kN)		2nd Axle weight (kN)	
	Mean	St.d.	Mean	St.d.	Mean	St.d.	Mean	St.d.
1	59.05	9.29	4.27	0.58	25.34	6.38	33.71	7.85
2	117.53	20.68	4.81	0.73	40.99	10.17	76.54	18.32

_____
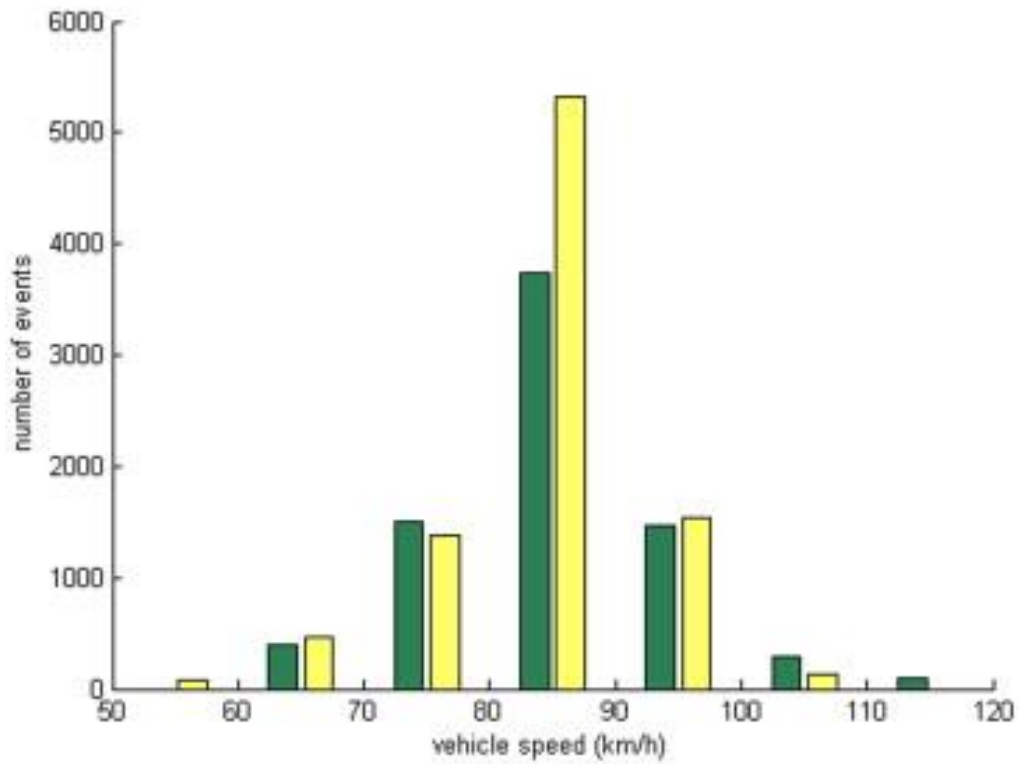
Figure 4.1: Vehicle velocities for: a) light vehicles shown in green, b) heavy vehicles shown in yellow

(Gonzalez *et al*., 2010).
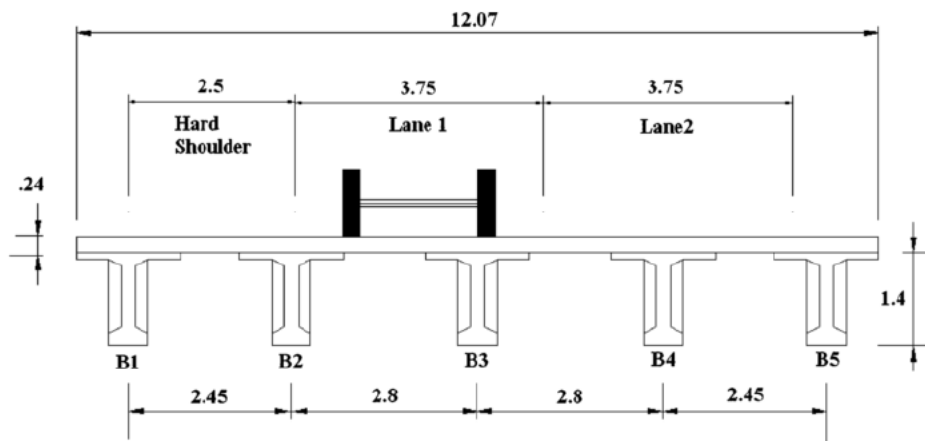
Figure 4.2: Cross-section of the Vransko bridge (Rowley *et al*., 2008)

4.3 Vehicle-Bridge Interaction Solution

In order to verify the VBI solution developed in Chapter 3 the interaction between the Vransko bridge and the set of 2-axle vehicles is simulated to compare the DAF produced. The double axle vehicles are modelled by collection of sprung masses, with a total of 4 degrees of freedom corresponding to the vertical displacement of the vehicle body, the pitch rotation of the vehicle body and the vertical displacement of both axles. Figure 4.3 presents an example of the 2-axle interaction model implemented in the VBI algorithm. The equations of motion for the 2-axle vehicle are fully derived and presented by OBrien, *et al., (2014)*.
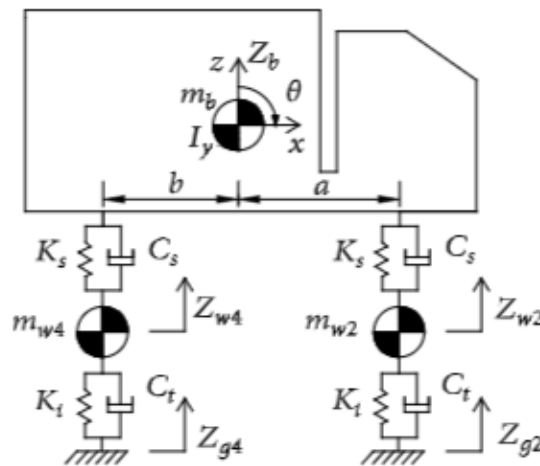
Figure 4.3: 2-axle vehicle model (Yu *et al.*, 2018).

 The dynamic interaction of the heavy group of vehicles is determined by implementing a Monte Carlo simulation to generate 5000 loading events according to the statistical variability described in Table 4.1. The velocities are generated between 50 km/h and 110 km/h, predominantly according to the velocity dispersion shown in Figure 4.1. The vehicles are simulated to have a 100 m approach length to traverse before the bridge is entered to take account for any vehicle vibrations induced by normal vehicle only dynamics. For each loading event, a random Class A road profile is generated for the full simulated road length (approach length + bridge span). The modulus of elasticity is specified as 35 GPa (Gonzalez *et al*., 2010).

In the available literature, information about the second moment of inertia and mass per meter of the Vransko bridge is not provided. Therefore, using the specified modulus of elasticity, span length and cross-section specification provided in Figure 4.2, the mass per meter and second moment of inertia are back estimated using the definition of the first natural frequency of a simply supported bridge. Any estimation of fundamental bridge properties can introduce more estimation inaccuracies in the final dynamic bridge response solution. However, knowing the first natural frequency which is inherently descriptive of the dynamic behaviour of the bridge significantly reduces these inaccuracies. The calculated DAFs using the VBI solution are compared and evaluated in Section 4.4.

4.4 Dynamic Amplification Comparison

The velocity of a vehicle is one of the most influential parameters with regards to extent to which a bridge experiences amplification. Any bridge has a critical velocity (also referred to as critical loading velocity) at which frequency matching occurs between the traversing vehicle and the bridge, also defined as bridge resonance. At these critical velocities, the largest DAFs tend to occur frequently. Considering the DAFs vs. vehicle velocity response, the critical velocities can easily be identified by the significant peaks observed in the DAFs response. It is therefore of fundamental importance that a VBI solution can accurately identify these critical velocities of a bridge, induced by a specific vehicle type/configuration.

The results of the average DAF vs. vehicle velocity induced by the population of vehicles defined in Table 4.1 are presented in Figure 4.4. The results from the field experiments on the Vransko bridge, which are presented by Gonzalez *et al.*, (2010), are compared to the results obtained from the VBI solution. The dynamic amplification response to velocity is shown for both the light and heavy groups as determined from the stain measurement and BWIM algorithm. The response of the group of heavy vehicles determined by the VBI solution is presented by the solid line graph in red.

Promising results are presented in terms of the DAF accuracy from the VBI solution. It is shown that the VBI solution can sufficiently identify the critical velocities of the Vransko bridge identified by the DAF peaks at approximately 63 km/h and 87 km/h. Furthermore, the average values of the DAFs are within a 10% margin of the measured field results which is significantly low considering the number of variable parameters within the vehicle-bridge interaction problem such as; road profiles, suspension properties, bridge properties, severity of expansion joints and the degree of simplification to which computerized simulation models are subjected.

Additionally the novel comparison between the BWIM and VBI solutions highlights the effectiveness of the two-dimensional VBI solution to be used for extensive dynamic amplification studies as also found by Kortiš and Daniel (2015). The verification presented here illustrates the effectiveness of the VBI algorithm to solve the vehicle-bridge interaction problem. The equations of motion of the 2-axle vehicle can now simply be replaced by those of the SA5, SA6 and BD7 to study the dynamic amplification induced by these vehicles on typical highway bridges.
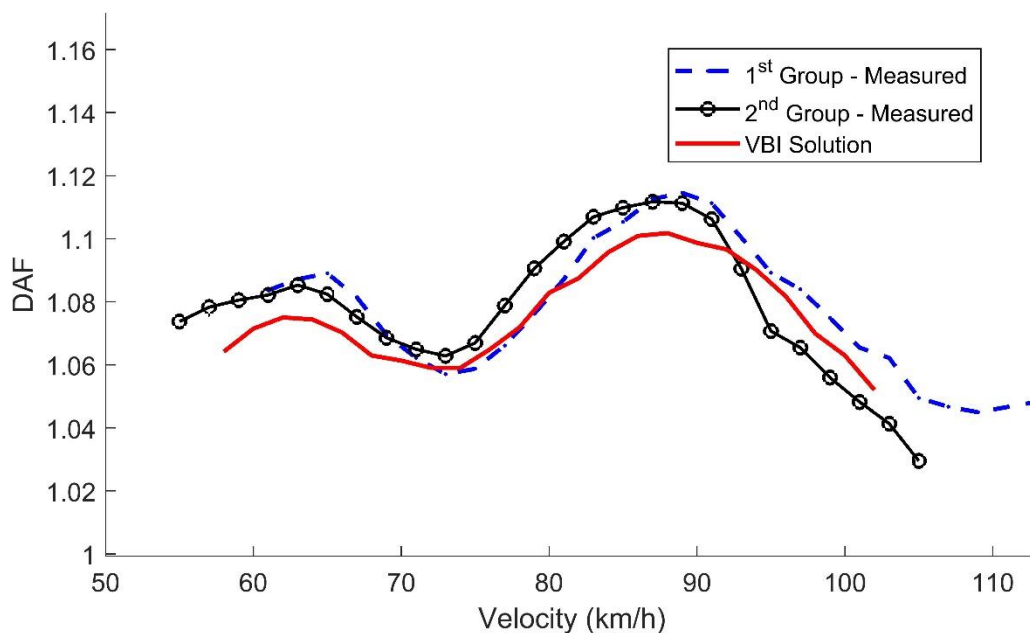
Figure 4.4: The DAF vs. velocity pattern from the measured and VBI solution of the Vransko bridge.

CHAPTER 5:   HEAVY VEHICLES AND BRIDGE STOCK

5.1 Introduction

The VBI models presented in Chapter 2 are developed in such a manner as to directly utilize filtered WIM data to identify the input parameters unique to each loading event. The research presented here is based on heavy vehicle population data sourced from extensive WIM measurement applications implemented on the national freight routes of South Africa. The purpose of this chapter is to define all the input parameters used in the VBI solutions to study the dynamic effects on common highway bridges. The mass of the vehicles are given in metric ton but will referred to in this document only as ton.

5.2 Heavy Vehicles Description

The WIM data measured at the Roosboom station are mainly used for the purpose of this research. The station is located on the N3 national road connecting Johannesburg to Durban with an ADTT of 2025 vehicles per day. This route experiences high numbers of heavy vehicles transporting freight from the Durban port to the financial capital of South Africa, Johannesburg. The N3 national road has two lanes with the WIM sensors set in the slow lane (Pérez Sifre, 2020). WIM data may contain inaccuracies and systematic errors which have to be removed in order to ensure accurate vehicle description. The errors in the WIM data from the Roosboom station have been removed by Pérez Sifre (2020).

The WIM data are filtered and all vehicles which classify as SA5, SA6 and BD7 configurations are categorized. The total number of vehicles for each configuration is; 21913, 220606 and 319076. The SA6 and BD7 vehicles combined account for more than 70% of the total truck traffic of South Africa while the BD7, being the most popular, accounts for 44% alone. With the focus of the present research being on the dynamic interactional behaviour of BD7 vehicles, the 5- and 6-axle single articulated vehicles, which are well known in Europe, are used as points of reference to study and compare the dynamic behaviour of the BD7 vehicles.

5.3 Vehicle Velocities

The following section presents the distribution of the velocities, from the WIM recordings of each of the three vehicle types considered. In Figures 5.1-5.3, the histograms indicate that the three vehicle types have approximately similar velocity distributions, all with means close to 80 km/h which is the legal limit of trucks for a range of countries, including South Africa. The statistical variability of the velocities is given in Table 5.1 below for each of the three vehicle types. The minimum velocities are all less than 10 km/h which is slow enough to neglect any dynamic amplification effects while the maximums are approximately at 120 km/h, at which significant bridge amplification can occur.

Table 5.1: Statistical parameters of velocities.

Vehicle Type	Min. velocity (km/h)	Mean velocity (km/h)	Max. velocity (km/h)
SA5	7	79.22	120
SA6	6	79.89	120
BD7	9	79.53	122
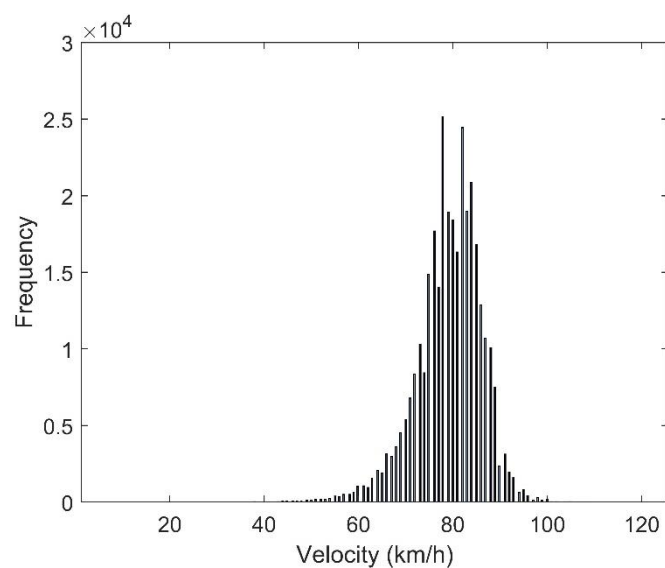
Figure 5.1: Velocity distribution of BD7 vehicles.
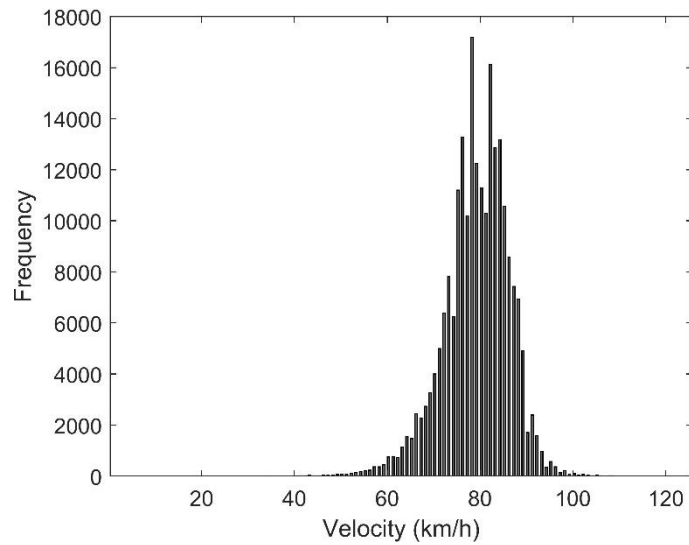
Figure 5.2: Velocity distribution of SA6 vehicles.
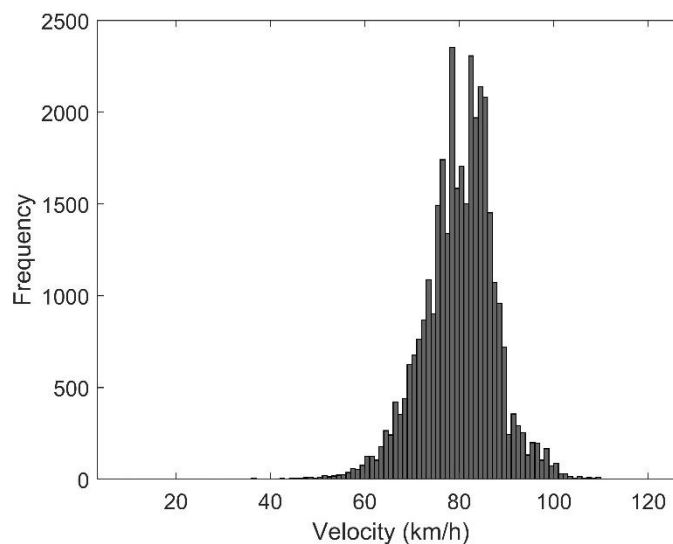
Figure 5.3: Velocity distribution of SA5 vehicles.

5.3.1 Gross Vehicle Mass

The details of the GVMs of each of the three vehicle types/configurations are shown in Table 5.2 with the histogram distributions shown in Figures 5.4-5.6. As expected, the BD7 are the heaviest vehicles with an average GVM of 45.35 ton and a maximum of 82.7 ton, which is significantly overloaded with 56 ton being the legal limit for GVM in South Africa as stated by the Department of Transport of South

Africa (TRH-11, 2009). Similarly, overloading is recorded for the SA6 vehicles with a maximum GVM of 82.85 ton.

Considering the minimum GVM values recorded by the WIM measurements, it can be concluded that these vehicles are smaller sized vehicles carrying light freight with large volumes which share similar axle configurations compared to the heavy freight vehicles. The unloaded masses for SA5, SA6 and BD7 heavy vehicles range from approximately 15 ton up to 25 ton depending on the type of freight the vehicles are designed to carry (Thorogood et al., 2009). Therefore, for the purpose of this research BD7 vehicles weighing less than 25 ton are assumed to be unloaded and are not included in VBI investigations.

Table 5.2: GVM description of heavy vehicles.

Vehicle type	Min. GVM (ton)	Mean GVM (ton)	Max. GVM (ton)
SA5	7.1	23.6	52
SA6	7.4	36.2	72.85
BD7	9.26	45.35	82.7
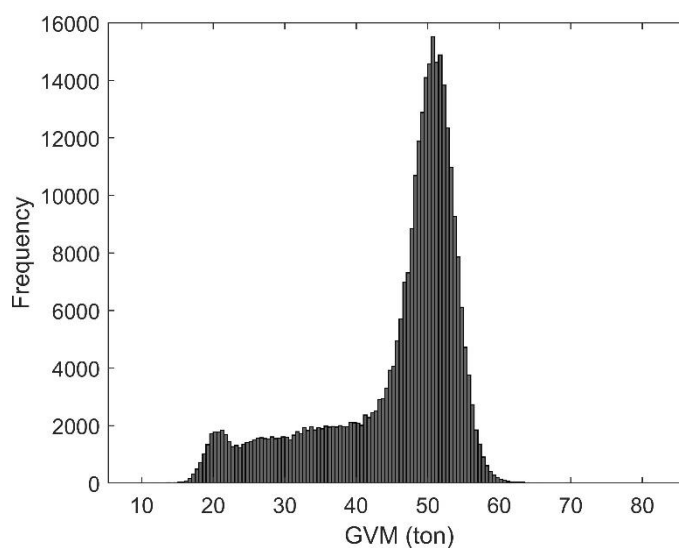
Figure 5.4: GVM of BD7 vehicles.
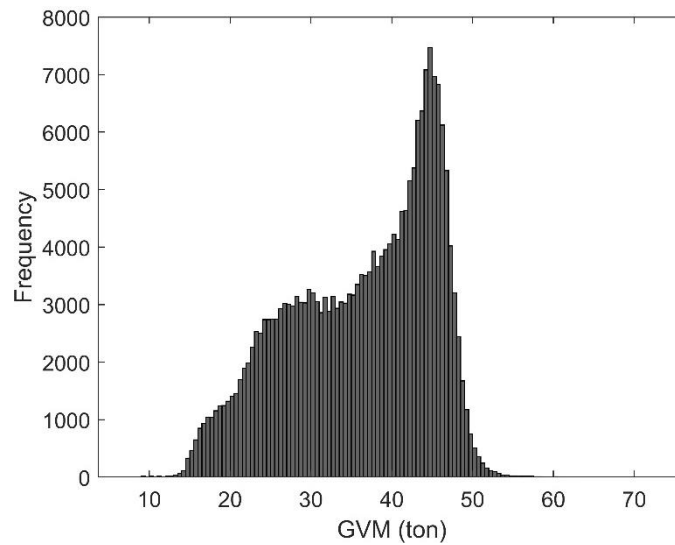
Figure 5.5: GVM of SA6 vehicles.
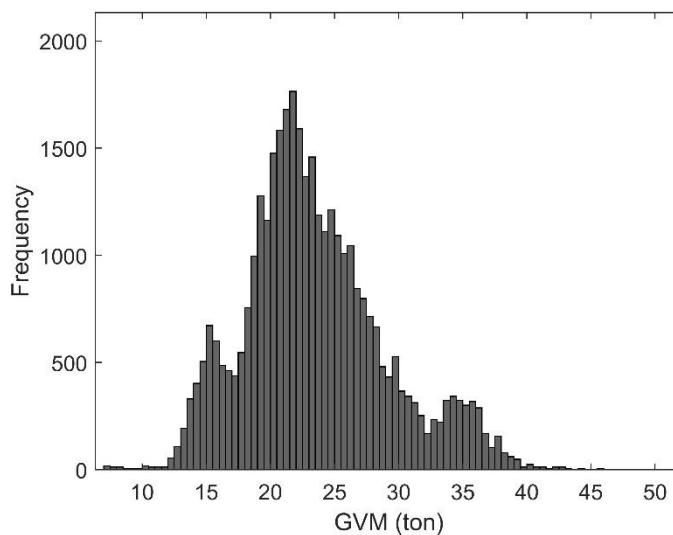
Figure 5.6: GVM of SA5 vehicles.

5.3.2 Axle Loads

Tables 5.3-5.5 present the axle loads for the BD7, SA6 and SA5 vehicles from the Roosboom WIM data. All axles of the three vehicle types are double wheel axles except for the first axles being the steering axle of the truck tractor (also referred to as the prime mover). Both BD7 and SA6 vehicles consist of similar tractors with one steering axle and two drive axles, hence the similarities in average axle loads for the first three axles of these two vehicle types, especially the first axles which

predominantly carry the weight of the engine and cabin. The main difference between the SA5 and SA6 vehicles is that the SA5 vehicles consist of only one driving axle, evidently lowering the total load capacity of these vehicles. The axle load distributions for all the axles of the three vehicle types are presented by the histograms shown in Appendix B.1

Table 5.3: Description of BD7 axle loads.

BD7 Axles	Min. Axle load (ton)	Mean Axle load (ton)	Max. Axle load (ton)
1	1.04	6.22	11.46
2	0.85	6.62	14.34
3	0.95	6.67	14.1
4	0.85	6.65	14.87
5	0.85	7.03	14.35
6	0.85	6.06	14.81
7	0.85	6.28	14.21

Table 5.4: Description of SA6 axle loads.

SA6 Axles	Min. Axle load (ton)	Mean Axle load (ton)	Max. Axle load (ton)
1	1.04	6.13	10.13
2	0.86	6.63	15.11
3	0.86	6.7	14.33
4	0.85	5.38	15.21
5	0.85	5.56	14.8
6	0.85	5.8	15.08

Table 5.5: Description of SA5 axle loads.

SA5 Axles	Min. Axle load (ton)	Mean Axle load (ton)	Max. Axle load (ton)
1	0.95	5.54	8.5
2	0.995	6.59	15.33
3	0.88	3.53	10.71
4	0.96	3.75	10.54
5	0.85	3.9	9.81

5.3.3 Axle Spacing

The axle spacing of heavy vehicles is one of the most important variables with regards to the interaction between bridge and vehicle. The axle spacing predominantly accounts for the identification of vehicle types from WIM measurements by identifying the axle groups of each vehicle. In this investigation an axle group is defined when the spacing between two or more adjacent axles is less than or equal to 1.6 m. The minimum, maximum and mean values for the axle spacing of the three vehicle types are given in Tables 5.6-5.8, while the distributions are shown in Appendix B.2.

The similarity in axle spacing between the tractors (defined by axle spacing of 1-2 and 2-3) of the SA6 and BD7 vehicles is an indication that the same type of tractors, in terms of specification, are predominantly used for both applications. Furthermore, the mean values of axle spacing within one axle group are all close to 1.4 m when rounded to the first decimal. The similarity in axle spacing among axles within an axle group can also be seen when comparing the histograms of these axle spacing provided in Appendix B.2. The average spacing between axles of each of the three vehicle types is presented in Figure 5.7. These averages are used for a parametric study of the effect of axle configurations on dynamic amplification discussed in Chapter 6.
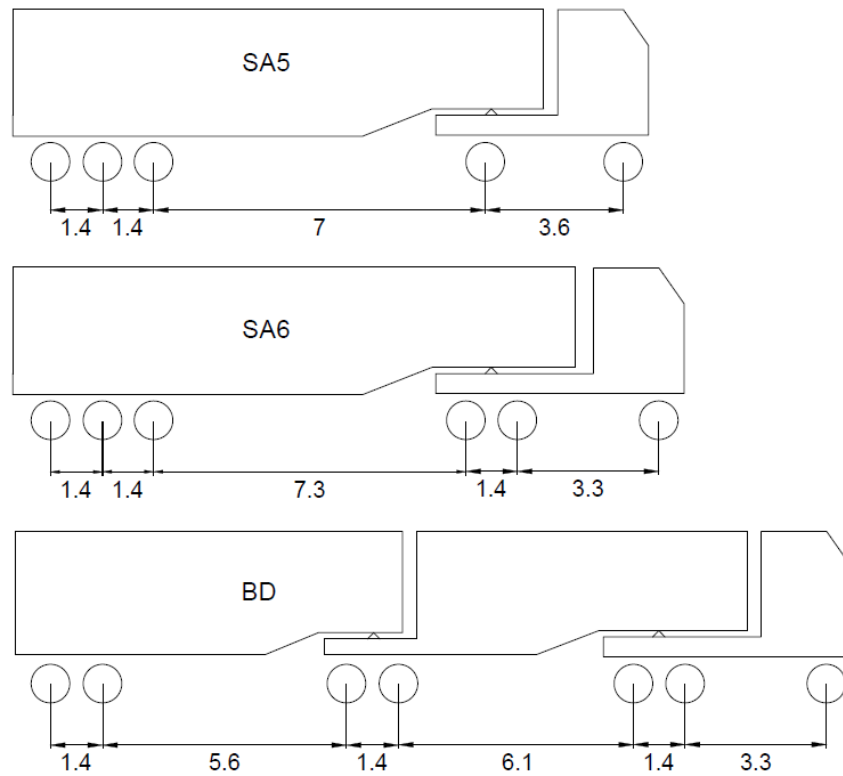
Figure 5.7: Three vehicle types/configurations with average vehicle spacing in meters.

Table 5.6: Axle spacing of BD7 vehicles.

BD7 Axle spacing	Min. Axle spacing (m)	Mean Axle spacing (m)	Max. Axle spacing (m)
1-2	2.25	3.28	5.96
2-3	1.04	1.37	1.59
3-4	3.07	6.08	9.98
4-5	0.88	1.36	1.5
5-6	1.16	5.68	8.45
6-7	0.8	1.35	1.5

Table 5.7: Axle spacing of SA6 vehicles.

SA6 Axle spacing	Min. Axle spacing (m)	Mean Axle spacing (m)	Max. Axle spacing (m)
1-2	2.23	3.31	6.11
2-3	1.04	1.35	1.6
3-4	3.67	7.34	10
4-5	0.96	1.35	1.5
5-6	0.91	1.35	1.5

Table 5.8: Axle spacing of SA5 vehicles.

SA5 Axle spacing	Min. Axle spacing (m)	Mean Axle spacing (m)	Max. Axle spacing (m)
1-2	1.27	3.62	6.47
2-3	2.32	6.95	9.98
3-4	0.97	1.35	1.49
4-5	0.96	1.35	1.48

5.3.4 Mechanical Vehicle Properties

The mechanical properties which define the undercarriage dynamics of the vehicles, such as the suspension and tyres, are presented here. There is a variety in mechanical properties amongst different heavy vehicles. Therefore, the suspension properties are varied, using a Monte Carlo simulation for each vehicle loading event, within a range chosen to be representative and generally accepted within the field of vehicle-bridge dynamic studies. The suspension properties are normally distributed. (Cantero *et al.*, 2009; Cantero, *et al*., 2009; Gonzalez, 2010; O'Brien, *et al*., 2014). Table 5.9 presents the suspension and tyre stiffness ranges used for the three vehicle types. Table 3.10 presents the

Stellenbosch University https://scholar.sun.ac.za

The Characterization of the Dynamic Interaction between Highway Bridges and Long, Multi-Trailer Heavy Vehicles
_____

damping coefficients of the vehicle suspension which have been widely implemented for VBI studies of heavy vehicles while the damping coefficients of the tyres are assumed to be zero, ensuring a more conservative approach as done by Cantero *et al.*, (2009), O'Brien, Mcgetrick and González, (2014). The mass of all steering axles is taken as 700 kg, the drive axles 1100 kg and the trailer axles as 750 kg. The mass of the SA5 tractor without axles is 4 890 kg and the mass of the tractor used for the SA6 and BD7 vehicles is 6420 kg without axles (Cantero *et al.*, 2009; Cantero, *et al.*, 2009; Thorogood *et al.*, 2009). The unloaded masses of the trailers are back calculated from the static WIM axle loads.

Table 5.9: Vehicle Stiffness Properties

Suspension Stiffness (N/m)			
Location	**Minimum**	**Mean**	**Maximum**
Steering Axles	250×10^3	400×10^3	550×10^3
Drive and Trailer Axles	1000×10^3	1250×10^3	1500×10^3
Tyre Stiffness (N/m)			
Steering Tyres	1500×10^3	1750×10^3	2000×10^3
Drive and Trailer Tyres	3000×10^3	3500×10^3	4000×10^3

Table 5.10: Vehicle suspension damping properties.

Suspension Damping (Ns/m)	
Steering Axles	10×10^3
Drive and Trailer Axles	20×10^3

5.4 Bridge Stock

In order to establish a concrete understanding of how BD7 vehicles interact with highway bridges it is necessary to consider a wide range of bridge spans due to the significant dynamic differences, such as

natural frequencies, amongst bridges of different span lengths. Therefore the stock of bridges considered for the present research range from short (10-20 m) to medium span (20-40 m) simply supported bridges. Due to the popularity of simply supported concrete beam and slab bridges around the world, these bridge types are chosen as the dynamic interaction platform to investigate the unique dynamic behaviour induced by BD7 vehicles. The representative bridge properties are presented in Table 5.11 and are based on typical cross-sections of beam and slab bridges designed according to BS5400-4. The Young's Modulus, E, for all spans is set to 3.5×10^{10} N/m^2 and bridge damping kept constant at 3%, unless otherwise specified. (BS5400-4, 1990; Li, *et al*, 2006; González, *et al*, 2011; O'Brien, *et al.*, 2014). These bridge properties have been widely implemented in VBI studies for smaller vehicles and are considered an accurate representation to capture the dynamic behaviour of beam and slab simply supported bridges (Li, *et al*, 2006; González, *et al*, 2011; O'Brien, *et al.*, 2014).

Table 5.11: Bridge stock parameters modelled as FEM beams.

Span Length [m]	Type of Beam	Mass/Meter (kg/m)	Flexural Rigidity (Nm^2)	Natural Frequency (Hz)
10	T	18 750	5.6×10^9	8.61
11	T	20625	7.28×10^9	7.71
12	T	22500	9.65×10^9	7.14
13	T	24375	1.2×10^{10}	6.53
14	T	26250	1.52×10^{10}	6.12
15	T	28 125	1.85×10^{10}	5.66
16	T	30000	2.27×10^{10}	5.33
17	T	31875	2.71×10^{10}	5.01
18	T	33750	3.22×10^{10}	4.73

Table 5.11: Bridge stock parameters modelled as FEM beams (continued).

Span Length [m]	Type of Beam	Mass/Meter (kg/m)	Flexural Rigidity (Nm²)	Natural Frequency (Hz)
19	T	35625	3.75×10^{10}	4.47
20	T	37 500	4.4×10^{10}	4.26
21	Y	16530	3.05×10^{10}	4.84
22	Y	16975	3.47×10^{10}	4.64
23	Y	17419	3.9×10^{10}	4.44
24	Y	17889	4.38×10^{10}	4.27
25	Y	18 358	4.9×10^{10}	4.1
26	Y	18865	5.42×10^{10}	3.94
27	Y	19372	5.97×10^{10}	3.78
28	Y	19929	6.6×10^{10}	3.65
29	Y	20486	7.22×10^{10}	3.51
30	Y	21 068	7.9×10^{10}	3.39
31	Y	21650	8.63×10^{10}	3.26
32	Super Y	20552	9.41×10^{10}	3.28
33	Super Y	20952	1.03×10^{11}	3.19
34	Super Y	21352	1.11×10^{11}	3.1
35	Super Y	21 752	1.2×10^{11}	3,01
36	Super Y	22152	1.29×10^{11}	2.92
37	Super Y	22552	1.38×10^{11}	2.84
38	Super Y	22952	1.48×10^{11}	2.76
39	Super Y	23352	1.6×10^{11}	2.7
40	Super Y	23752	1.7×10^{11}	2.62

5-52

_____

CHAPTER 6: DYNAMIC AMPLIFICATION AND BRIDGE ACCELERATION

6.1 Introduction

The extent of dynamic amplification induced by the typical BD7 vehicles on short to medium span bridges is investigated and compared to the smaller SA5 and SA6 vehicles. The well-established relationship between the GVM and DAF is tested for the B-Double and single articulated vehicle configurations using input parameters gathered from WIM data. This investigation produced somewhat contradictory results with regards to the generally accepted relationships between dynamic amplification, bridge span lengths and GVM of vehicles. Further investigation of the root cause of the latter, unearthed a novel relationship which exists between the DAF and bridge acceleration which is linked to the influence of axle configurations of these vehicles.

Section 6.2 demonstrates the influence of GVM on dynamic amplification for the different vehicle types and compares the DAFs induced by these vehicles at short to medium span bridges. This section incorporates the study of parametric vehicles in which the axle loads, axle spacing and mechanical properties are kept constant as well as a study where these input parameters are varied using WIM data. The road roughness is taken as smooth so to focus the dynamic effects of the vehicles itself. Dynamic loads will still occur even though perfect road conditions are assumed due to the inertia effects of the bridge induced by the axle loads and the interaction between the vehicle and bridge.

Section 6.3 explores the novel relationship between the DAF and bridge acceleration by considering the interaction of parametric vehicles of each of the three vehicle types at a range of velocities and bridge spans. Finally the latter relationship is shown to hold for road Class A and B surface conditions.

Section 6.4 explores the influence of axle configurations of the three vehicle types and demonstrates how the bridge acceleration and evidently, the extent of dynamic amplification can be influenced by the latter.

The work presented in this Chapter has been documented in (Meyer, *et al.*, 2021).

6.2 Dynamic Amplification and Gross Vehicle Weight

In a single degree of freedom system, as the mass increases, the amplitude and the frequency of the response decrease. The same applies to highway bridges traversed by heavy vehicles. Many researchers have established that an increase of GVM leads to a decrease in dynamic amplification (Huang, *et al*, 1993; Broquet *et al.*, 2004; Ashebo, *et al*, 2007; Caprani, 2017). However, this relationship may not be generally true, especially when comparing heavy vehicles of different axle group configurations.

To illustrate the differences, Figure 6.2 presents the mean DAFs according to the VBI numerical solution of three parametric vehicles traversing a range of short and medium span bridges at a fixed speed of 80 km/h. The GVM, axle spacing, axle loads and mechanical properties of the SA5, SA6 and BD7 parametric vehicles are kept constant with these input values equal to the means presented in Chapter 5. The axle spacing for the three parametric vehicles is shown again in Figure 5.7.

The DAFs are calculated at midspan at the instant where the maximum total bending moment is observed. To reiterate, for this research bridges with span lengths shorter than 20 m are categorized as "short" and bridges within the range of 20 m up to 40 m as "medium" span bridges. It can be seen in Figure 6.1a that for the majority of short spans, the shorter and lighter SA5 and SA6 vehicles govern the dynamic amplification. As for the medium span lengths, the heavier BD7 vehicle governs the majority of the spans. It is noted that this result contradicts the often-presented inverse relationship between the DAF and the GVM. The BD7 vehicle is heavier in comparison to both SA5 and SA6 vehicles and should, in theory, exhibit lower dynamic amplification.
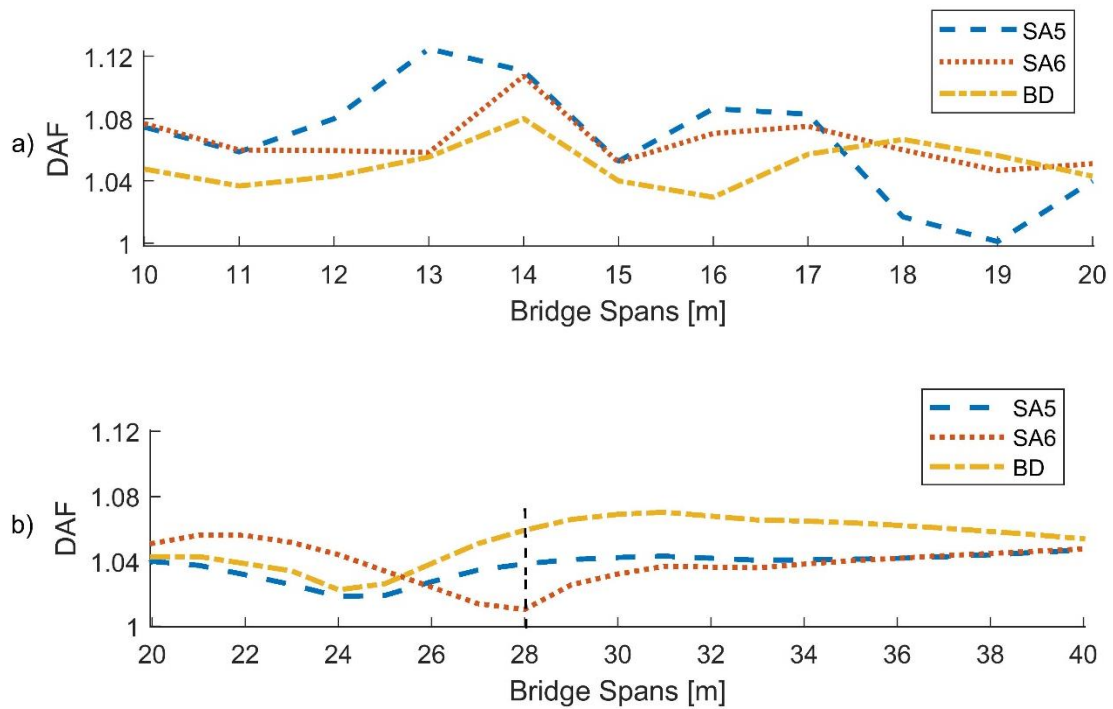
Figure 6.1: a) DAF at short spans, b) DAF at medium spans. The black dashed line indicates 28 m span.

To explore this result further, a set of 10 000 vehicles of each type, based on the WIM data, was simulated crossing the 28 m span bridge. The bridge is indicated by the black vertical line in Figure 6.1b and is chosen because of the large differences in DAF between vehicles at this span length. The input parameters such as axle loads, axle spacing and vehicle velocities are gathered directly from the cleaned and calibrated WIM data. The WIM data is used to support the results obtained and is shown in Figure 6.1 by incorporating a larger number of vehicles contributing to the average response. The results of this WIM VBI analysis are shown in Figure 6.2 by comparing the moving average dynamic amplification to the GVM of each of the three vehicle types.

The DAFs produced by the BD vehicles are shown to be consistently large across the GVM spectrum in comparison to the single articulated vehicles. This confirms the result from the parametric VBI analysis previously discussed. Additionally, it is observed that the SA5 and SA6 vehicles amplify the 28 m bridge similarly because they share a similar trailer and axle configuration. In contrast, the BD7 vehicles have different trailer and axle group configurations emphasizing the distinct trend.

Stellenbosch University https://scholar.sun.ac.za

The Characterization of the Dynamic Interaction between Highway Bridges and Long, Multi-Trailer Heavy Vehicles
_____
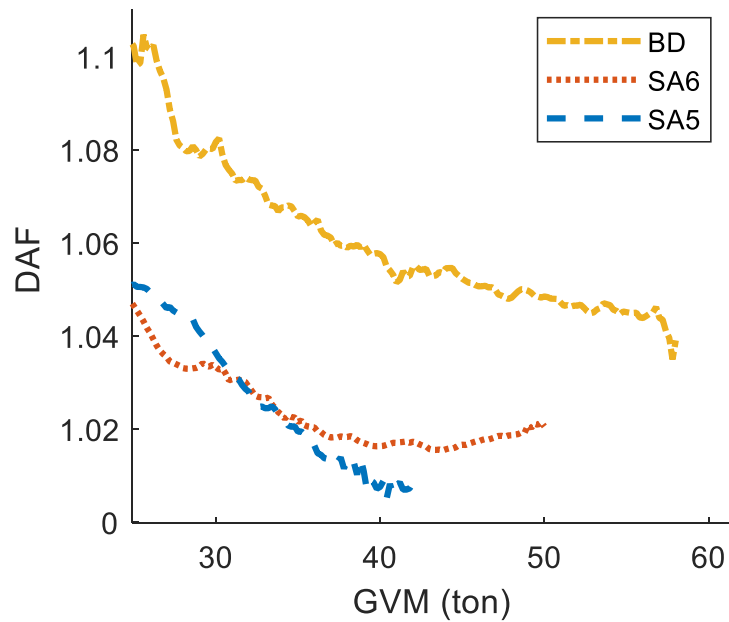
Figure 6.2: DAF for different vehicle types for a 28 m simply supported bridge at a range of GVM.

The axle group configuration, defined by the number of axle groups and axle group spacing, plays a significant role in the dynamic amplification experienced by a bridge (Guo & Liu, 2015). A number of axle groups depends on the type of vehicle considered. A group is characterized by axles which are situated in close proximity to each another, approximately within 1.6 m. The more axle groups a vehicle has, the more interaction situations between the vehicle and the bridge. Hence they influence the displacement, velocity and acceleration responses experienced by the bridge. Upon further investigation of the various responses and parameters, an important relationship between the acceleration and DAFs emerged and is discussed in Section 6.3.

6.3 DAF versus Acceleration

In order to institute the reason behind the higher amplification of BD7 vehicles, a novel relationship linking the dynamic amplification to the corresponding midspan acceleration of the bridge is introduced here. The DAF induced by a vehicle is typically calculated at the instant when the bridge experiences the highest total bending moment. However, the midspan acceleration of the bridge is not necessarily the maximum at that time. This acceleration experienced by the bridge at the instant of highest total

bending moment is termed here the "corresponding acceleration". It is shown in Section 6.4, that the entry of axle groups situated further back along the vehicle has a significant influence on this acceleration.

6.3.1 Parametric Vehicles at a Range of Velocities

By performing a VBI analysis for all three of the parametric vehicles at a range of velocities ascending from 40 km/h up to 120 km/h in 1 km/h intervals, and recording the acceleration experienced by the same 28 m bridge at the specific instant of DAF calculation, an approximately linear relationship can be observed. A linear function is fitted to this data as shown in Figure 6.3 for all three parametric vehicles. A perfect positive linear correlation between two variables has a correlation coefficient (r) equal to 1. Figure 6.3 indicates a strong linear correlation between the two variables for all three vehicles with correlation coefficients equal to 0.99 for each.
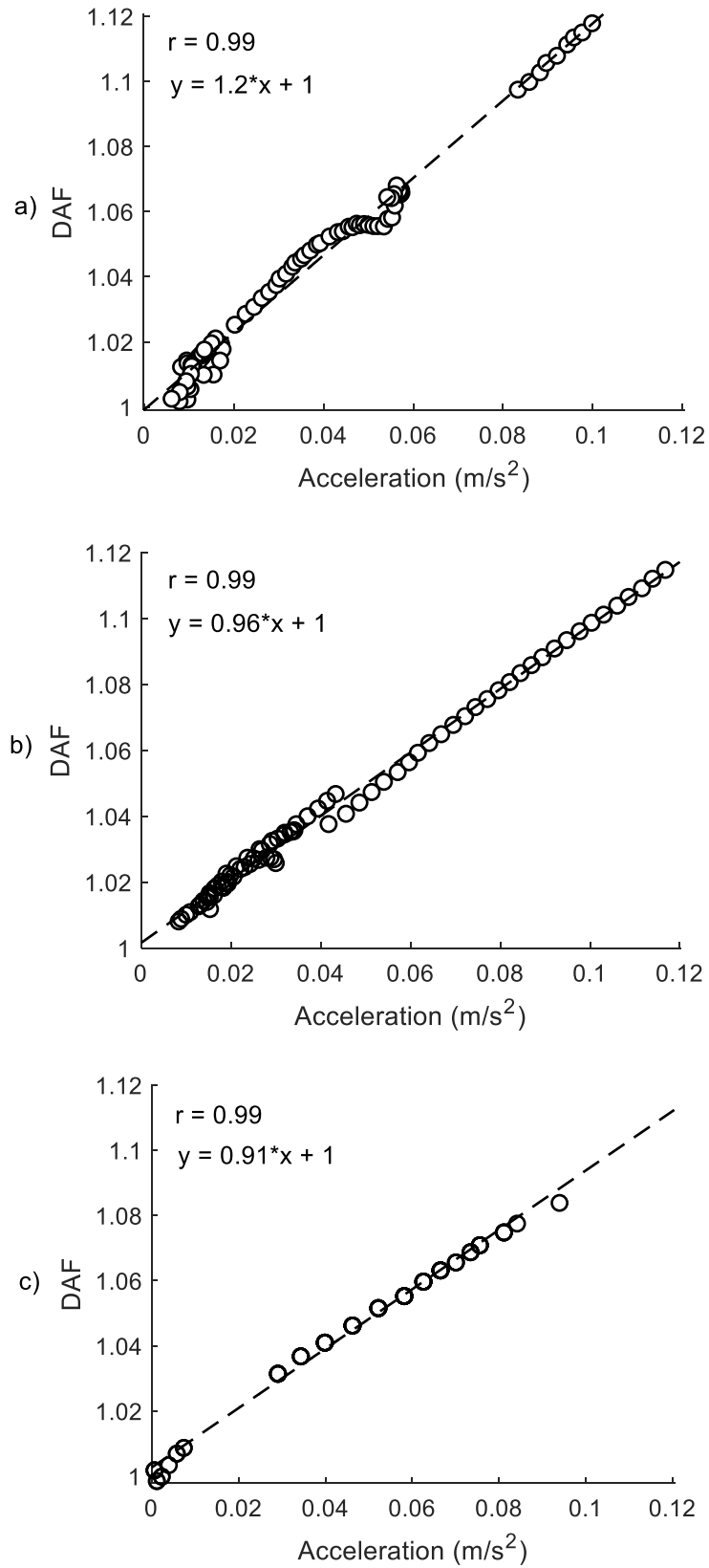
Figure 6.3: Correlation between the DAF and acceleration at a range of velocities for a) SA5, b) SA6 and c) BD7 vehicles.

It can be seen that the gradients (m) of the linear correlation functions for the three parametric vehicles are not exactly the same due to the physical differences in spacing between axle groups, number of axles per axle group and the number of axle groups. These all influence the midspan acceleration.

6.3.2 Parametric Vehicles at a Range of Bridges

It also necessary to investigate how the relationship between acceleration and dynamic amplification is affected when comparing a range of bridges with different properties, lengths and natural frequencies. Figure 6.4 indicates the results for the parametric vehicles travelling at a velocity of 80 km/h over the full range of short and medium bridges, starting at 10 m and continuing up to 40 m in 5 m span increments. The linear correlations between the DAF and the instantaneous acceleration are not as strong as in the previous case but are still significant with correlation coefficients of 0.88 for SA5 and BD7 and 0.96 for SA6. The result is understandable when recognizing that one type of heavy vehicle does not interact in the same manner with a range of bridges defined by different physical properties and natural frequencies.
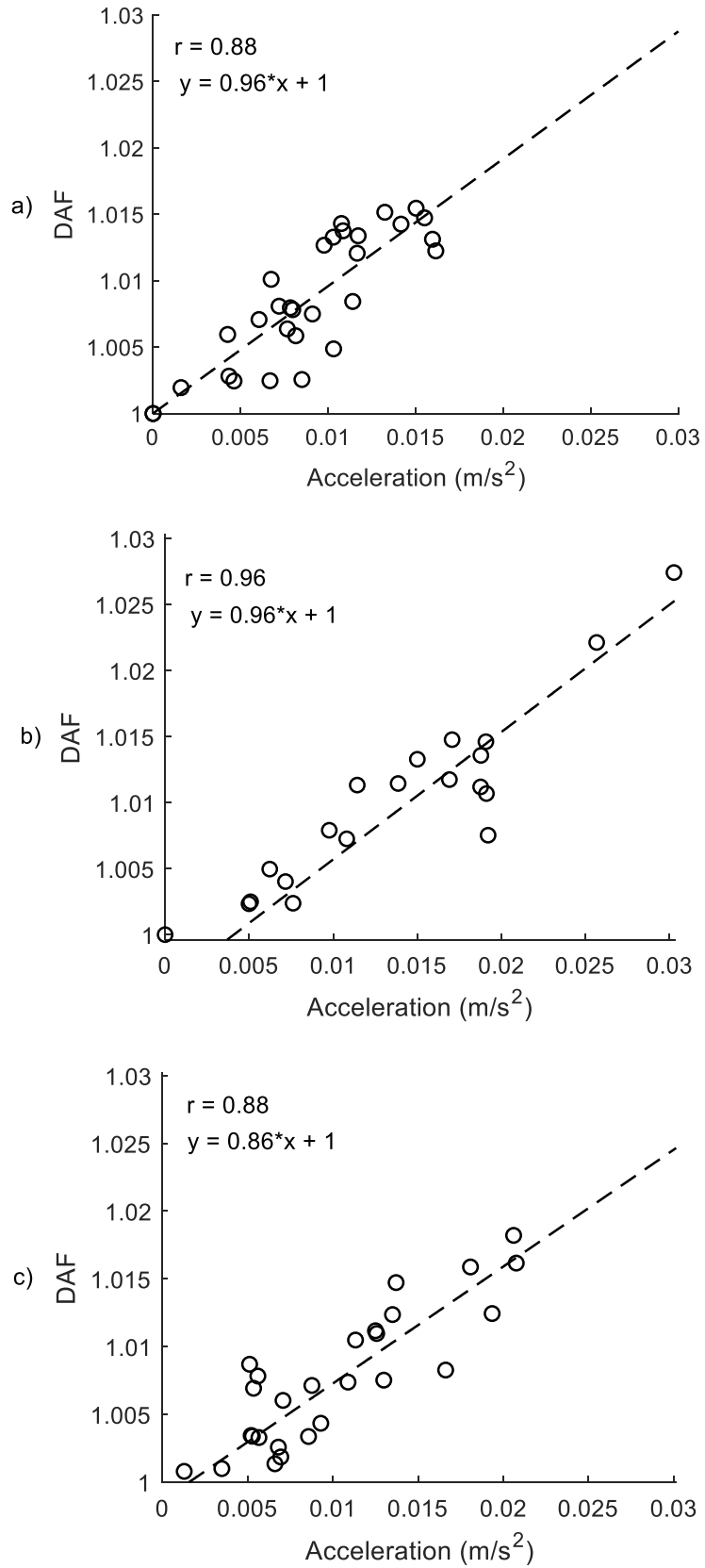
Figure 6.4: Correlation between the DAF and acceleration at short and medium bridges for a) SA5, b) SA6 and

c) BD vehicles.

The use of VBI models with parametric vehicles is necessary in identifying potential trends between variables. However, it is also essential to investigate whether the trends identified remain true when considering a full range of non-parametric vehicles and capturing the on-road variability within a fleet of vehicles.

6.3.3 WIM Vehicles

The same set of 10 000 vehicles, as used in Section 6.2 for the GVM and DAF comparison, each with distinctive properties based on WIM data, is utilized in a VBI analysis of 15 m, 25 m and 35 m span bridges. All vehicles are traversing the bridges with unique velocities as recorded by the WIM station. Table 6.1 lists the linear correlation coefficients and gradients of the linear functions which describe the correlation between the DAF and acceleration for the three span lengths considered.

Strong correlation exists between the DAF and the midspan acceleration for each of the bridges considered, although differences in the gradients of the linear correlation functions amongst the three vehicles types are observed. The main culprits are the different axle group configurations of vehicles, number of axle groups and axle group spacing. However, considering that these trends incorporate the variability of 10 000 vehicles of each type traversing three bridges, the assumption of linearity between the DAF and the acceleration might not be unreasonable.

Table 6.1: Linear correlation details between the DAF and midspan acceleration.

Vehicle Type	Bridge Spans					
	15 m		25 m		30 m	
	r	m	r	m	r	m
SA5	0.9	1	0.89	0.93	0.88	1.2
SA6	0.85	0.85	0.88	0.77	0.95	1
BD	0.9	0.98	0.94	0.78	0.94	1.1

_____

6.3.4 Vehicle Suspension and Road Roughness

To incorporate the variation in mechanical properties such as stiffness these properties are varied according to the statistical variation given in Table 4.9. This is done for the three vehicle types and studied within a Monte Carlo simulation. The Monte Carlo simulation used the same 10 000 WIM vehicles of each vehicle type to determine the mean DAFs at short and medium bridge spans.

The influence of road profiles is also included using a spectral density function as specified in Chapter 3. In this case, the road profile of the bridges is taken at a constant Class A profile for every loading event. All vehicles are simulated with an approach length to the bridge of 100 m to capture the pre-existing vehicle excitations which are present before the vehicle enters the bridge. Figure 6.5 illustrates the resulting mean DAFs of the three vehicle types at short and medium bridge spans. The results in Figure 6.5 agree with that of Figure 6.1 but, most importantly, it is shown that the BD7 vehicles (with road roughness and suspension variability included) also govern the greater range of medium span bridges.
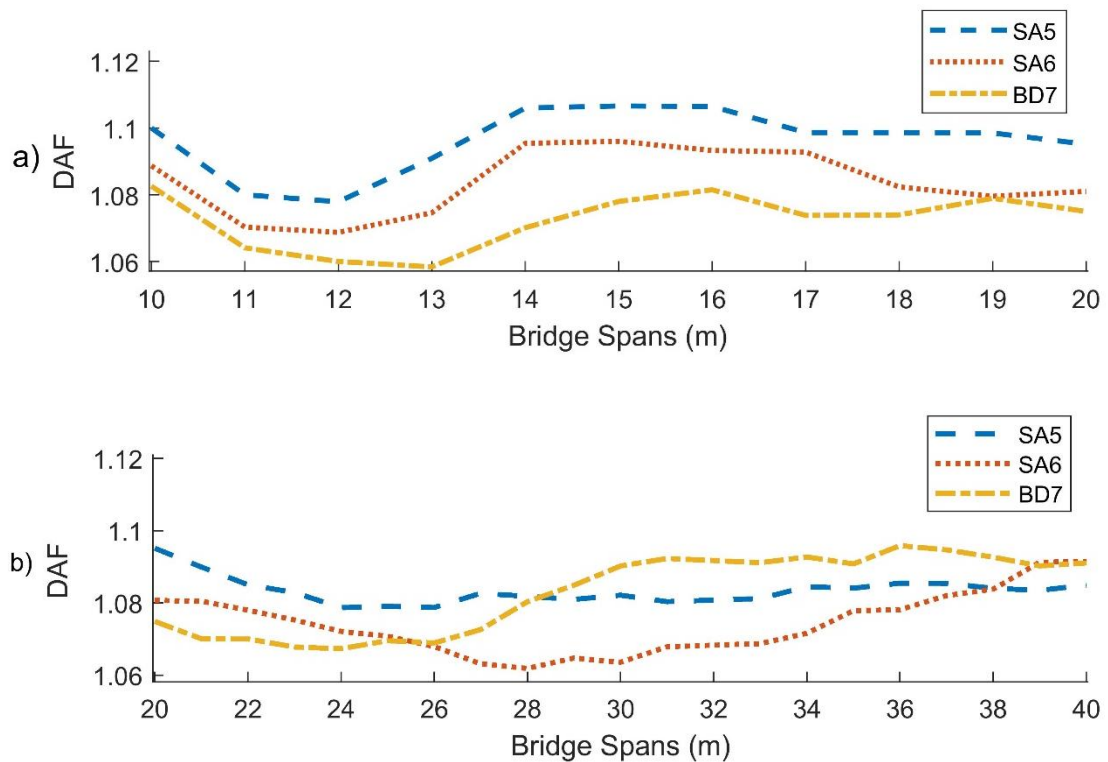
Figure 6.5: The mean DAFs at road Class A and varying suspension properties at a) short spans and b) medium spans.

Furthermore, the relationship between the DAF and the corresponding midspan acceleration for the BD7 vehicles is shown in Figure 6.6 for road Class A and for Class B at the 28 m bridge as considered previously. The linear correlation for road Class B is less than road Class A as expected due to the rougher road conditions and irregularities. Nevertheless, there exists a promising linear relationship between the two parameters when road roughness is included, which supports the previous findings.

Stellenbosch University https://scholar.sun.ac.za

The Characterization of the Dynamic Interaction between Highway Bridges and Long, Multi-Trailer Heavy Vehicles
_____
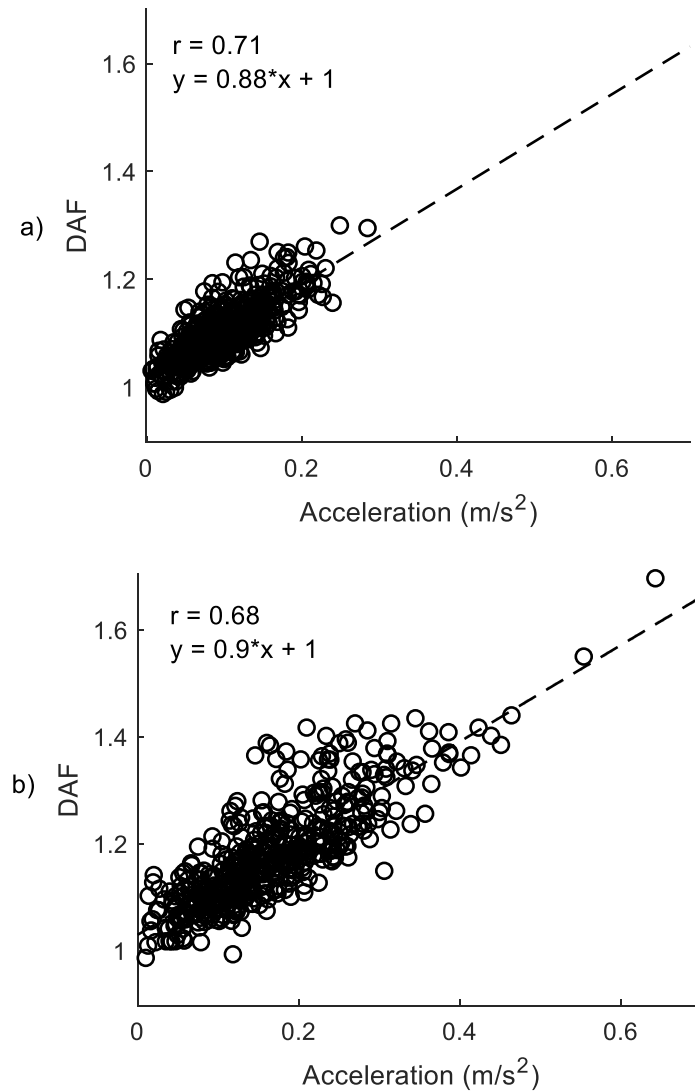
Figure 6.6: Correlation between the DAF and acceleration for road condition of a) Class A and b) Class B.

The relationship between the DAF and acceleration along with the effect of axle group configurations, is key to the exploration of the dynamic dominance of the BD7 vehicles at medium spans, which is discussed in Section 6.4.

6.4 Axle group Configurations

In order to fully understand the BD7 behaviour on medium span length bridges, the introduced linearity between DAF and corresponding acceleration needs to be further extended by exploring the influence of a particular axle group configuration on the dynamic response. Heavy vehicles have different axle configurations which inevitably influence the dynamic response of the bridge as the vehicle crosses

Stellenbosch University https://scholar.sun.ac.za

The Characterization of the Dynamic Interaction between Highway Bridges and Long, Multi-Trailer Heavy Vehicles
_____

(Guo & Liu, 2015). It is well known in bridge dynamics that shorter span bridges tend to experience higher degrees of amplification in comparison to longer ones with the exception of resonance occurring between the bridge and the vehicle (Caprani, 2017; Lu Deng *et al*., 2015). The dynamic dominance of the BD7 vehicles at medium span bridges can be attributed to a higher degree of resonance occurring in comparison to the behaviour of SA5 and SA6 vehicles. Resonance between a bridge and a moving vehicle occurs if any multiple of the loading frequencies (frequencies due to axles and axle spacing) or driving frequency (frequencies due to the velocity of the vehicle) match the natural frequency of the bridge. The challenge lies in pinpointing the matching frequencies within an intricate harmonic system of multiple degrees of freedom. In this sense, it is the inter-axle spacing coupled with the velocity that determines the loading frequency of each axle. The loading frequency, f_{li}, is directly proportional to the vehicle velocity and inversely proportional to the distance between axles, which is defined by:

$$f_{li} = \frac{v}{d_i} \tag{6.1}$$

where, v is the velocity of the vehicle and d_i is the distance between axles. There is a range of influencing parameters such as the mechanical properties of suspension and axle loads which can influence the loading frequency to some extent, while the the travelling velocity and distance between axles will dominate the loading frequency. Considering the three different vehicle types, each vehicle has a different number of axle groups, resulting in unique loading frequencies. It is quite complex to explore the effect of the loading frequencies of different vehicles with varying axle spacing. This is compounded when considering the presence of harmonics, which means that any multiple of these frequencies can also influence the final dynamics. All these frequencies contribute to the final dynamics but the loading frequencies due to axle groups are in closer proximity to the resonance frequency. In other words, the axle groups tend to be more influential than the individual axles within of the group. Considering the axle group as one entity, the loading frequencies of that axle group are then inversely proportional to the spacing between axle groups, which is measured between the centres of any two axle groups, defined by d_i.

The spacing between axle groups along with the vehicle velocity determines the time of axle group entry on to the bridge deck. This event largely influences the extent of the midspan acceleration of the bridge. As the first axle group (axle 1) of the vehicle enters the bridge deck, the midpoint of the bridge starts to experience a sinusoidal acceleration response with approximately the same frequency as that of the first natural frequency of the bridge as shown in Figure 6.7. As soon as the following axle groups enter the bridge, the initial response is disturbed. Figure 6.7 also illustrates the midspan acceleration as the parametric SA6 vehicle traverses a simply supported bridge at 80 km/h.

Due to the spacing between the first axle group and the second axle group (axles 2 and 3) there is a reduction in the amplitude of the acceleration. The opposite occurs when the third axle group enters the bridge. This is because the midspan is experiencing a negative acceleration at the time at which the second axle group enters the bridge and therefore increases the acceleration response. The acceleration amplitude in this case just before the entry of the third axle group is just less than 0.02 m/s^2. However, after this axle group has entered the bridge, the negative acceleration amplitude is increased to roughly 0.03 m/s^2.
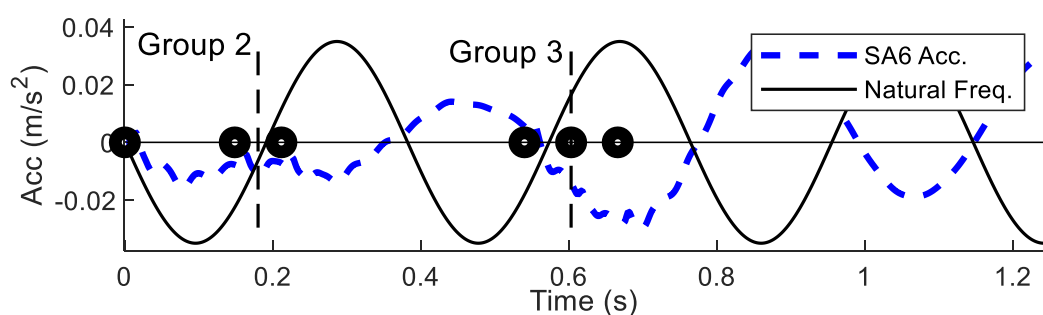

Figure 6.7: Midspan acceleration response of a simply supported bridge. Dashed vertical lines indicate the entry time of the second and third axle groups.

It can be concluded that the time at which an axle group enters the bridge, has either an amplifying or reducing effect on the acceleration response at midspan through the superposition of loading effects. If

_____

the axle group enters at an instant where the midpoint of the bridge is experiencing a negative acceleration gradient, the succeeding amplitude will be increased. The opposite applies if the axle group enters at a positive acceleration gradient. Recalling the correlation between the DAF and the corresponding acceleration presented in Section 6.3, the following also holds – if an axle group enters a bridge deck while the bridge is experiencing a positive midspan acceleration, the acceleration is decreased and finally results in a smaller DAF.

6.4.1 Axle Group Spacing of Single Articulated Vehicles

To encompass the axle group configuration influencing the dynamic response, the spacing value between two axle groups of one single articulated vehicle is varied. Referring to Figure 6.1b, at 28 m span length, the SA6 vehicle produces a significantly lower DAF in comparison to the SA5 and the BD7 vehicles. The DAF induced by the SA6 on the 28 m span can be manipulated by only changing the spacing between axle groups. The geometry of the given vehicle can be adjusted in a manner to favour the acceleration amplitude increases and therefore also the linearly related DAF. Three cases are considered, each with a different axle group spacing:

Case A:

The inter-axle spacing follows the geometry defined in Figure 5.7, the spacing between axle groups, d_1 and d_2 is equal to 4 m and 9.4 m. The spacing configuration causes the second axle group to enter the bridge while the acceleration response is at a positive crest at roughly 0.2 s as shown in Figure 6.8a. The third axle group enters at a positive acceleration gradient. Both axle groups cause a reduction in midspan acceleration and therefore a reduction in the dynamic response of the bridge at the instant of the maximum static moment, indicated by the red vertical line. This corresponds with the small DAF of 1.01 seen in Figure 6.1b.

Case B:

In Case B, d_2 is decreased to 7.1 m while d_1 is kept the same as in Case A. This particular reduction of d_2 allows the third axle group to enter at the instant when the acceleration gradient is negative, which increases the amplitude from 0.033 m/s² before the entry of the axle group to 0.056 m/s² after entry of the axle group, shown in Figure 6.8b. Consequently, the final midspan acceleration increases from 0.01 m/s² in Case A to 0.048 m/s² in Case B and results in a higher DAF of 1.046.

Case C:

In Case C, d_2 remains at 7.1 m as in Case B, while d_1 is increased from 4 m to 5.7 m to allow the second axle group to enter the bridge deck later at 0.26 s. Both axle groups now contribute to an amplifying effect on the acceleration amplitude, by entering at a negative acceleration gradient, as shown in Figure 6.8c. The midspan acceleration increases to 0.058 m/s² at the instant when the governing static moment occurs, resulting in the highest DAF of 1.057 of the three cases.
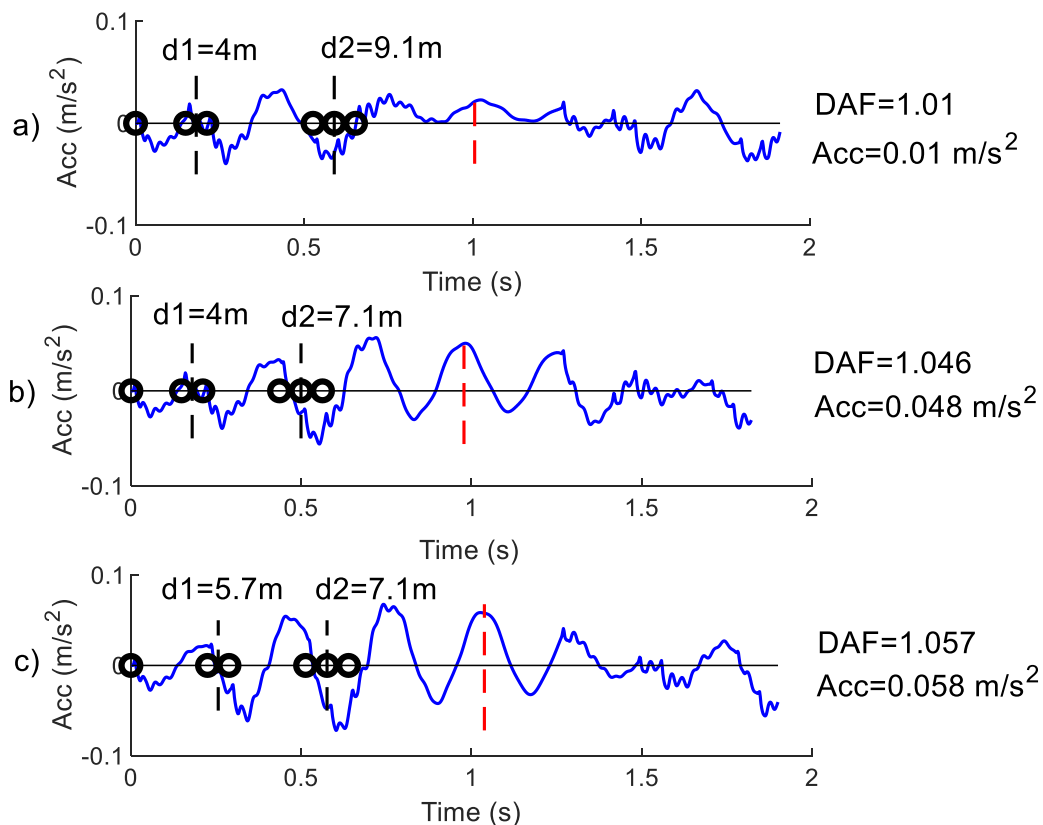

Figure 6.8: Midspan acceleration response for a) Case A, b) Case B and c) Case C. The black dashed lines indicate the entry of the axle groups and the red dashed line indicates the instant of DAF calculation.

In this case study all input parameters are kept constant except the spacing between axle groups, which illustrates how sensitive the dynamic amplification of a bridge can be to the spacing between axle groups.

6.4.2 Axle Group Configurations of B-Doubles

A typical BD vehicle differs from a single articulated vehicle by the number of axle groups, trailer configuration and dimensions. The most notable difference is the additional axle group – or one more set of loaded axles that interact with the bridge. To illustrate why BD7 vehicles produce a higher amplification in comparison to single articulated vehicles at certain spans, shown in Figure 6.1, a detailed investigation of dynamic responses of the BD7 and the SA6 parametric vehicles is necessary. The dynamic response of both vehicles crossing a 28 m span is shown in Figure 6.9a and 6.9b. Both figures consist of three sub-figures, the first showing the static and total bending moment as the vehicles traverse the bridge. The second, showing only the dynamic moment and the third showing the midspan acceleration response including the positions of the axles and axle groups of each vehicle at the time of entry. All figures indicate in red the instant at which the maximum total moment occurs, and DAFs are calculated.

The spacing between the first and second axle groups is the same for both vehicles. The second axle group of both vehicles enters while the midspan acceleration response is experiencing a positive acceleration, therefore reducing the acceleration. The third and fourth axle groups of the BD vehicle both cause an increase in the acceleration amplitude, while the third axle group of the SA6 causes an amplitude reduction. Thus, the BD vehicle induces a higher acceleration, dynamic moment and DAF compared to the SA6 vehicle. It is concluded that the extra axle group, along with its spacing, causes the BD vehicle to induce higher amplification for most medium bridge spans.

Stellenbosch University https://scholar.sun.ac.za

The Characterization of the Dynamic Interaction between Highway Bridges and Long, Multi-Trailer Heavy Vehicles
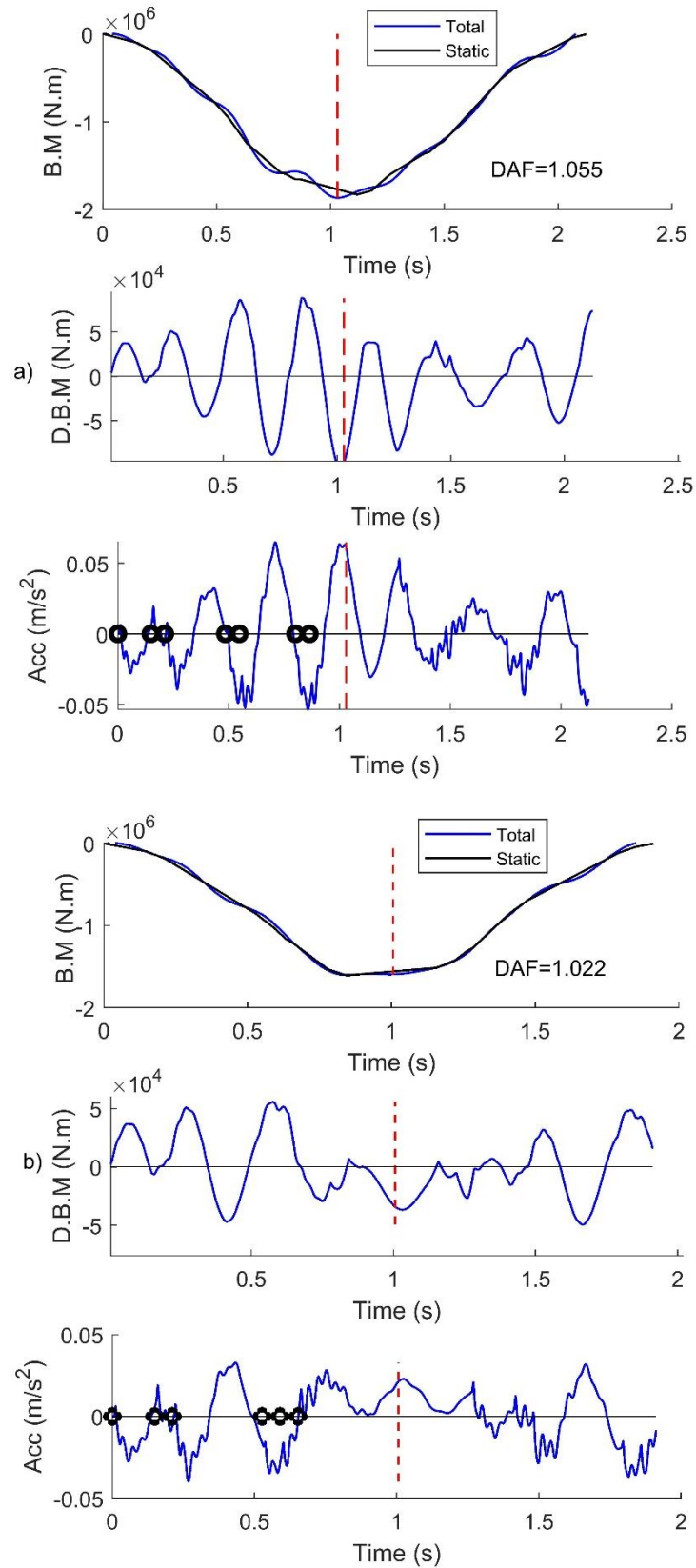_____

Figure 6.9: Dynamic bridge response of a 28 m bridge due to a) BD7 and b) SA6 vehicles. The red dashed lines indicate the time of DAF calculation.

To illustrate this concept further, the dynamic response of the BD7 parametric vehicle crossing the 25 m, 30 m and 40 m spans is considered. Referring to Figure 6.1b, it can be seen that at 25 m the BD7 vehicle produces a lower DAF than the SA6 vehicle. But as the span length increases, the BD7 starts to govern. At the 30 m, the DAF induced by the BD7 vehicle reaches close to the maximum with a slight decrease in DAFs onward to the 40 m span.

A comparison of the midspan acceleration responses is shown in Figure 6.10 for the three bridges considered. Due to the natural period of the 25 m bridge, the fourth axle group of the BD7 enters at a positive acceleration gradient which significantly decreases the amplitude as shown in Figure 6.10a. As the span length increases, the natural period increases. Such results in the time of entry of the axle group tend to be more aligned with the negative acceleration gradients as in the case up to 30 m as seen in Figure 6.10b. As a result, amplitudes increase, and higher degrees of amplification are observed.

Beyond 30 m, the entry of axle groups moves closer to the positive acceleration gradients and causes a slight decrease in the acceleration. As the span length increases, the entry of axle groups becomes more favourable for a decrease in the acceleration. Finally, at 40 m the third and fourth axle groups enter close to the acceleration crest, shown in Figure 6.10c, ultimately causing an amplitude reduction and a lower DAF compared to the DAF at 30 m. The DAFs and the acceleration values of each case are given next to each of the acceleration responses of the three bridges in Figure 6.10 for comparison.

Stellenbosch University https://scholar.sun.ac.za

The Characterization of the Dynamic Interaction between Highway Bridges and Long, Multi-Trailer Heavy Vehicles
_____
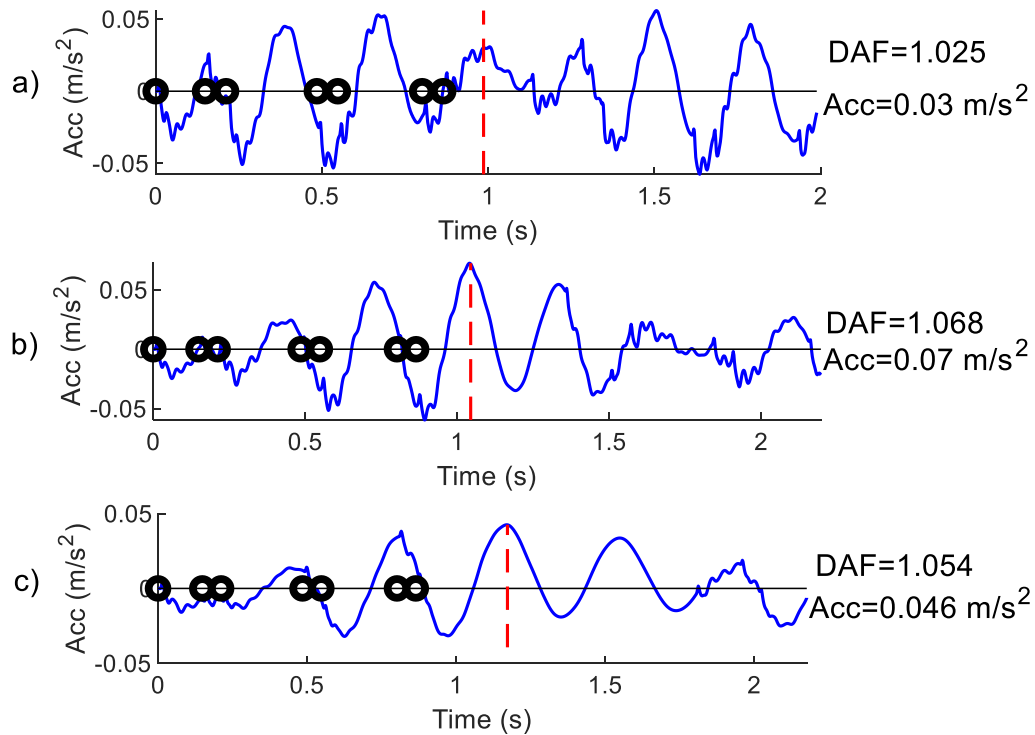
Figure 6.10: Midspan acceleration response of BD7 parametric vehicle at a) 25m at b) 30m and c) 40m.

It is evident that axle groups and the respective spacing thereof cannot be ignored when considering the dynamic effect of long, multi-trailer vehicles. It may be a dominant variable when considering dynamic amplification.

6.5 Conclusion

This Chapter explores the dynamic amplification characteristics induced on bridges by the BD7 configuration compared to the smaller SA5 and SA6 heavy vehicles. The findings suggest that the heavier BD7 vehicles produce higher levels of dynamic amplification at medium spans compared to the typically lighter single articulated vehicles due their inherent axle configurations. This is an indication that the often-presented relationship between the dynamic amplification and the GVM needs to be revised to also characterize the dynamic effects of these new longer truck configurations. The study suggests that the time of entry of an axle group and both the magnitude and the direction of the midspan acceleration at that instant are beneficial for the estimation of the dynamic amplification.

6-73

Furthermore, the relationship established here between the dynamic amplification and the corresponding acceleration has been shown to have significant relevance towards the estimation of the dynamic amplification of bridges.

CHAPTER 7: DYNAMIC AMPLIFICATION FACTOR OF B-DOUBLE VEHICLES

7.1 Introduction

The vehicle-bridge interaction solution is not only useful in identifying and studying vehicle-specific dynamic amplification characteristics as shown in Chapter 6, but can also do so with great efficiency and versatility. A significant advantage of the vehicle-bridge interaction solution is the ability to investigate a large number of interactions scenarios within a relatively short period of time and at an insignificant cost compared to field studies. The VBI solution developed for the present research allows for the study of the full BD7 vehicle population of 319 076 vehicles, as recorded at the Roosboom WIM station, traversing the stock of bridges while incorporating the statistical variability of the suspension stiffness using a Monte Carlo simulation. Highway road surfaces are generally well maintained by authorities to fall within Class A road surface category. Therefore, the bridge surface quality is set to fall within Class A conditions and is randomly generated for each simulated BD7 vehicle to account for the inherent variability present in real life surface conditions. A 100 m approach length to the bridge is set to account for the pre-existing vehicle vibrations which are present as the bridge is entered.

The dynamic amplification factors induced by the full population of BD7 vehicles on the stock of short and medium span bridges are presented in this Chapter with specific focus on the influence of velocity and GVM. The objective is to gain insight with regards to the expected amplification that can be induced by the BD7 vehicles traversing a range of short to medium span simply supported bridges.

7.2 Mean Dynamic Amplification Factors of Bridge Stock

The mean DAFs induced by the BD7 vehicle population on the short and medium span stock of bridges are given in Figure 7.1. The top three largest means are indicated on the figure at 35 m, 10 m and 40 m spans. The mean DAFs reduce from 10 m to 22 m after which the means predominantly increase

_____

towards the longer, medium span. The BD7 vehicles amplify the medium span bridges, especially from 30 m to 40 m, to a greater extent than the shorter bridges. This finding somewhat contradicts the generally accepted theory that longer span bridges experience lower amplifications compared to shorter span bridges. However, referring back to Chapter 6, it is shown that this is due to the effect of the inherent axle configuration combined with the typical velocity of the BD7 vehicles. The vehicle velocity determines the time of entry onto the bridge for each of the axle groups which have an amplifying or reducing effect on the midspan acceleration experienced by the bridge.

The DAF peaks shown in Figure 7.1 are the result of the amplification of the midspan acceleration discussed in Chapter 6. The larger the DAF peaks, the closer is the time of axle group entry aligned to a negative midspan acceleration, which amplifies the acceleration response to a greater extent. These time dependent axle group entry events can also be interpreted as the loading frequencies induced by the BD7 vehicles on the bridge. The traversing velocity at which the amplification peaks occur for a specific bridge and vehicle type can also be defined as the critical load velocity of the bridge. Section 7.3 elaborates on the latter.
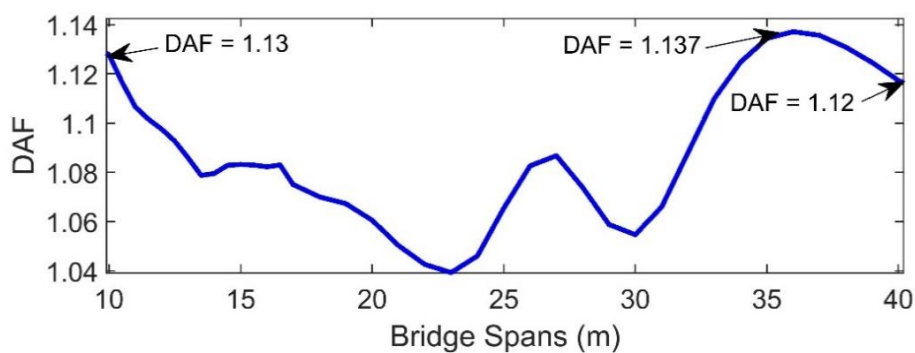

Figure 7.1: Mean DAF for short to medium span simply supported bridges.

Stellenbosch University https://scholar.sun.ac.za

The Characterization of the Dynamic Interaction between Highway Bridges and Long, Multi-Trailer Heavy Vehicles
_____

7.3 Influence of Gross Vehicle Mass and Vehicle Velocity

Figure 7.2 presents the moving means of the DAF vs. the GVM, summarized in 5 m bridge span increments from 10 m to 40 m span length. The moving means are calculated by taking the average of the DAFs within each 5 ton increment of the GVM from 25 to 80 ton. The three largest moving means are that of the 35 m, 10 m and 40 m bridges as expected, of which the scatter plots and moving means are shown in Figure 7.2. Refer to Appendix C.1 for the DAF vs. GVM responses of all the bridges presented in Figure 7.2.

A general decrease in DAFs with the increase of GVM can be observed for the population of BD7 vehicles. However, for the majority of the medium span bridges, the BD7 vehicles with GVMs over 70 ton induced a higher degree of dynamic amplification than the average lighter vehicles. It is shown in Figures 7.3b and 7.3c for both the 35 m and 40 m bridges. This is due to the critical loading velocities of these bridges. A critical load velocity can also be defined as the velocity at which a traversing vehicle generates matching load frequencies to that of the natural frequency of the bridge, causing local dynamic amplification peaks in the bridge response. Critical load velocities are dependent on the physical configurations of the traversing vehicles. Single articulated vehicles have fewer axles and axle groups than the B-double vehicles, inducing different loading frequencies, thus different critical loading velocities.

The vehicles which caused the increase in the average DAF from 70 ton, highlighted by the black box in Figure 7.2, were all travelling at a velocity between 85 and 100 km/h which falls within the critical load velocity range of these bridges. Figure 7.4 presents the mean DAFs vs. vehicle velocities for the governing 10 m, 35 m and 40 m bridges where the critical velocities of each are indicated by the peaks in the moving means of the DAFs. The 35 m and 40 m bridges both have critical loading velocities at approximately 90 km/h where high degrees of dynamic amplification are experienced. Contrastingly, at 90 km/h the 10 m bridge experiences a minimum in DAFs while its critical loading velocity is

Stellenbosch University https://scholar.sun.ac.za

The Characterization of the Dynamic Interaction between Highway Bridges and Long, Multi-Trailer Heavy Vehicles
_____

approximately at 75 km/h, hence the decrease in average DAF vs. GVM shown in Figure 7.2. The individual DAF vs. velocity responses of the bridges presented are given in Appendix C.2.
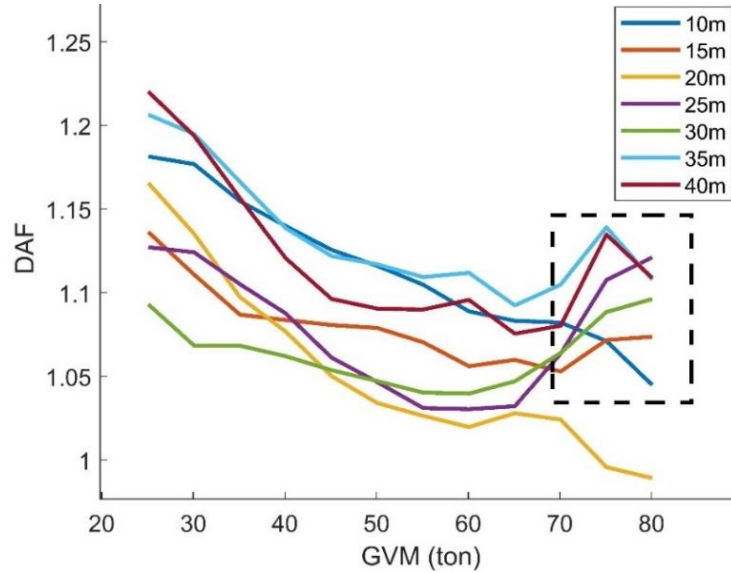

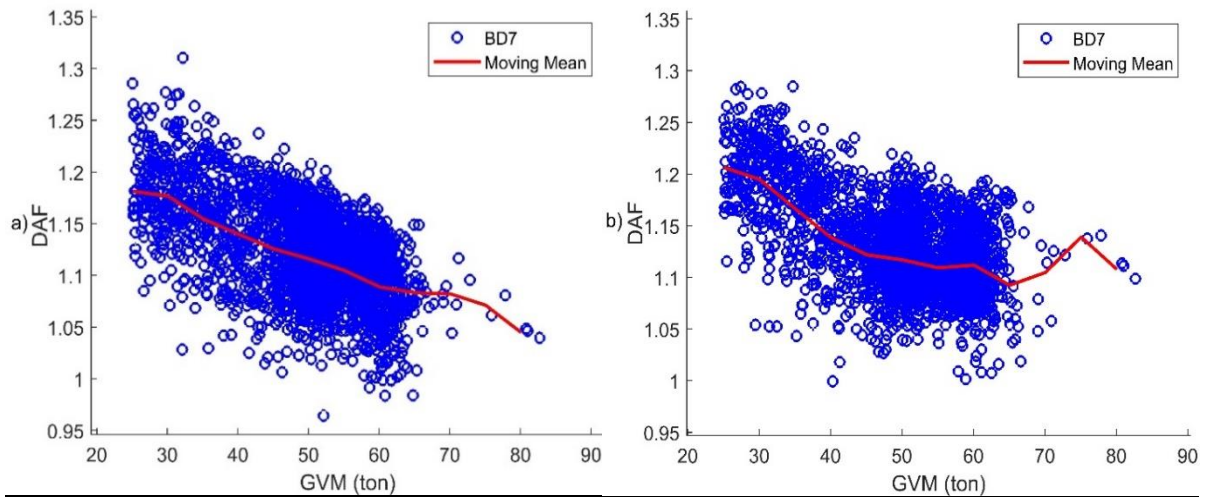Figure 7.2: Mean DAFs vs GVMs for short to medium span bridges.

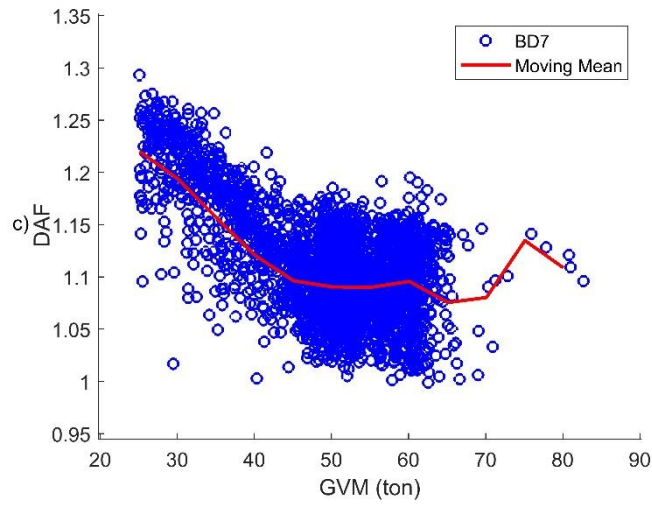Figure 7.3: DAF vs GVM for: a) 10m, b) 35m.

Figure 7.3: DAF vs GVM for: c) 40m.
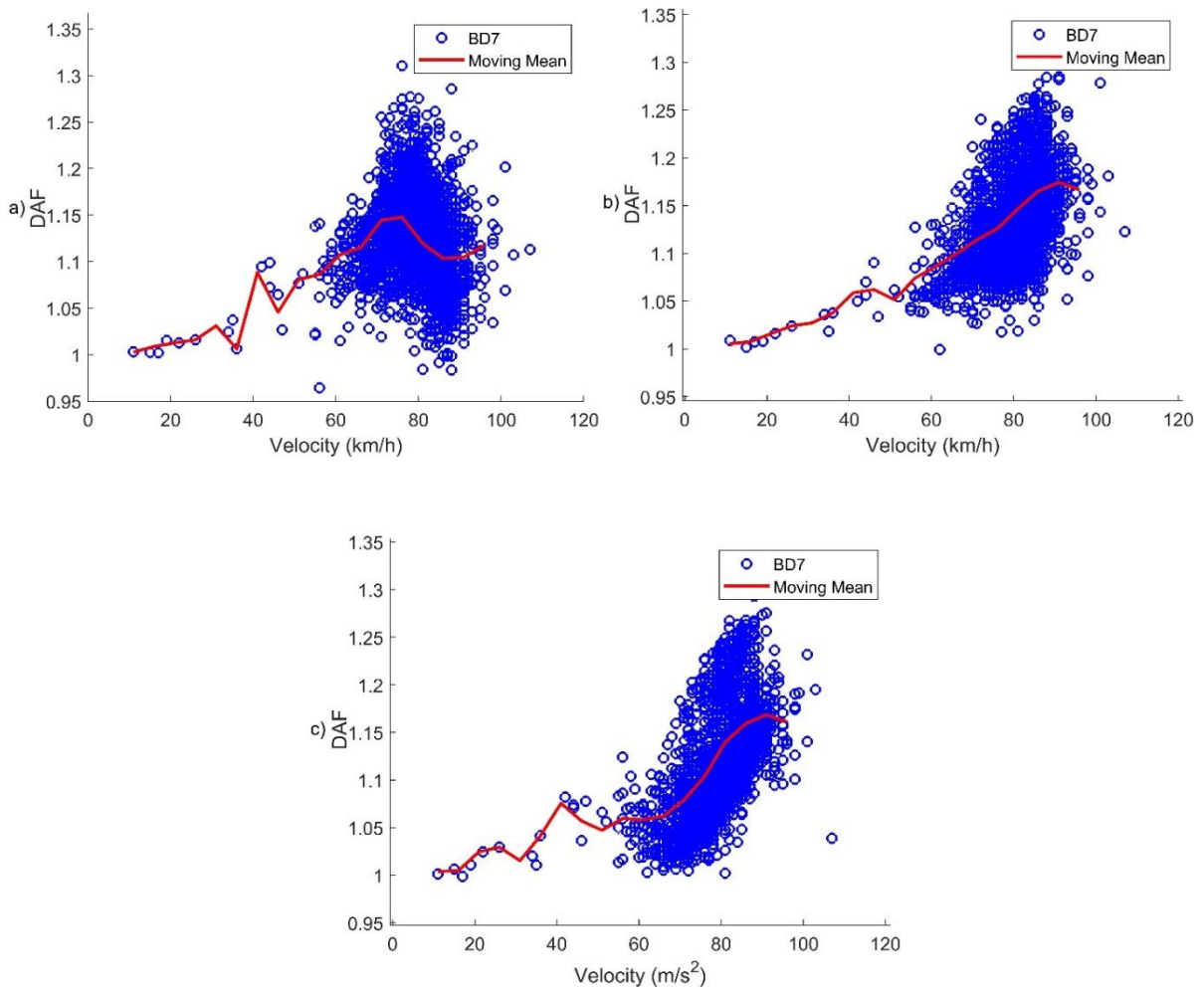
Figure 7.4: DAF vs Velocity for: a) 10m, b) 35m, c) 40m.

The influence of velocity on the DAF induced by BD7 vehicles for the full bridge stock is presented by the contour plots given in Figure 7.5. The dark yellow clusters visualize the most critical loading velocities at which the highest DAFs are observed within the stock of bridges. The average vehicle velocity of the BD7 population is 80.25 km/h, thus producing the high DAFs observed for the bridges with critical loading velocities in close proximity to this average velocity. The range of bridges in each of these governing clusters is in a good agreement with the mean DAF peaks shown in Figure 7.1. According to the results presented in Figure 7.5 it can be concluded that the DAF dominance by BD7 vehicles at medium span bridges is due to critical loading velocities, unique to their configuration, which produce matching loading frequencies to that of the natural frequencies of these bridges.

Figure 7.5: DAF vs. vehicle velocity and bridge span in; a) plane view.
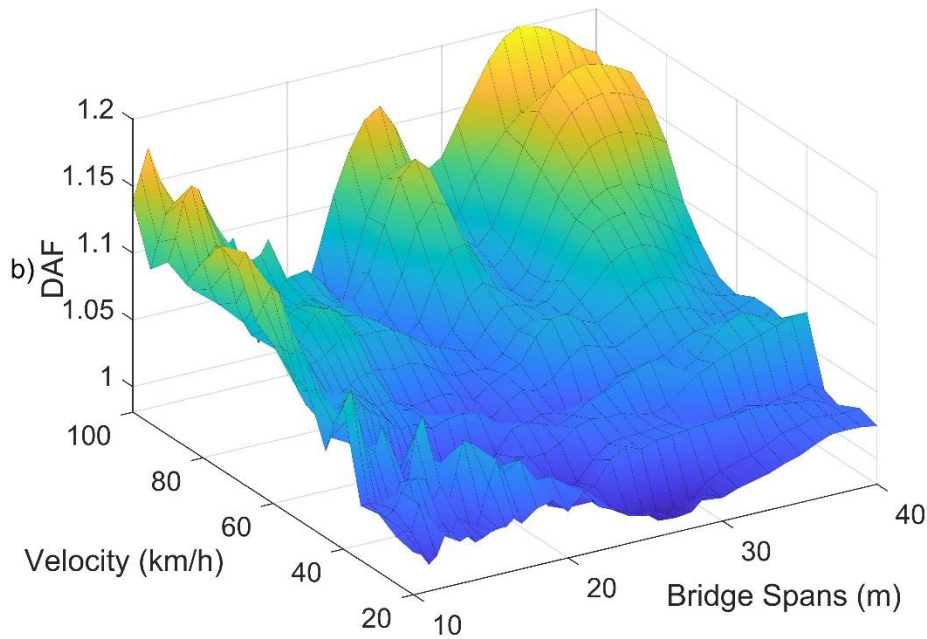
Figure 7.5: DAF vs. vehicle velocity and bridge span in; b) three-dimensional view.

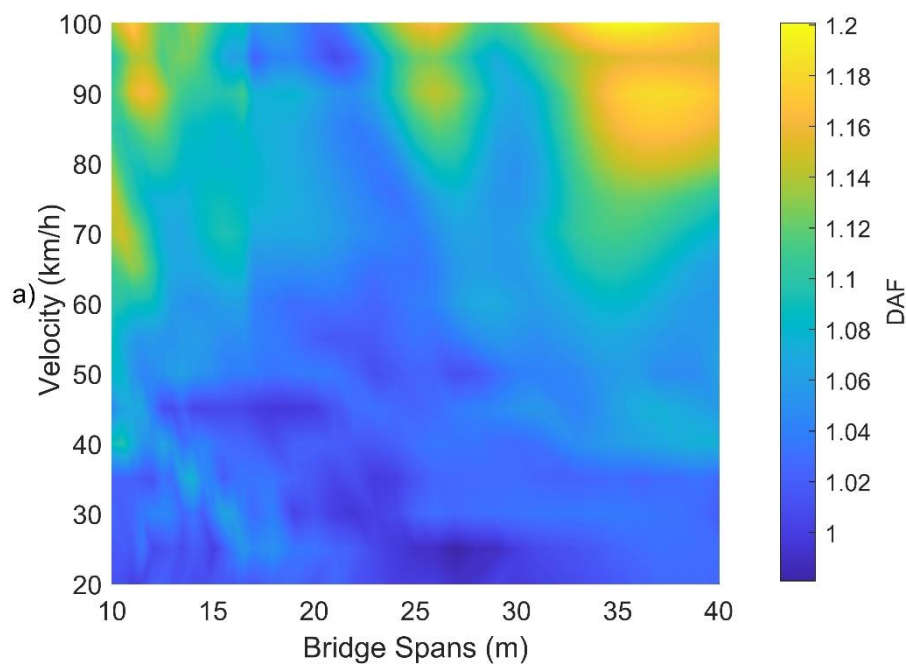Ultimately it is insightful to consider the dynamic amplification factors of the short and medium span bridges combined to establish a sense of the degree of amplification induced by the BD7 multi axle and trailer heavy vehicles. Figure 7.6 presents the combined DAF vs. GVM responses for the short and medium span bridges, all with road Class A surface conditions. As expected, the lighter vehicles produce the largest DAFs after which a steady decrease in dynamic amplification is observed as the vehicles increase in weight. The solid line graph indicates the mean DAF at the shown GVM range for all the bridges combined. As discussed above, the slight increase in the average dynamic amplification observed from 70 ton is due to the majority of the medium span bridges experiencing critical load velocities at the typical traversing velocities of these vehicles.

The 95 percentile confidence intervals for the mean DAFs are presented in Figure 7.7. It shown that the largest mean DAF is at 25 ton with a value of 1.156 after which a decrease in amplification is observed down to a mean DAF of 1.057 at 65 ton respectively. Moving from 65 ton, the means increase to a peak of 1.087 at 75 ton with 95 percentile values equal to 1.074 and 1.1. The 95 percentile confidence interval

values of the DAFs for the heavier vehicles from 50 ton onwards, which govern the overall bridge
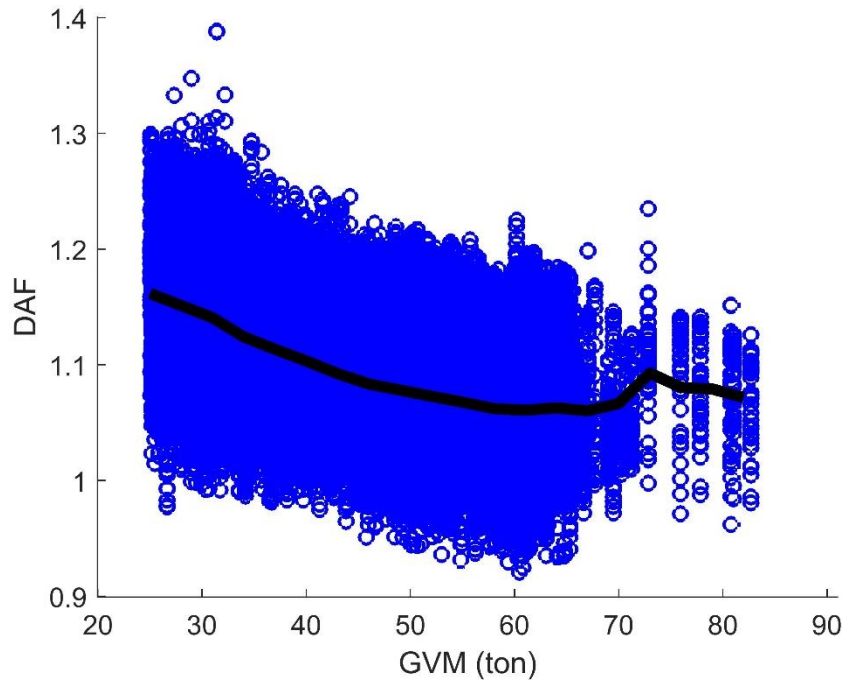
loading events, are presented in Table 7.1.

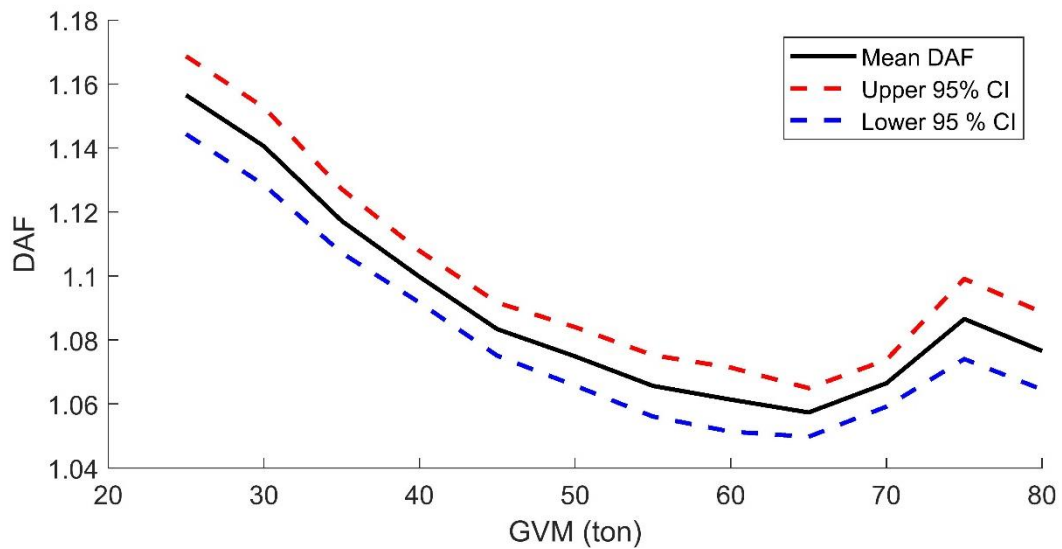Figure 7.6: DAF vs. GVM for short and medium span bridges with road Class A surface conditions.

Figure 7.7: 95 Percentile confidence interval of the DAF vs. GVM.

The Characterization of the Dynamic Interaction between Highway Bridges and Long, Multi-Trailer Heavy Vehicles
_____

Table 7.1: DAFs at 95 percentile confidence intervals.

GVM (ton)	Mean DAF	Lower C.I. DAF	Upper C.I. DAF
50	1.075	1.066	1.084
55	1.066	1.056	1.075
60	1.061	1.051	1.071
65	1.057	1.05	1.065
70	1.067	1.059	1.074
75	1.087	1.074	1.099
80	1.077	1.065	1.089

7.4 Damping Sensitivity

The bulk of this research assumes a constant bridge damping factor of 3 % due to the focus being on the characterization of vehicle specific interaction dynamics and not bridge dynamic design purposes. However, due to the variability of infield bridge damping factors it is of interest to consider the different degrees of dynamic amplification induced by the population of BD7 vehicles at lower levels of bridge damping. Figure 7.8 presents the the mean DAFs for each considered span length at 1 % and 2 % compared to mean DAFs at 3 % bridge damping also presented in Figure 7.1.

It is shown that the degree of dynamic amplification increases as the levels of bridge damping are reduced, as anticipated. The differences in dynamic amplification between the three levels of bridge damping are not uniform due to the variability within a vehicle-bridge interaction system as a consequence of the randomization of the surface roughness for each loading event. Considering the significant reduction in bridge damping from 3 % to 1 %, the maximum factor of increase in dynamic amplification between the two is only 1.0114 occurring at the governing 35 m span bridge. The mean factor of increase in DAFs between the 3 % damping bridge range and the 1 % and 2 % damping bridge

ranges is 1.009 and 1.004. It is evident that the dynamic amplification experienced by the range of bridges are more sensitive to lower levels of bridge damping which agrees with the generally accepted theory of dynamic amplification and bridge damping. The degree of bridge damping is one of the important dynamic bridge properties which has to be taken into account when considering vehicle-bridge interaction. However, considering the work discussed in Section 7.3 it apparent that the dynamic amplification is more sensitive to the variables unique to the vehicle such as the travelling velocity, axle loads and configuration.
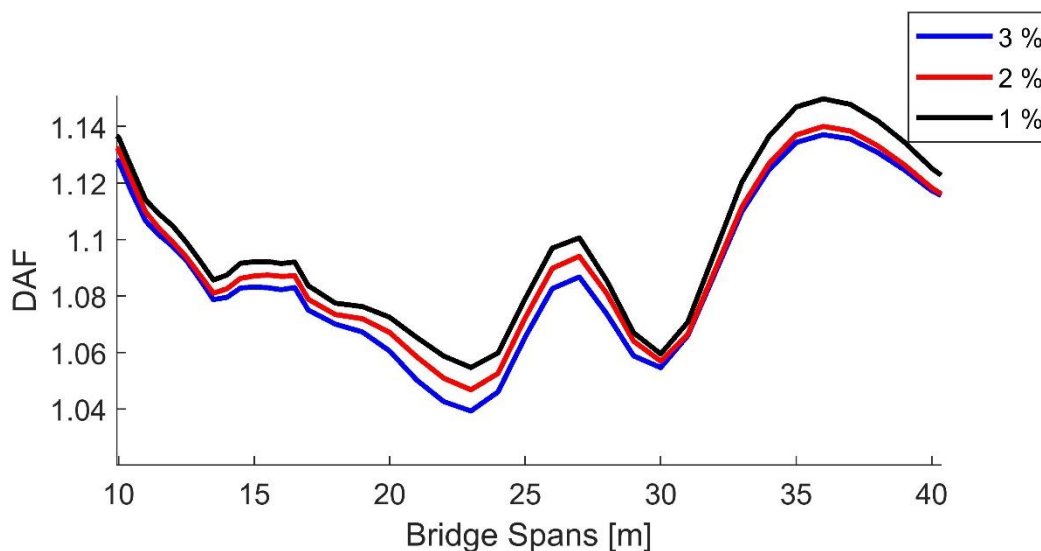
Figure 7.8: Dynamic amplification sensitivity to bridge damping.

7.5 Conclusion

This chapter presents the results of the VBI solution of the full BD7 vehicle population interacting with the stock of short and medium span bridges with a Class A road surface. The dynamic amplification dominance at medium span bridges is again illustrated by the DAF peaks which occur at the ranges of 25 m to 30 m and 35 m to 40 m spans and are presented in Figure 7.1. Furthermore the critical loading velocities of the bridge stock, induced by the BD7 population, are presented and shown to be accountable for the peaks observed in the DAF vs. bridge span response. The average DAF at 95

confidence levels is presented for all bridges combined, short and medium. Finally, the sensitivity of the dynamic amplification to three levels of bridge damping is explored.

CHAPTER 8:   DYNAMIC LOAD SIGNATURE

8.1 Introduction

The dynamic amplification induced by rigid and single articulated vehicles, especially the 5-axle (SA5) vehicles, has been addressed and investigated thoroughly over the past decade; however, this is not the case for the larger BD7 vehicles. This is addressed by the development of a exemplary Dynamic Load Signature (DLS) which defines the dynamic loads induced by these vehicles on the range of short to medium span bridges. A novel method of estimating the DAFs induced by the BD7 vehicles, without knowing the static loads, on simply supported highway bridges is introduced by the utilization of the DLS. The method utilizes a relationship between the dynamic loads, bridge accelerations and the first natural frequency of the bridge to determine the dynamic load component induced per loading event. Strain measurements can then be implemented to determine the maximum total load component, where after the static loads can be back-calculated to finally determine the DAF.

Section 8.2 demonstrates that the DAF vs. acceleration relationship discussed in Chapter 6 has one limitation which can be addressed by removing the static component to rather consider the dynamic loads vs. acceleration. Section 8.3 presents the newly developed linear correlation between dynamic loads vs. bridges for short to medium span bridges and how they differ. Sections 8.4 presents the development of the surface function which describes the dynamic DLS of the BD7 vehicles. Sections 8.5 and 8.6 demonstrate and verify the method developed to estimate the DAFs by using the DLS along with strain and acceleration measurements.

8.2 Dynamic Loads versus Dynamic Amplification

Chapter 6 has shown that the well documented inversely proportional relationship between the DAF and the GVM holds when comparing one type of heavy vehicle configuration, but may be contradicted if different heavy vehicle configurations are compared (e.g. Single Articulated vs B-Double) in one test. However, this chapter only considers the BD7 configuration and therefore the latter relationship holds,

_____

which is shown by the scatter plot of the DAF vs GVM in Figure 8.1. Vehicles that are not fully loaded produce higher DAFs than the more heavily loaded vehicles. Two distinctive groups of results are observed and highlighted in red and blue; vehicles which weigh less than 45 ton and vehicles heavier than 45 ton. For the purpose of this example the two groups will be referred to as "light" and "heavy" vehicles. The notable differences in DAFs between the light and heavy vehicles are indicative of their unique degree of interaction.
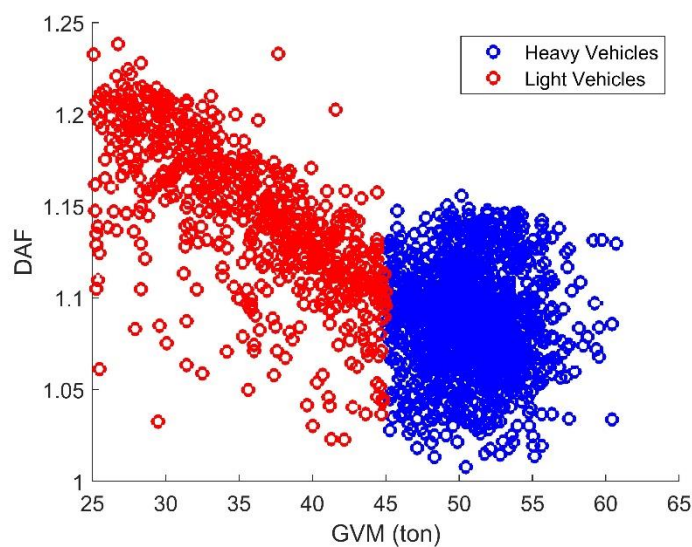
Figure 8.1: DAF vs GVM of BD7 vehicles.

These interaction differences are highlighted in the linear relationship between the DAFs and the bridge accelerations. Considering the scatter plot of the DAFs vs. accelerations, shown in Figure 8.2, the light and heavy vehicles can be easily distinguished from one another. In this case the presence of the lighter vehicles does not allow the data to be described by one linear function, which is the desirable solution. The relationship between the induced DAFs and bridge accelerations is shown to depend on the extent to which these vehicles are loaded. Both groups of vehicles activate a similar range of bridge accelerations. However, the lighter vehicles induce higher DAFs at the same accelerations as the heavier vehicles.
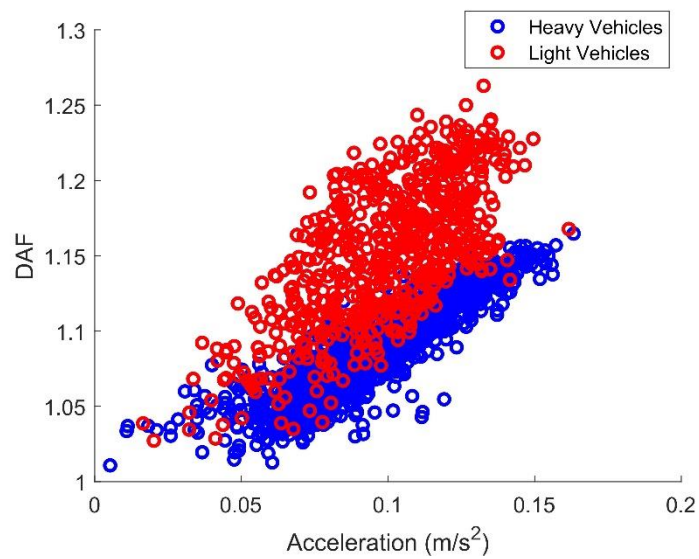
Figure 8.2: DAF vs acceleration of BD7 vehicles.

A stronger linear relationship exists between the bridge accelerations and the induced dynamic loads when compared to the relationship between bridge accelerations and DAFs. The DAFs are calculated using the static load contributions, by removing the influence of the static loads and only considering the dynamic loads, a single trend is observed. Figure 8.3 presents the dynamic loads vs. accelerations for the case under consideration. The light and heavy vehicles are shown to follow a similar trend which allows a single linear function to describe the full range of unloaded to loaded vehicles. The relationship between the dynamic loads and the bridge accelerations is thus independent of vehicle weight, which enables it to be a superior measure of dynamic bridge responses to be used for prediction purposes.

_____
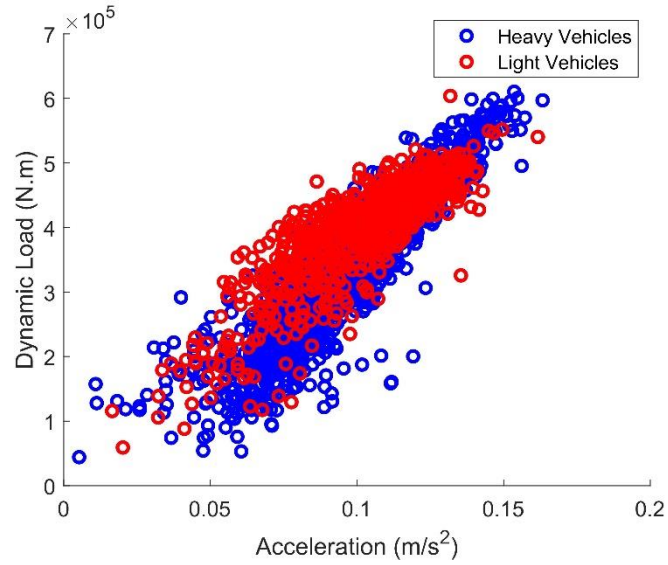
Figure 8.3: Dynamic load vs. acceleration for BD7 vehicles.

A correlation coefficient of 0.89 of the linear trend line indicates a strong relationship between the midspan accelerations and the dynamic loads as is shown Figure 8.4 for the particular case traversed by the population of BD7 vehicles.

Figure 8.4: Linear fit of dynamic loads and acceleration.

The linear relationship can be defined by a function which estimates the dynamic loads caused by BD7 vehicles at a certain midspan acceleration for a specific bridge. The dynamic load function can therefore be defined by:
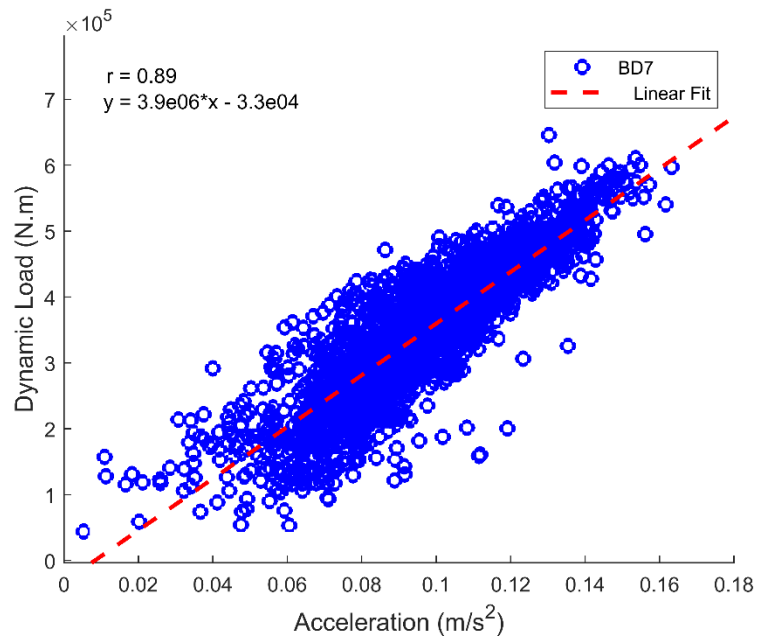
$$DL(\ddot{v}) = A \cdot \ddot{v} + B \tag{8.1}$$

where $\ddot{v}$ is the midspan acceleration and A and B are constants dependent on the fit. The dynamic load function is also described as the dynamic load signatures of BD7 vehicles for the bridges considered. The dynamic load function can now be explored for the entire stock of bridges which includes short and medium span bridges.

8.3 Dynamic Loads at Short and Medium Bridges

This section explores the proposed linearity between the dynamic load response and acceleration for the entire stock of bridges ranging from short to medium spans for Class A road surface conditions. Bridges with similar structural properties will experience similar dynamic load functions and vice versa. For example, there is a significant difference in the dynamic load functions of the 10 m and the 40 m span bridges. Longer span bridges will experience larger midspan static loads/moments compared to short span bridges. Inherently, the longer span bridges will also experience larger dynamic loads than the shorter span bridges at the same bridge accelerations. This is shown in Figure 8.5.

Figure 8.5 summarized the dynamic loads vs. bridge accelerations for the range of short to medium span bridges from the 10 m to the 40 m span in 5 m span increments. The acceleration range of each bridge is divided into increments of 0.0025 m/s^2 of which the average dynamic load is calculated for each increment which is defined as the moving mean. The moving mean of each of the bridge responses is shown in red to illustrate the inherent linearity between the dynamic loads and accelerations throughout the range of bridges. The significant changes at the start and end of the acceleration spectra may be ignored due to the low frequency of loading events occurring at these accelerations.

Short bridges, (10 - 20 m) tend to produce a weaker linear relationship between the dynamic loads and accelerations. This can be caused by the effective loading length of the BD7 vehicles. The average loading length for BD7 vehicles from the first axle to the last axle is approximately 19 m. Therefore, for all bridges with span lengths shorter than 19 m, the maximum total load of the bridge is experienced at some instance where only a section of the vehicle is active on the bridge. Essentially this effect simulates a smaller and lighter vehicle crossing the bridge which, along with the influence of vehicle velocity, results in a weaker linear trend between the dynamic loads and accelerations. This can be observed in Figure 8.5a and 8.5b.

These situations become more pertinent with decreasing span length. For the 10 m bridge, the maximum total load occurs when only one of the axle groups (two axles) is active on the bridge. These dynamic interaction events are more susceptible to localized influencing parameters unique to the specific axle group, such as the suspension properties, spacing and the difference in loads of the axles in the group, resulting in a greater variety of dynamic responses. Table 8.1 presents the linear correlation coefficients between the dynamic loads and the bridge accelerations. It is shown that for the 20 m to 40 m bridge spans the correlation coefficients significantly increase, indicating a stronger linear relationship for the medium span bridges.

Dynamic load functions/signatures induced by BD7 vehicles can be derived for all bridges being considered – from short to medium span bridges. However, it is not desirable to have a single dynamic load signature for a single bridge span, this will evidently result in a cumbersome approach of defining the dynamic signature of the BD7 vehicle. It is possible to develop a single dynamic load signature function capable of describing the dynamic signatures for short and medium span bridges. Chapter 8.4 explores the development of a single bivariate function which describes the dynamic load signatures for short and medium span bridges for the BD7 vehicles.

Table 8.1: Correlation coefficients between dynamic loads and bridge accelerations.

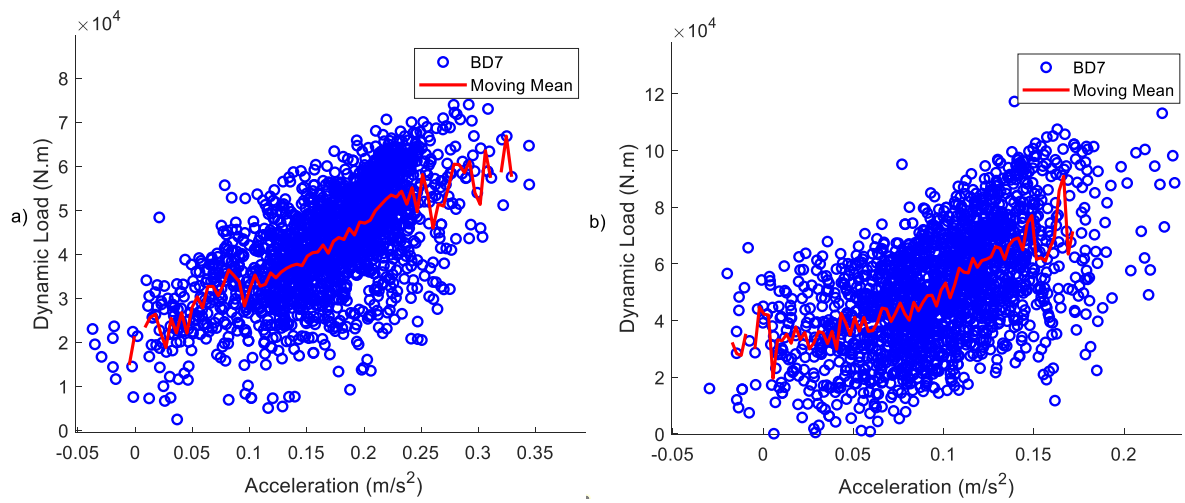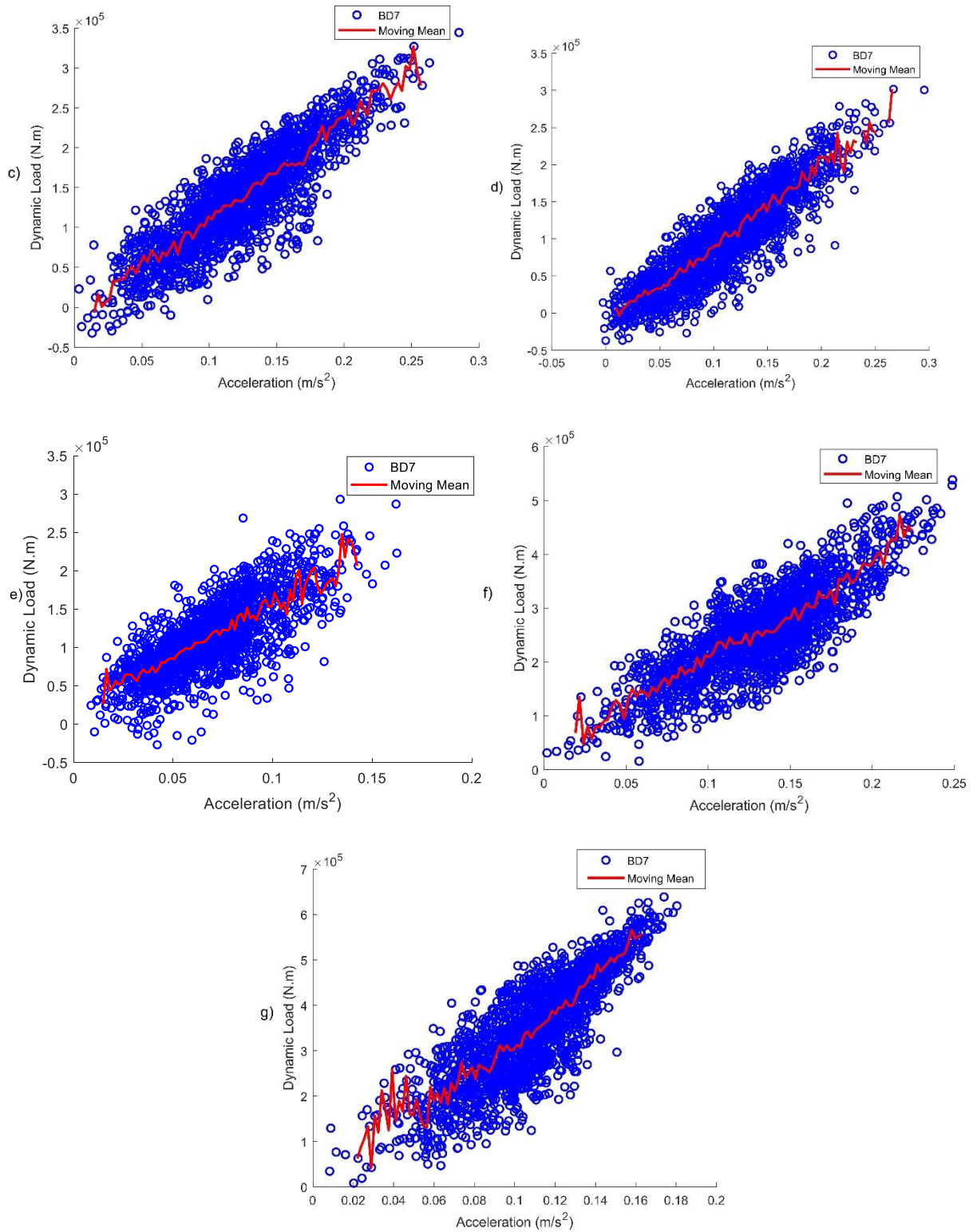| Bridge Span (m)	Correlation Coefficient, r
10	0.69
15	0.66
20	0.87
25	0.88
30	0.77
35	0.82
40	0.84

Figure 8.5: Dynamic loads vs acceleration for bridge spans of: a) 10 m, b) 15 m.

Figure 8.5: Dynamic loads vs acceleration for bridge spans of: c) 20 m, d) 25 m, e) 30 m, f) 35 m, g) 40 m.

Stellenbosch University https://scholar.sun.ac.za

The Characterization of the Dynamic Interaction between Highway Bridges and Long, Multi-Trailer Heavy Vehicles
_____

8.4 Dynamic Load Signature Function

The Dynamic Load Signature (DLS) is defined as a function describing the expected mean dynamic loads for simply supported bridges with Class A surface roughness carrying BD7 vehicles. The DLS defines a load signature unique to the BD7 heavy vehicle population induced on typical short to medium span bridges.

Chapter 8.2 introduced the linear correlation between the dynamic loads and bridge acceleration which can be interpreted as the DLS of a single bridge; hence a single linear function which defines the mean dynamic loads of the bridge. However, by introducing a third variable which describes each of the bridges which are defined in the bridge stock, it is possible to define the DLS with a single, bivariate surface function. The first natural bridge frequency is a fundamental bridge property which is descriptive of the dynamic nature of a bridge itself. The main advantage of using the natural frequency to distinguish between the bridges is that it allows the DLS to be applied on any simply supported bridge which has a natural frequency which falls within the frequency range from which the DLS is derived. The frequency range is based on frequencies of the stock of bridges considered for this investigation which range from 8.61 – 2.61 Hz (10 – 40 m spans).

The moving means of dynamic loads and bridge accelerations of the entire stock of bridges, including those shown in Figure 8.5 above, are presented in Figure 8.6 below. Each colour response represents the moving mean dynamic loads of a specific bridge identified by its natural frequency, starting at the 10 m span bridge and ending at the 40 m bridge with 1 m span increments in between. Figure 8.6 presents the dynamic loads vs. acceleration for all the short and medium span bridges defined in Chapter 5. The gradual increase in sensitivity of the dynamic loads to the accelerations as the natural bridge frequencies decrease is due to the higher degree of overall loads experienced at midspan by longer span bridges.

The linear correlations between the dynamic loads and bridge accelerations can be distinctly observed. As the natural frequencies decrease, the gradient of the linear correlations increases gradually which introduces the possibility of defining the range of dynamic loads by one surface function. The DLS can then consequently be described in the form of:

$$DLS = F(\ddot{v}, f_n) \hspace{3cm} (8.2)$$

where $\ddot{v}$ is the midspan acceleration due to vehicle passage and f_n is the first natural frequency of the bridge.
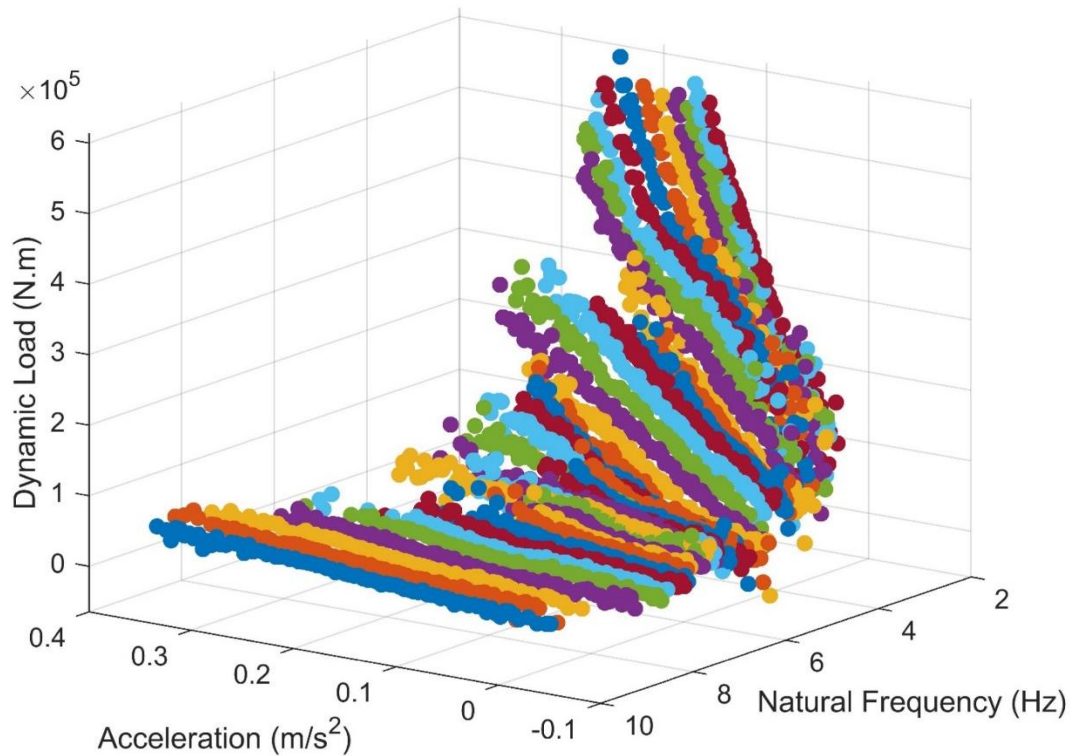
Figure 8.6: Dynamic loads vs. bridge acceleration vs. natural frequency.

8.5 Cross-Validation of Dynamic Load Signature

The three-dimensional dynamic loads shown in Figure 8.6 indicates that the mean dynamic loads become more sensitive to bridge accelerations as the span lengths increase from 10 m to 40 m, i.e. as the natural frequency decreases. In the acceleration plane the dynamic loads increase linearly with the bridge accelerations and in the frequency plane at the higher accelerations the dynamic loads increase

Stellenbosch University https://scholar.sun.ac.za

The Characterization of the Dynamic Interaction between Highway Bridges and Long, Multi-Trailer Heavy Vehicles
_____

to an exponential degree as the natural frequencies decrease. However, at the lower accelerations closer to zero, the dynamic load increase is to a lower degree as the natural frequencies decrease. To account for these differences at the higher and lower accelerations three bivariate functions were considered ranging from first to third exponential degree of the natural frequency variable. The three functions are given in Table 8.2.

Due to the large quantity of available data points, cross-validation is implemented to establish which bivariate function fits the data best. Cross-validation is defined as a statistical method used in machine learning to compare and evaluate algorithms or functions. The main data set is subdivided into smaller sets to train and test the algorithm or function. The aim of cross validation is that the train and test data sets must cross over in consecutive iterations so that each data point has been validated against. The k-fold cross-validation procedure is implemented to determine which of the three bivariate functions defines the dynamic response data the most accurately. In k-fold cross-validation the data set is divided into k segments, also referred to as folds, of equal size. Thereafter k iterations of training and testing are performed, where one fold of the data subsets is left out for testing and the remaining k-1 folds are used to train the algorithm or function (Liu, 2009).

The procedure of k-fold cross-validation is shown in Figure 8.7 and can be outlined as follows:

1. Divide the data set in k equal subsets.

2. Fit the function considered to k-1 subsets.

3. Calculate the test error of prediction by testing the function on the kth subset (test set).

4. Iterate k times, while using each of the subsets as the test set.

5. Calculate the final prediction error of the function by taking the average of the k errors recorded.

Stellenbosch University https://scholar.sun.ac.za

The Characterization of the Dynamic Interaction between Highway Bridges and Long, Multi-Trailer Heavy Vehicles
_____
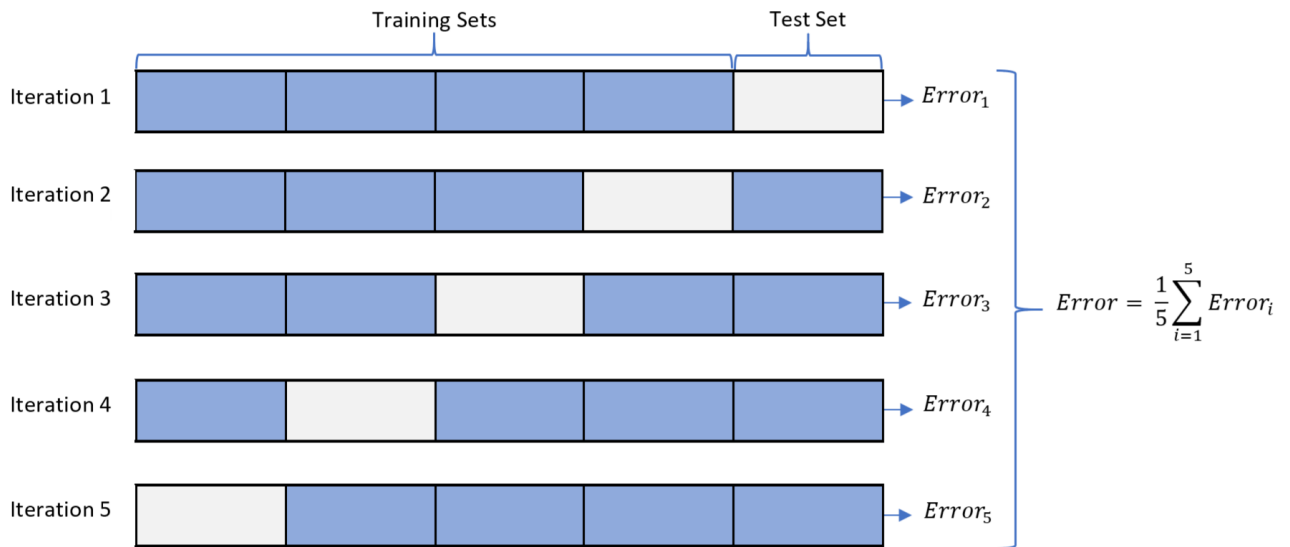
Figure 8.7: K-fold cross-validation procedure (Patro, 2021).

The *k*-fold cross-validation method is not tied to a specific number of folds, instead the number of folds should be chosen in such a manner that the size of the train and test sets is large enough to be statistically representative of the entire data set (Kohavi, 2000). The general rule of thumb is to use five or ten folds, in this case to only determine which of the three bivariate functions fits the data the best, five folds were used and proved to be adequate.

Implementing a 5-fold cross-validation means that the total data set is divided into five equal subsets of which four sets are used to fit the function (train) and the set left-out is used to test the accuracy of the function. Table 8.2 indicates the functions considered, the root mean square error (RMSE) after each fold iteration and the final average RMSE. The second function is shown to produce significantly smaller estimation errors and therefore indicates that it is best suited to be used to define the DLS surface.

Table 8.2: Cross-Validation Results.

$\mathbf{F}(\ddot{v}, f_n)$		RMSE (10^4)					
		$K=1$	$K=2$	$K=3$	$K=4$	$K=5$	Ave. RMSE
1	$a \cdot \dfrac{\ddot{v} - b}{f_n}$	7.41	7.31	7.36	7.24	7.27	7.32
2	$a \cdot \dfrac{\ddot{v} - b}{f_n^{\,2}}$	**4.08**	**4.04**	**4.07**	**3.96**	**4.06**	**4.03**
3	$a \cdot \dfrac{\ddot{v} - b}{f_n^{\,3}}$	7.49	7.47	7.49	7.39	7.57	7.47

In addition, to further substantiate the selection of the surface function, the Akaike Information Criteria (AIC) is implemented. The AIC is defined by:

$$AIC = N \cdot \ln\left(\frac{sse}{N}\right) + 2k \qquad (8.3)$$

where k is the number of function parameters, sse is sum of squared errors and N is the number of observations. The function with the lowest AIC value will fit the data the best (Akaike, 1974). The AIC values for the three functions are given in Table 8.3. The Akaike criteria also indicates that the second surface function fits the data best by having the lowest AIC value.

Table 8.3: Akaike Information Criteria.

	$\mathbf{F}(\ddot{v}, f_n)$	AIC (10^4)
1	$a \cdot \dfrac{\ddot{v} - b}{f_n}$	390
2	$a \cdot \dfrac{\ddot{v} - b}{f_n}$	**369**
3	$a \cdot \dfrac{\ddot{v} - b}{f_n^{\,3}}$	391

_____

Fitting the function to the dynamic load data of the BD7 vehicles introduced in this research, the constants, a and b, are found to be equal to 1.81×10^7 (95% Conf. Intervals: $[1.79 \times 10^7\ \ 1.83 \times 10^7]$) and 0.0171 (95% Conf. Intervals: $[0.0157\ \ 0.0185]$). By substituting in these constants, the final DLS for BD7 vehicles for simply supported bridges is defined by:

$$DLS(\ddot{v}, f_n) = 1.81 \cdot 10^7 \cdot \frac{\ddot{v} + 0.0171}{f_n^{\,2}}$$

$$(8.4)$$

The DLS, fitted to the data set is presented in Figure 8.8 from two points of view. The DLS correlates well with the data set with a correlation coefficient of 0.97. The DLS developed here can be used in bridge assessment studies to determine the expected midspan dynamic loads and DAFs induced by BD7 vehicles. The DLS can be applied to simply supported bridges of beam and slab configuration if the natural frequency falls within the specified frequency range of the DLS while the surface quality conforms to Class A. Due to the unique loading nature of the BD7 vehicle, the DLS developed here only applies to BD7 vehicles. The DLS shown in Figure 8.8 should be implemented with caution when considering low bridge frequencies and high levels of acceleration due to substantial extrapolation in these areas. Although it is unlikely that measurements will fall within these sensitive areas, it is recommended that the DLS should not be used for accelerations higher than 0.2 m/s^2 for bridges with natural frequencies less than 8 Hz.

Smaller single articulated vehicles will not share the same DLS function due to the significant differences in axle configurations. The DLS function presented here can easily be implemented by countries which use, or plan to use, similar BD7 vehicles in their fleet of heavy vehicles to transport freight along routes with highway bridges.
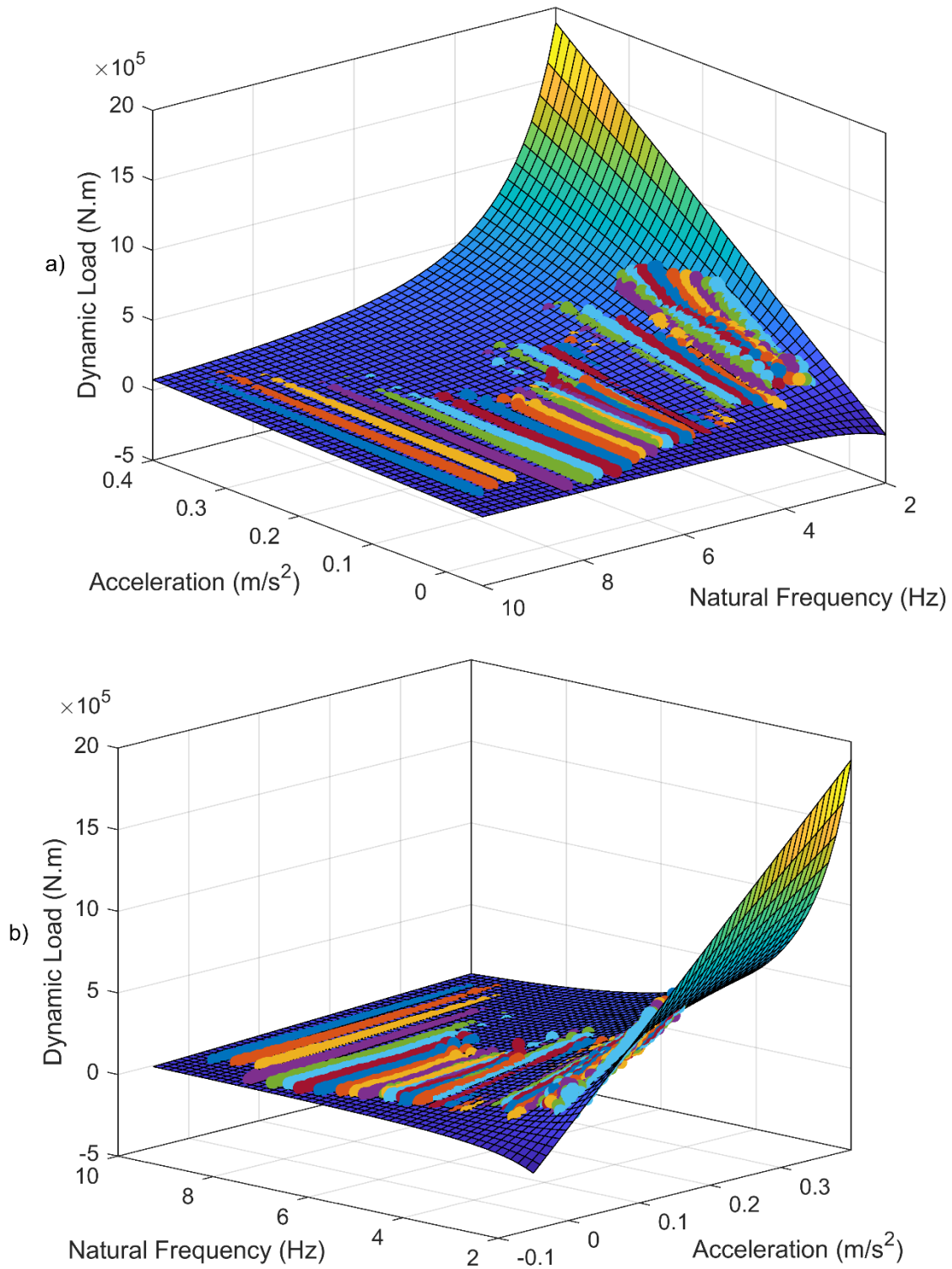
Figure 8.8: Dynamic Load Signature for BD7 vehicles.

Stellenbosch University https://scholar.sun.ac.za

The Characterization of the Dynamic Interaction between Highway Bridges and Long, Multi-Trailer Heavy Vehicles
_____

8.6 Implementation of the DLS to Estimate DAFs

The DLS can be used infield to estimate the dynamic loads induced on simply supported bridges traversed by a BD7 heavy vehicle population. The method proposed here utilizes infield strain and acceleration measurements to finally determine the expected dynamic loads and DAFs. The following requirements need to be met to ensure an accurate loads prediction:

- Simply supported bean and slab bridge configuration.

- 3 % bridge damping.

- Road Class A surface conditions.

- Strain gauge and accelerometer positioned at midspan in the slow lane.

- The first natural bridge frequency to be known.

- BD7 vehicle interaction.

If the first natural frequency of the bridge is not known, it can be determined by:

$$f_n(L, EI, \mu) = \frac{\pi}{2 \cdot L^2} \cdot \sqrt{\frac{EI}{\mu}} \qquad (8.5)$$

where L is span length of the bridge, EI is the flexural rigidity and μ the mass per meter of the bridge. In the case of older bridges which might have undergone some deterioration, the flexural rigidity will need to be estimated to determine the natural frequency. This can be done by implementing drive-by methods to determine the accelerations using an instrumented vehicle from which the bridge deflections can be calculated using double integration. The curvature is calculated by taking the second derivative of the deflection with respect to distance. The flexural rigidity can then be determined using the ratio of bending moment to curvature. This method of determining the flexural rigidity of a bridge is termed the Direct Stiffness Calculation (Martinez, *et al.*, 2020).

A strain gauge is used to determine the time step at which the bridge experienced the maximum total load at midspan due to the interaction of a BD7 vehicle. From the acceleration history recorded from the accelerometer, the midspan bridge acceleration, at the specific time step at which the maximum total load occurred, can then be determined. Finally, the acceleration and first natural frequency can be substituted into the DLS function to determine the expected dynamic loads. The calculation of the dynamic loads now enables the DAFs to be quantified by calculating midspan total loads by utilizing the maximum measured strains at midspan. The maximum midspan bending moments can be calculated by:

$$T_{BM}(\varepsilon, EI, y) = \frac{-\varepsilon \cdot EI}{y}$$

(8.6)

where ε is the maximum strain for the load event, EI is the flexural rigidity of the bridge and y is the depth to the neutral axis of the bridge. Having determined the total and dynamic loads at midspan the DAF induced by a BD7 vehicle, can be determined by:

$$DAF = \frac{T_{BM}(\varepsilon, EI, y)}{T_{BM}(\varepsilon, EI, y) - DLS(\ddot{v}, f_n)}$$

(8.7)

The summarized methodology to estimate dynamic loads and DAFs using strain and acceleration measurements with the DLS is given in Figure 8.9 below.
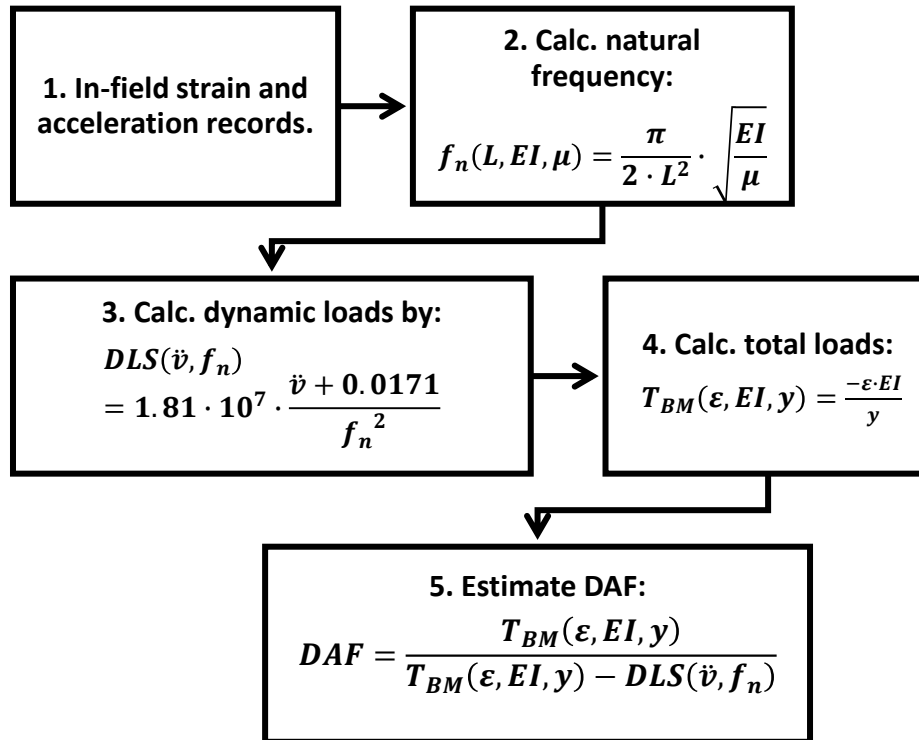
```
┌────────────────────────┐     ┌──────────────────────────────┐
│ 1. In-field strain and │ ──► │      2. Calc. natural        │
│  acceleration records. │     │         frequency:           │
└────────────────────────┘     └──────────────────────────────┘
```

$$f_n(L, EI, \mu) = \frac{\pi}{2 \cdot L^2} \cdot \sqrt{\frac{EI}{\mu}}$$

3. Calc. dynamic loads by:

$$DLS(\ddot{v}, f_n) = 1.81 \cdot 10^7 \cdot \frac{\ddot{v} + 0.0171}{f_n^2}$$

4. Calc. total loads:

$$T_{BM}(\varepsilon, EI, y) = \frac{-\varepsilon \cdot EI}{y}$$

5. Estimate DAF:

$$DAF = \frac{T_{BM}(\varepsilon, EI, y)}{T_{BM}(\varepsilon, EI, y) - DLS(\ddot{v}, f_n)}$$

Figure 8.9: Methodology to estimate dynamic loads and DAFs.

8.6.1 Validation of DLS Methodology

The methodology is validated against the VBI solution of the Vransko bridge, defined in Chapter 4, from interacting with 2000 BD7 vehicles randomly selected from the population of BD7 vehicles. These vehicles are simulated to cross the bridge with a Class A road surface and 100 m approach length. To ensure a credible test it is important to note that the Vransko bridge is not part of the bridge stock and was not used to develop the DLS. All that is known of the simply supported bridge is its first natural frequency.

The dynamic loads forming the VBI solution are shown in Figure 8.10 below. These are the loads to which the predicted dynamic loads from the DLS methodology will be validated against to test the accuracy. The blue scatter indicates each BD7 loading event on the bridge and the red line the moving mean of the dynamic loads. Henceforth, knowing the natural frequency of the bridge and the accelerations of maximum total loads, the DLS can be used to determine the predicted dynamic loads.

Stellenbosch University https://scholar.sun.ac.za

The Characterization of the Dynamic Interaction between Highway Bridges and Long, Multi-Trailer Heavy Vehicles
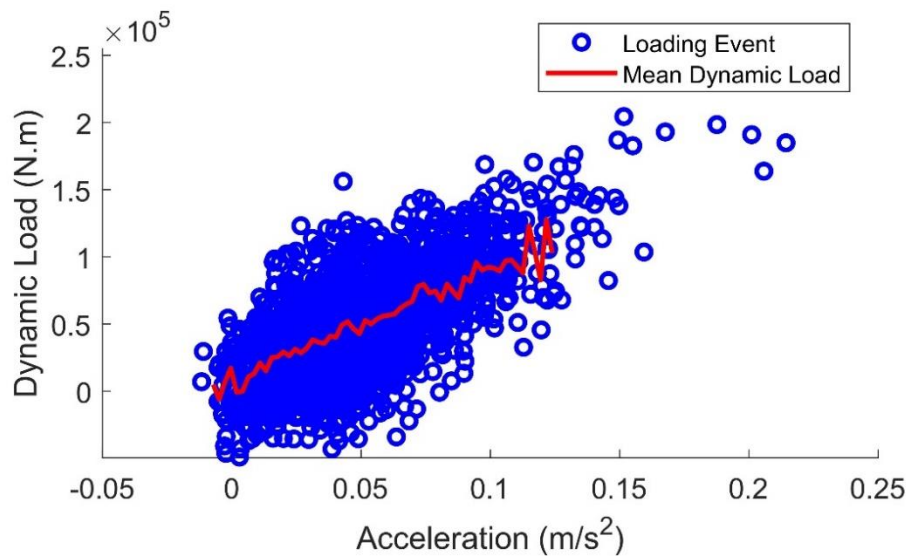_____

Figure 8.10: Dynamic loads of BD7 on Vransko bridge.

Figure 8.11 presents the comparison of the linear fit of the recorded moving mean from the VBI solution vs. the predicted dynamic loads according to the DLS. The linear fit of the moving means are shown in blue while the predicted dynamic loads according to the DLS are given in black. The results indicate that the predicted dynamic loads are accurate with only small deviations at the start and end accelerations where the density of loading events is lower.
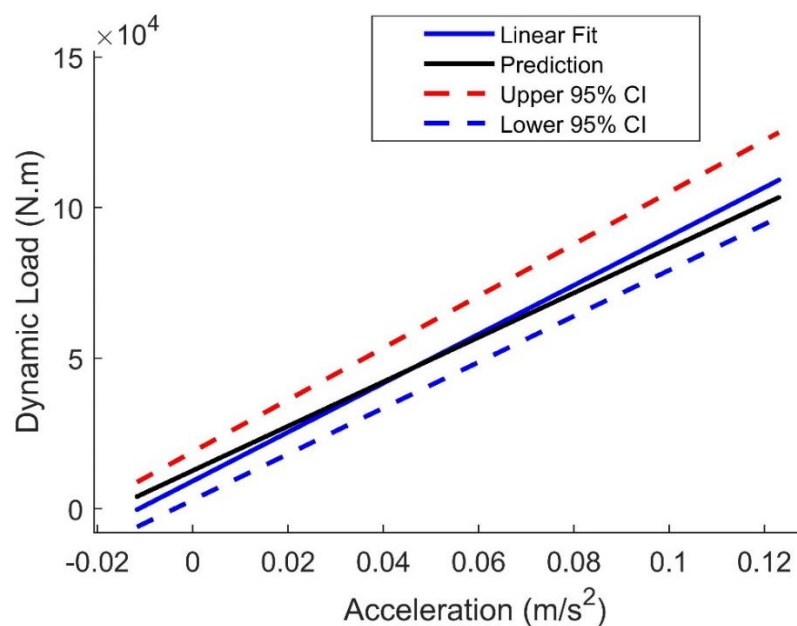

Figure 8.11: Comparison of predicted and measured dynamic loads.

The strain measurements can then be used to determine the total bending moments, using Equation 8.6 above, of which the predicted dynamic moments can be subtracted to determine the predicted static loads induced on the bridge. Figure 8.12 below compares the recorded static loads to the predicted static loads determined using the DLS method. The similarity in means of the predicted, shown in black, to the recorded, shown in red, reflects the promising accuracy of the prediction. Calculating the error in estimation reveals that the average prediction error of the DLS method is 1.7% with a maximum outlier error of 11.5%, shown in Figure 8.13 below.

Finally, the average degree of dynamic amplification induced by the 2000 BD7 vehicles on the Vransko bridge can be calculated by considering the ratio of total to static loads to produce the DAF for each loading event. The average recorded DAF from the VBI solution produced a factor of 1.0396 while the DLS methodology produced factor of 1.0350. The accuracy indicates the effectiveness of the DLS to estimate the average DAFs for simply supported bridges traversed by the BD7 vehicles.
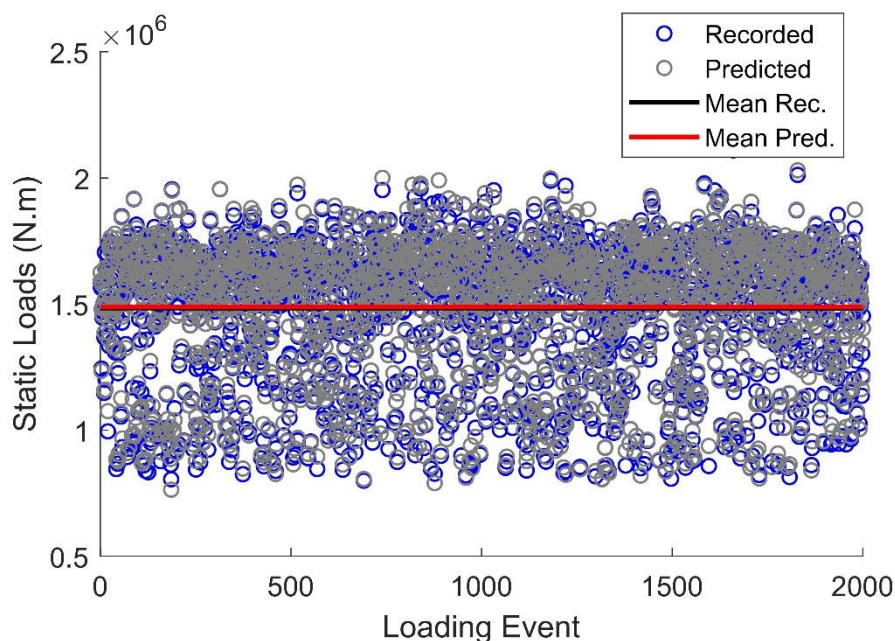

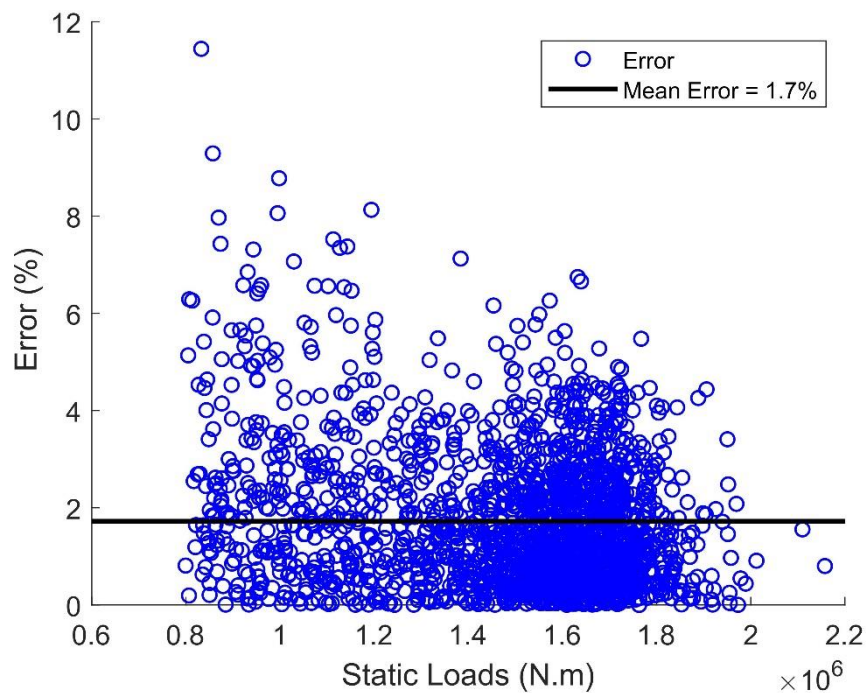Figure 8.12: Recorded vs. predicted static loads.

Figure 8.13: Static load prediction errors.

8.6.2 Conclusion

Around the world more countries are investing in greener means of transport which entails the use of larger BD7 vehicles which have not yet been studied in depth elsewhere. The DLS proves to be a useful tool which defines how these BD7 vehicles interact with existing concrete beam and slab simply supported bridges. The novel DLS methodology to study dynamic loads and bridge amplification is unparalleled with regards to computational efficiency provided that the specified requirements are met. The DLS provides the researchers with a quick and simple method to compare and study the degree of dynamic interaction induced by these multi-trailer heavy vehicles.

Stellenbosch University https://scholar.sun.ac.za

The Characterization of the Dynamic Interaction between Highway Bridges and Long, Multi-Trailer Heavy Vehicles
_____

CHAPTER 9:   CONCLUSIONS

The transportation industry is the largest contributor to the global carbon footprint and is under significant pressure to transform into a greener industry in a time with an increasing demand for freight to be transported by road. This has led to countries investigating more efficient means of road freight transportation. One of the solutions identified is the implementation of larger, multi-trailer heavy vehicles without compensating on manoeuvrability within the existing infrastructure. One of the most common solutions is the B-Double vehicle configuration of which a thorough bridge interaction analysis to investigate the dynamic loads accompanying these vehicles has not yet been undertaken. Additionally, some countries that have already incorporated these vehicles into their fleets follow foreign bridge design specifications which may not account for these types of heavy vehicles. This research aims to address the unknowns that exist in the field of dynamic interaction between the BD7 heavy vehicles and typical highway bridges. This is achieved by determining the dynamic loads and dynamic amplification factors induced on a range of short to medium span bridges and exploring clear trends unique to these vehicles.

A comparative dynamic amplification study of the three vehicles interacting with short and medium span bridges (Chapter 6) found several novel trends which are explored. It is found that the generally accepted inverse relationship between the DAF and GVM does not hold when considering the DAFs of vehicles with different axle configurations. It is concluded that the relationship between the DAF and GVM should be revised to accommodate vehicles with different trailer and axle configurations. Furthermore, the study found that the larger BD7 vehicles produce higher levels of dynamic amplification at medium span bridges compared to the smaller single articulated vehicles. Upon further investigation of the above-mentioned phenomena, it was found that BD7 vehicles can cause higher levels of dynamic amplification at certain medium span bridges due to the inherent axle configurations of these vehicles.

Stellenbosch University https://scholar.sun.ac.za

The Characterization of the Dynamic Interaction between Highway Bridges and Long, Multi-Trailer Heavy Vehicles
_____

An in-depth investigation of the factors which influence dynamic amplification, identified a novel relationship that exists between the midspan bridge accelerations and the dynamic component generated during interaction (Chapter 6). It is shown that a reliable linear relationship exists between the dynamic amplification factor and accelerations experienced at midspan of simply supported beam and slab concrete bridges. It is found that this relationship can be distorted by the presence of both loaded and unloaded vehicles. To overcome the latter, the static component can be removed to produce an improved linear relationship between the dynamic loads and midspan accelerations (Chapter 8).

The extensive dynamic interaction study of the full population of BD7 vehicles recorded at the Roosboom WIM station identified the critical loading velocities of the stock of bridges at which high dynamic amplification occurs (Chapter 7). The critical loading velocity can be defined as the unique travelling velocity of the vehicles which induce loading frequencies which aligns with the natural frequency of the bridge. At these velocities significant increases in dynamic amplification are observed. The investigation found that the largest average DAF for the BD7 vehicles heavier than 50 ton is observed at 75 ton with an average of 1.087 (Conf. Intervals: [1.065 1.089]). Finally using the dynamic interaction results of the extensive study the Dynamic Load Signature (DLS) for BD7 vehicles is introduced. The DLS is a surface function which defines the midspan dynamic loads induced by typical BD7 vehicles as a function of the midspan acceleration and first natural frequency of the bridge. This function is first of its kind and provides a simplified procedure, which does not include extensive numerical VBI simulations, to determine the expected dynamic loads induced on simply supported bridges by BD7 vehicles. Finally a novel method of estimating the DAFs induced by a BD7 vehicles is introduced which utilizes the DLS, strain and acceleration measurements. The developments presented here can be implemented by countries which use, or plan to use, similar BD7 heavy vehicles to preform preliminary dynamic bridge loads studies.

The investigation of the dynamic amplification induced by BD7 vehicles are certainly open for further developments. In this research the range of considered bridges were utilized as a platform to investigate

the unique dynamic behaviour of BD7 vehicles. In order to specifically study the unique trends in dynamic amplification induced by the vehicle itself, the flexural rigidity and bridge damping were set to constant values which have been shown to be representative of typical slab and beam bridges. However, assuming constant values, limits the findings of these research to a certain extent which should be addressed in future work when considering dynamic loads for final design purposes. Additionally, this investigation can be extended to incorporate a wider variety of bridge types and configurations such as composite bridges, integral and continuous span bridges. Finally, with regards to bridge assessment studies, it is recommended to investigate the influence of varying bridge deck stiffness and settled approach slab conditions on the dynamic loads induced by the BD7 vehicles. These developments will only ensure a better understanding of the intricacies associated with the dynamic amplification induced by larger multi-trailer vehicles on highway bridges so to finally produce safer bridge design values.

REFERENCES

Akaike, H. (1974). A New Look at the Statistical Model Identification. *IEEE Transactions on Automatic Control*.

Ashebo, D. B., Chan, T. H. T., & Yu, L. (2007). Evaluation of Dynamic Loads on a Skew Box Girder Continuous Bridge part I: Field Test and Modal Analysis. *Engineering Structures*, *29*(6), 1052–1063.

Brady, S. P., O'Brien, E. J., & Znidaric, A. (2010). The Effect of Vehicle Velocity on the Dynamic Amplification of a Vehicle crossing a Simply Supported Bridge. *Journal of Bridge*, *40*(1), 67–77.

Broquet, C., Bailey, S. F., Fafard, M., & Brühwiler, E. (2004). Dynamic Behavior of Deck Slabs of Concrete Road Bridges. *Journal of Bridge Engineering*, *9*(2), 137–146.

BS5400-4. (1990). *Steel, Concrete and Composite Bridges - Part 4: Code of Practice for Design of Concrete Bridges*.

Cantero, D., González, A., & O'Brien, E. J. (2009). Maximum Dynamic Stress on Bridges Traversed by Moving Loads. *Proceedings of the Institution of Civil Engineers: Bridge Engineering*, *162*(2), 75–85.

Cantero, D., O'Brien, E. J., & González, A. (2010). Modelling the Vehicle in Vehicle-Infrastructure Dynamic Interaction Studies. *Proceedings of the Institution of Mechanical Engineers, Part K: Journal of Multi-Body Dynamics*, *224*(2), 243–248.

Cantero, D., McGetrick, P., Kim, C. W., & O'Brien, E. J. (2019). Experimental Monitoring of Bridge Frequency Evolution During the Passage of Vehicles with different Suspension Properties. *Engineering Structures*, *187*, 209–219.

Cantero, D., O'Brien, E. J., González, A., & Enright, B. (2009). Highway Bridge Assessment for Dynamic Interaction with Critical Vehicles. *International Conference on Safety, Reliability and Risk of Structures, ICOSSAR*.

Caprani, C. C. (2017). Dynamic Load Allowance - A Synthesis of the State of the Art. *10th Austroads Bridge Conference*.

Stellenbosch University https://scholar.sun.ac.za

The Characterization of the Dynamic Interaction between Highway Bridges and Long, Multi-Trailer Heavy Vehicles
_____

Cary, R., Gerdes, D. Del, Haverberg, J., Pratt, R. I., Carolina, S., Roush, N. H., Virginia, W., Ruff, W. T., & Wilson, R. (2000). *American Association of State Highway Officials*.

Chang, D., & Lee, H. (1994). Impact Factors for Simple-Span Highway Girder Bridges. *Journal of Structural Engineering, ASCE*.

Chen, Y. H., & Li, C. Y. (2000). Dynamic Response of Elevated High-Speed Railway. *Journal of Bridge Engineering*, *5*, 124–130.

Committee of State Road Authorities. (1981). *TMH7 Parts 1 and 2: Code of Practice for the Design of Highway Bridges and Culverts in South Africa*.

Csagoly, P. F., & Dorton, R. A. (1975). *The Development of the Ontario Highway Bridge Design Code*.

Deng, L., & Cai, C. S. (2010). Development of Dynamic Impact Factor for Performance Evaluation of Existing Multi-Girder Concrete Bridges. *Engineering Structures*, *32*, 21–31.

Deng, Lu, Yu, Y., Zou, Q., & Cai, C. S. (2015). State-of-the-art Review of Dynamic Impact Factors of Highway Bridges. *Journal of Bridge Engineering*, *20*(5), 1–14.

Deng, Y., & Phares, B. M. (2016). *Investigation of the Effect of Speed on the Dynamic Impact Factor for Bridges with Different Entrance Conditions*.

EN 1991-2 (2003). (1 C.E.). *Actions on Structures - Part 2: Traffic Loads on Bridges*.

Eurocode 1: Actions on Structures - Part 2: Traffic Loads on Bridges. (2011).

Frangopol, D. M. . (2011). *Moving Loads – Dynamic Analysis and Identification Techniques*.

Frýba, L, & Yau, J. D. (2009). Suspended Bridges Subjected to Moving Loads and Support Motions due to Earthquake. *Journal of Sound and Vibration*, *319*(1–2), 218–227.

Frýba, Ladislav. (1972). *Vibration of Solids and Structures Under Moving Loads* (p. 494).

González, A., Znidaric, A., Casas, J.R., Enright, B., O'Brien, E.J., Lavric, I. & Kalin, J. (2009). *ARCHES Recommendations on Dynamic Amplification Allowance*.

Gonzalez, A. (2010). Vehicle-Bridge Dynamic Interaction Using Finite Element Modelling. *Finite Element Analysis*.

González, A., Cantero, D., & O'Brien, E. J. (2011). Dynamic Increment for Shear Force due to Heavy Vehicles Crossing a Highway Bridge. *Computers and Structures*, *89*(23–24), 2261–2272.

Gonzalez, A., O'Brien, E. J., Cantero, D., Li, Y., Dowling, J., & Znidaric, A. (2010). *Critical Speed for The Dynamics of Truck Events on Bridges with a Smooth Road Surface*. *329*, 2127–2146.

González, Arturo, Rattigan, P., O'Brien, E. J., & Caprani, C. (2008). Determination of Bridge Lifetime Dynamic Amplification Factor Using Finite Element Analysis of Critical Loading Scenarios. *Engineering Structures*, *30*(9), 2330–2337.

Green, M. F., & Cebon, D. (1992). *Dynamic Response of Highway Bridges to Heavy Vehicle Loads: Theory and Experimental Validation*.

Green, M. F., & Cebon, D. (1997). Dynamic Interaction Between Heavy Vehicles and Highway Bridges. *Computers and Structures*, *62*(2), 253–264.

Guo, T., & Liu, Z. (2015). *Fatigue Reliability Assessment of Orthotropic Steel Bridge Decks based on Probabilistic Multi-scale Finite Element Analysis*.

Harris, N. K., O'Brien, E. J., & González, A. (2007). Reduction of Bridge Dynamic Amplification through Adjustment of Vehicle Suspension Damping. *Journal of Sound and Vibration*, *302*(3), 471–485.

Henchi, K., Fafard, M., Talbot, M., & Dhatt, G. (1998). An Efficient Algorithm for Dynamic Analysis of Bridges Under Moving Vehicles using a Coupled Modal And Physical Components Approach. *Journal of Sound and Vibration*, *212*(4), 663–683.

Huang, D., Wang, T., & Shahawy, M. (1993). *Vibration and Impact in Multigirder Steel Bridges*.

Jeffcott, H. H. (1929). On the Vibration of Beams under the Action of Moving Loads. *The London, Edinburgh, and Dublin Philosophical Magazine and Journal of Science*, *8*(48).

Khadri, Y., Tekili, S., Daya, E. M., Daouadji, A., Guenfoud, M., & Merzoug, B. (2009). Analysis of the Dynamic Response of Bridges under Moving Loads. *International Review of Mechanical Engineering*, *3*(1), 91–99.

Kim, C. W., Kawatani, M., & Kim, K. B. (2005). Three-dimensional Dynamic Analysis for Bridge-Vehicle Interaction with Roadway Roughness. *Computers and Structures*, *83*, 1627–1645.

Kirkegaard, P., Nielsen, S. R., & Enevoldsen, I. (1997). *Heavy Vehicles on Minor Highway Bridges*.

Koç, M. A., Kesercioğlu, M. A., Esen, İ., & Çay, Y. (2016). Vehicle-Bridge-Interaction Analysis using

Stellenbosch University https://scholar.sun.ac.za

The Characterization of the Dynamic Interaction between Highway Bridges and Long, Multi-Trailer Heavy Vehicles
_____

Half-Car Model. *International Symposium on Innovative Technologies in Engineering and Science*.

Kohavi, R. (2000). A Study of Cross-Validation and Bootstrap for Accuracy Estimation and Model Selection. *International Joint Conference on Artifcial Intelligence*.

Kortiš, J., & Daniel, L. (2015). The Comparison between the Results of the Two-dimensional and Three-dimensional Models of Vehicle Bridge Interaction. *Procedia Engineering*, *111*, 425–430.

Kwasniewski, L., Li, H., & Wekezer, J., Malachowski, J. (2006). Finite Element Analysis of Vehicle-Bridge Interaction. *Finite Elements in Analysis and Design*, *42*, 950–959.

Kwasniewski, L., Wekezer, J., Roufa, G., Li, H., Ducher, J., & Malachowski, J. (2006). *Experimental Evaluation of Dynamic Effects for a Selected Highway Bridge*. *24*, 11–24.

Lenner, R. (2018). Traffic Characteristics and Bridge Loading in South Africa. *Journal of the South African Institution of Civil Engineering*, *59*(4), 34–46.

Li, H. (2005). Dynamic Response of Highway Bridges Subjected to Heavy Vehicles. *Tallahassee: The Florida State University*, 1–162.

Li, Y., O'Brien, E. J., & González, A. (2006). The Development of a Dynamic Amplification Estimator for Bridges with Good Road Profiles. *Journal of Sound and Vibration*, *293*(1–2), 125–137.

Liu, R. P. T. L. L. H. (2009). Cross-Validation. In *Database Systems* (p. 154). Springer, Boston, MA.

Malekjafarian, A., McGetrick, P. J., & O'Brien, E. J. (2015). A Review of Indirect Bridge Monitoring using Passing Vehicles. *Shock and Vibration*, *2015*(March), 2015–2019.

Martinez, D., Malekjafarian, A., & O'Brien, E. J. (2020). Bridge Flexural Rigidity Calculation using Measured Drive-by Deflections. *Journal of Civil Structural Health Monitoring*, *10*(5), 833–844.

Meyer, M. W., Cantero, D., & Lenner, R. (2021). Dynamics of long Multi-Trailer Heavy Vehicles Crossing Short to Medium Span Length Bridges. *Engineering Structures*, *247*, 113149.

Meyer, M. W., Lenner, R., & Van Der Spuy, P. F. (2019). The Development of a Vehicle-Bridge Interaction Model for South African Traffic . In A. Zingoni (Ed.), *Advances in Engineering Materials, Structures and Systems: Innovations, Mechanics and Applications*. Taylor & Francis.

Mohammed, O., Gonzalez, A., & Cantero, D. (2018). Dynamic Impact of Heavy Long Vehicles with

Stellenbosch University https://scholar.sun.ac.za

The Characterization of the Dynamic Interaction between Highway Bridges and Long, Multi-Trailer Heavy Vehicles
_____

Equally Spaced Axles on Short-span Highway Bridges. *Baltic Journal of Road and Bridge Engineering*, *13*(1), 1–13.

Mohammed, Omar, González, A., & Cantero, D. (2018). Dynamic Impact Of Heavy Long Vehicles with Equally Spaced Axles on Short-Span Highway Bridges. *Baltic Journal of Road and Bridge Engineering*, *13*(1), 1–13.

Newpher, B., Laman, J. A., & Boothby, T. E. (2014). *Dynamic Response of Three Historic Through-Truss Bridges*. *3*(6), 1–11.

O'Brien, E. J., McGetrick, P. J., & Gonzalez, A. (2014). A Drive-By Inspection System Via Vehicle Moving Force Identification. *Smart Structures and Systems*, *13*, 821–848.

OBrien, E. J., Mcgetrick, P. J., & González, A. (2014). A Drive-by Inspection System via Vehicle Moving Force Identification. *Smart Structures and Systems*, *13*(D), 821–848.

Patro, R. (2021). Cross-Validation: K Fold vs Monte Carlo. *Towards Data Science*.

Paultre, P. (2003). Dynamics of Structures. In *Dynamics of Structures*. John Wiley and Sons.

Pérez Sifre, S. (2020). *Site Specific Traffic Load Factor Approach for the Assessment of Existing Bridges*.

Rao, G. V. (2000). Linear Dynamics of an Elastic Beam under Moving Loads. *Journal of Vibration and Acoustics.*, *122*, 281–289.

Rattigan, P., O'Brien, E. J., & Gonzalez, A. (2005). The Dynamic Amplificaion on Highway Bridges due to Traffic Flow. *Proceedings of Young Researchers Seminar*.

Rowley, C., O'Brien, E. J., & González, A. (2008). Experimental Testing of a Moving Force Identification Bridge Weigh-in-Motion Algorithm. *Experimental Mechanics*, *49*, 743–746.

Schwarts, M., & Laman. (2001). *Response of Prestressed Concrete I-Girder Bridges to Live Load*. *6*, 1–8.

Shi, X., & Cai, C. S. (2006). Structural Performance of Approach Slab and its Effect on Vehicle Induced Bridge Dynamic Response. *Civil Engineering*, *Ph.D*.

ITF (2019), High Capacity Transport: Towards Efficient, Safe and Sustainable Road Freight. *International Transport Forum Policy Papers*, No. 69, OECD Publishing, Paris.

Stellenbosch University https://scholar.sun.ac.za

The Characterization of the Dynamic Interaction between Highway Bridges and Long, Multi-Trailer Heavy Vehicles
_____

States, M. (1996). Directive 96/53/EC. *Official Journal of the European Communities*, *L*, 59–75.

Stokes, G. (1896). Discussion of a Differential Equation Relating to the Breaking of Railway Bridges. In *Transactions of the Cambridge Philosophical Society*.

Thorogood, R., Bright, G., Nordengen, P., & Lyne, P. (2009). Performance Based Analysis of Current South African Semi Trailer and B-Double Trailer Designs. *South African Sugar Technologists Association*, *December*, 132–150.

Timoshenko, S. (1908). *Forced Vibration of Prismatic Bars*.

Timoshenko, S. (1922). On the Forced Vibraiton of Bridges. *Philosophical Magazine*, *6*(43), 1018–1019.

Timoshenko, S. (1953). History of the Strength of Materials. *McGraw-Hill, New York*.

TRH-11. (2009). *Dimensional and Mass Limitations and Other Requirements for Abnormal Vehicles*.

Van Der Spuy, P. F. (2019). *Derivation of a Traffic Load Model for the Structural Design Of Highway Bridges in South Africa*.

Van Der Spuy, P. F., Lenner, R., & Meyer, M. W. (2019). *Dynamic Amplification Factor for South African Bridges*.

Yang, J., & Duan, R. (2013). *Modelling and Simulation of a Bridge Interacting with a Moving Vehicle System*.

Yang, Y.-B., Liao, S.-S., & Lin, B.-H. (1995). Impact formulas for vehicles moving over simple and continuous beams. *Journal of Structural Engineering, ASCE*, *121*(11), 1644–1650.

Yang, Y. B., & Chang, K. C. (2014). *Effect of Road Surface Roughness on Extraction of Bridge Frequencies by Moving Vehicle*.

Yang, Y. B., & Lin, C. W. (2005). Vehicle-Bridge Interaction Dynamics and Potential Applications. *Journal of Sound and Vibration*, *284*(1–2), 205–226.

Yang, Y. B., Yau, J. D., & Wu, Y. S. (2004). Vehicle–Bridge Interaction Dynamics. In *Vehicle–Bridge Interaction Dynamics*.

Yang, Y., Chang, C., & Yau, J. D. (1999). An Element for Analysing Vehicle–Bridge Systems Considering Vehicle's Pitching Effect. *International Journal for Numerical Methods in*

Stellenbosch University https://scholar.sun.ac.za

The Characterization of the Dynamic Interaction between Highway Bridges and Long, Multi-Trailer Heavy Vehicles
_____

Engineering, *46*(7), 1031–1047.

Youcef, K., Sabiha, T., El Mostafa, D., Ali, D., & Bachir, M. (2013). Dynamic Analysis of Train-Bridge System and Riding Comfort of Trains with Rail Irregularities. *Journal of Mechanical Science and Technology*, *27*(4), 951–962.

Yu, H., Wang, B., Li, Y., Zhang, Y., & Zhang, W. (2018). Road Vehicle-Bridge Interaction Considering Varied Vehicle Speed Based on Convenient Combination Of Simulink and ANSYS. *Shock and Vibration*.

Zheng, D. Y., Cheung, Y. K., Au, F. T. K., & Cheng, Y. S. (1998). Vibration of Multi-Span Non-Uniform Bridges under Moving Loads by Using Modified Beam Vibration Functions. *Journal of Sound and Vibration*, *212*, 455–467.

Žnidarič, A. (2015). Heavy-Duty Vehicle Weight Restrictions in the EU. In *European Automibile Manufacturers Association*.

APPENDIX A.1

The equations of motion of the 7-axle B-Double (BD7) vehicle are presented here in matrix form.

- **Mass matrix:**

$M_v(1:4, 1:4)$

$$= \begin{pmatrix} m_t + m_{s1} + m_{s2} & (m_{s1} + m_{s2}) \cdot b_{11} & m_{s1} \cdot b_{10} + m_{s2} \cdot (b_{10} + b_9) & m_{s2} \cdot b_8 \\ (m_{s1} + m_{s2}) \cdot b_{11} & b_{11}^2 \cdot (m_{s1} + m_{s2}) + I_t + m_{e1} \cdot a_1^2 & b_{11} \cdot (m_{s1} \cdot b_{10} + m_{s2} \cdot (b_{10} + b_9)) - m_{e1} \cdot a_1 \cdot a_2 & m_{s2} \cdot (b_{11} \cdot b_8) \\ m_{s1} \cdot b_{10} + m_{s2} \cdot (b_{10} + b_9) & b_{11} \cdot (m_{s1} \cdot b_{10} + m_{s2} \cdot (b_{10} + b_9)) - m_{e1} \cdot a_1 \cdot a_2 & b_{10}^2 \cdot m_{s1} + m_{s2} \cdot ((b_{10} + b_9)^2) + I_{s1} + (a_2^2) \cdot (m_{e2} + m_{e1}) & m_{s2} \cdot b_8 \cdot (b_{10} + b_9) - m_{e2} \cdot a_2 \cdot a_3 \\ m_{s2} \cdot b_8 & m_{s2} \cdot (b_{11} \cdot b_8) & m_{s2} \cdot b_8 \cdot (b_{10} + b_9) - m_{e2} \cdot a_2 \cdot a_3 & b_8^2 * m_{s2} + I_{s2} + m_{e2} * a_3^2 \end{pmatrix}$$

$$M_v(5:11, 5:11) = \begin{pmatrix} m_1 & 0 & 0 & 0 & 0 & 0 & 0 \\ : & m_2 & 0 & 0 & 0 & 0 & 0 \\ : & : & m_3 & 0 & 0 & 0 & 0 \\ : & : & : & m_4 & 0 & 0 & 0 \\ : & : & : & .. & m_5 & 0 & 0 \\ : & : & .. & .. & .. & m_6 & 0 \\ symm. & .. & .. & .. & .. & .. & m_7 \end{pmatrix}$$

116

_____

- **Damping Matrix:**

$$\boldsymbol{C_v}(1{:}4, 1{:}4) = \begin{pmatrix} c_{11} & c_{12} & c_{13} & c_{14} \\ \vdots & c_{22} & c_{23} & c_{24} \\ \vdots & & c_{33} & c_{34} \\ symm. & .. & .. & c_{44} \end{pmatrix}$$

$$c_{11} = c_{s1} + c_{s2} + c_{s3} + c_{s4} + c_{s5} + c_{s6} + c_{s7}$$

$$c_{12} = -b_1 \cdot c_{s1} + c_{s2} \cdot b_2 + c_{s3} \cdot b_3 + (c_{s4} + c_{s5} + c_{s6} + c_{s7}) \cdot b_{11}$$

$$c_{13} = c_{s4} \cdot (b_{10} + b_4) + c_{s5} \cdot (b_{10} + b_5) + (c_{s6} + c_{s7}) \cdot (b_{10} + b_9)$$

$$c_{14} = c_{s6} \cdot (b_8 + b_6) + c_{s7} \cdot (b_8 + b_7)$$

$$c_{22} = b_1^2 \cdot c_{s1} + b_2^2 \cdot c_{s2} + b_3^2 \cdot c_{s3} + b_{11}^2 \cdot (c_{s4} + c_{s5} + c_{s6} + c_{s7})$$

$$c_{23} = b_{11} \cdot (c_{s4} \cdot (b_{10} + b_4) + c_{s5} \cdot (b_{10} + b_5) + (b_{10} + b_9) \cdot (c_{s6} + c_{s7}))$$

$$c_{24} = c_{s6} \cdot b_{11} \cdot (b_8 + b_6) + c_{s7} \cdot b_{11} \cdot (b_8 + b_7)$$

$$c_{33} = c_{s4} \cdot (b_{10} + b_4)^2 + c_{s5} \cdot (b_{10} + b_5)^2 + c_{s6} \cdot (b_{10} + b_9)^2 + c_{s7} \cdot (b_{10} + b_9)^2$$

$$c_{34} = (b_{10} + b_9) \cdot (c_{s6} \cdot (b_8 + b_6) + c_{s7} \cdot (b_8 + b_7))$$

$$c_{44} = c_{s6} \cdot (b_8 + b_6)^2 + c_{s7} \cdot (b_8 + b_7)^2$$

The Characterization of the Dynamic Interaction between Highway Bridges and Long, Multi-Trailer Heavy Vehicles

_____

$$C_v(5{:}11,5{:}11) = \begin{pmatrix} c_{s1}+c_{t1} & 0 & 0 & 0 & 0 & 0 & 0 \\ : & c_{s2}+c_{t2} & 0 & 0 & 0 & 0 & 0 \\ : & : & c_{s3}+c_{t3} & 0 & 0 & 0 & 0 \\ : & : & : & c_{s4}+c_{t4} & 0 & 0 & 0 \\ : & : & : & .. & c_{s5}+c_{t5} & 0 & 0 \\ : & .. & .. & .. & .. & c_{s6}+c_{t6} & 0 \\ symm. & .. & .. & .. & .. & .. & c_{s7}+c_{t7} \end{pmatrix}$$

- **Stiffness matrix:**

$$K_v(1{:}4,1{:}4) = \begin{pmatrix} k_{11} & k_{12} & k_{13} & k_{14} \\ : & k_{22} & k_{23} & k_{24} \\ : & .. & k_{33} & k_{34} \\ symm. & .. & .. & k_{44} \end{pmatrix}$$

$$k_{11} = k_{s1} + k_{s2} + k_{s3} + k_{s4} + k_{s5} + k_{s6} + k_{s7}$$

$$k_{12} = -b_1 \cdot k_{s1} + k_{s2} \cdot b_2 + k_{s3} \cdot b_3 + (k_{s4} + k_{s5} + k_{s6} + k_{s7}) \cdot b_{11}$$

$$k_{13} = k_{s4} \cdot (b_{10} + b_4) + k_{s5} \cdot (b_{10} + b_5) + (k_{s6} + k_{s7}) \cdot (b_{10} + b_9)$$

$$k_{14} = k_{s6} \cdot (b_8 + b_6) + k_{s7} \cdot (b_8 + b_7)$$

$$k_{22} = b_1^2 \cdot k_{s1} + b_2^2 \cdot k_{s2} + b_3^2 \cdot k_{s3} + b_{11}^2 \cdot (k_{s4} + k_{s5} + k_{s6} + k_{s7})$$

$$k_{23} = b_{11} \cdot (k_{s4} \cdot (b_{10} + b_4) + k_{s5} \cdot (b_{10} + b_5) + (b_{10} + b_9) \cdot (k_{s6} + k_{s7}))$$

$$k_{24} = k_{s6} \cdot b_{11} \cdot (b_8 + b_6) + k_{s7} \cdot b_{11} \cdot (b_8 + b_7)$$

The Characterization of the Dynamic Interaction between Highway Bridges and Long, Multi-Trailer Heavy Vehicles
_____

$$k_{33} = k_{s4} \cdot (b_{10} + b_4)^2 + k_{s5} \cdot (b_{10} + b_5)^2 + k_{s6} \cdot (b_{10} + b_9)^2 + k_{s7} \cdot (b_{10} + b_9)^2$$

$$k_{34} = (b_{10} + b_9) \cdot \left(k_{s6} \cdot (b_8 + b_6) + k_{s7} \cdot (b_8 + b_7) \right)$$

$$k_{44} = k_{s6} \cdot (b_8 + b_6)^2 + k_{s7} \cdot (b_8 + b_7)^2$$

$$K_v(5\!:\!11, 5\!:\!11) = \begin{pmatrix} k_{s1} + k_{t1} & 0 & 0 & 0 & 0 & 0 & 0 \\ \vdots & k_{s2} + k_{t2} & 0 & 0 & 0 & 0 & 0 \\ \vdots & \vdots & k_{s3} + k_{t3} & 0 & 0 & 0 & 0 \\ \vdots & \vdots & \vdots & k_{s4} + k_{t4} & 0 & 0 & 0 \\ \vdots & \vdots & \vdots & .. & k_{s5} + k_{t5} & 0 & 0 \\ \vdots & .. & .. & .. & .. & k_{s6} + k_{t6} & 0 \\ symm. & .. & .. & .. & .. & .. & k_{s7} + k_{t7} \end{pmatrix}$$

- **Coupled system matrices:**

$$K_{bv} = \begin{pmatrix} 0 & .. & 0 & -H \begin{pmatrix} k_{s1} + k_{t1} & 0 & 0 & 0 & 0 & 0 & 0 \\ \vdots & k_{s2} + k_{t2} & 0 & 0 & 0 & 0 & 0 \\ \vdots & \vdots & k_{s3} + k_{t3} & 0 & 0 & 0 & 0 \\ \vdots & \vdots & \vdots & k_{s4} + k_{t4} & 0 & 0 & 0 \\ \vdots & \vdots & \vdots & .. & k_{s5} + k_{t5} & 0 & 0 \\ \vdots & .. & .. & .. & .. & k_{s6} + k_{t6} & 0 \\ symm. & .. & .. & .. & .. & .. & k_{s7} + k_{t7} \end{pmatrix} \end{pmatrix}_{n \times 11}$$
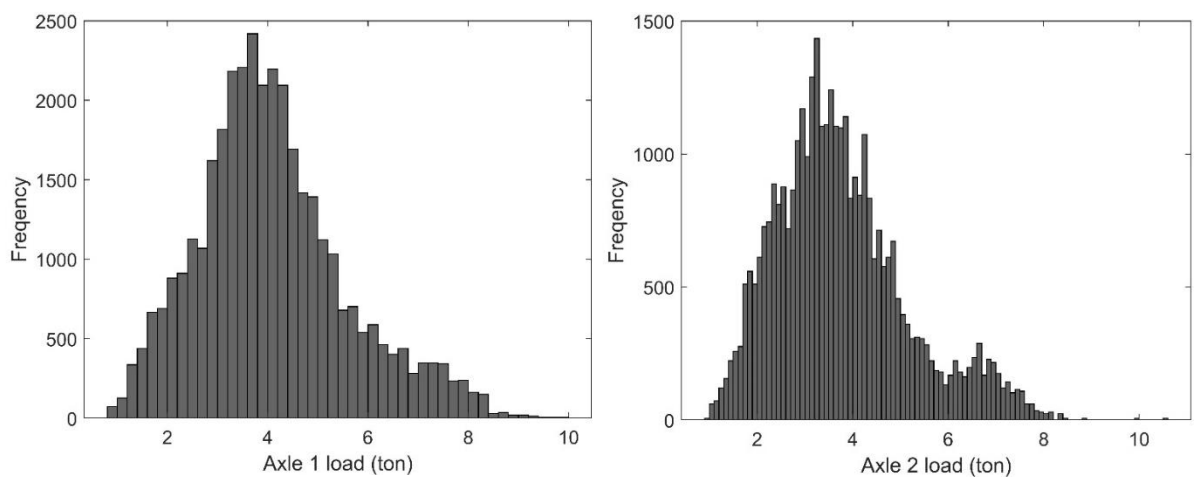
where *n* is the total number of beam degrees of freedom.

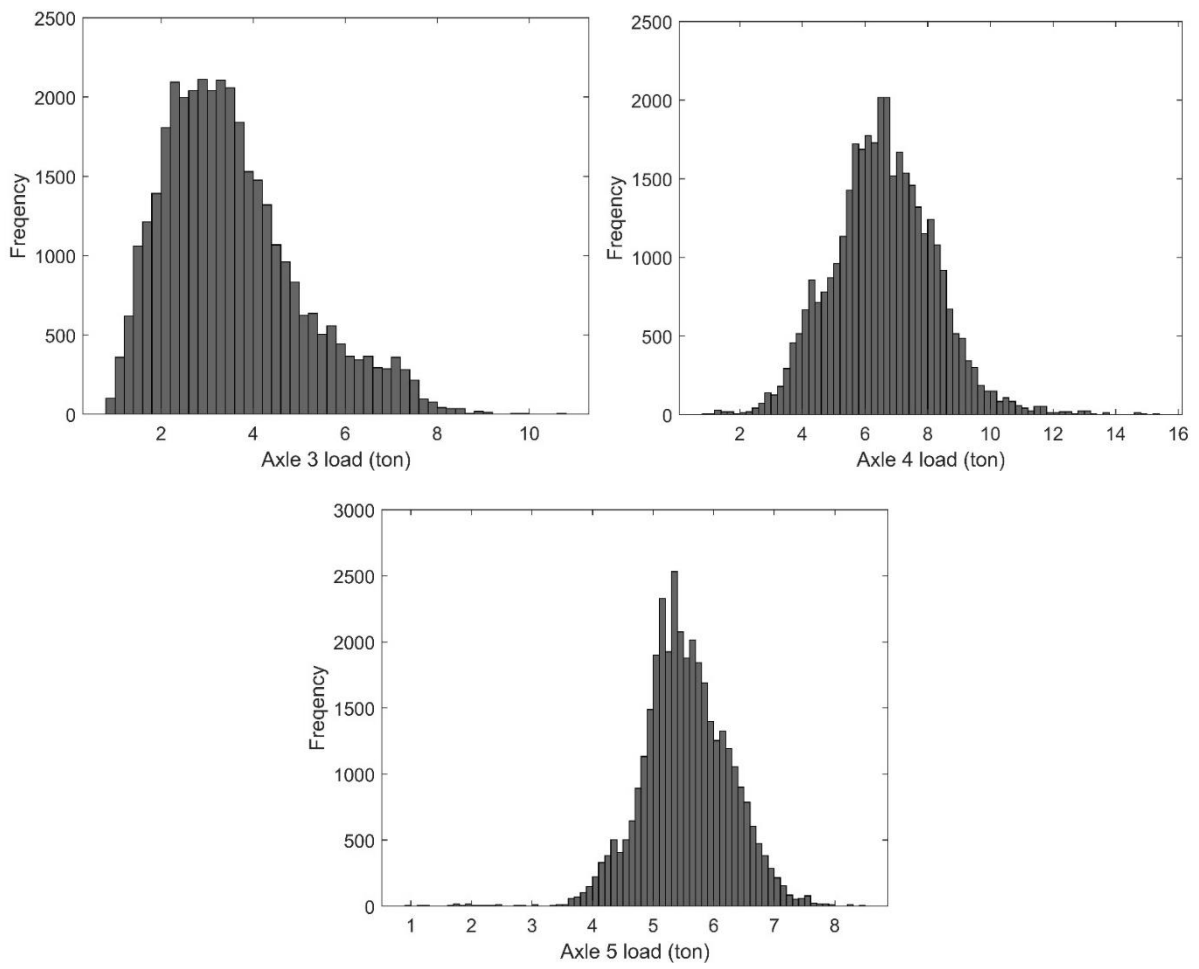The Characterization of the Dynamic Interaction between Highway Bridges and Long, Multi-Trailer Heavy Vehicles
_____

$$K_{vb} = K_{bv}{}^T$$

$$
H = \begin{pmatrix}
0 & 0 & 0 & 0 & 0 & 0 & 0 \\
0 & 0 & 0 & 0 & 0 & 0 & 0 \\
0 & 0 & 0 & 0 & 0 & 0 & N_{s7} \\
0 & 0 & 0 & 0 & 0 & N_{s6} & 0 \\
0 & 0 & 0 & 0 & 0 & 0 & 0 \\
0 & 0 & 0 & 0 & N_{s5} & 0 & 0 \\
0 & 0 & 0 & N_{s4} & 0 & 0 & 0 \\
0 & 0 & N_{s3} & 0 & 0 & 0 & 0 \\
0 & 0 & 0 & 0 & 0 & 0 & 0 \\
0 & N_{s2} & 0 & 0 & 0 & 0 & 0 \\
N_{s1} & 0 & 0 & 0 & 0 & 0 & 0 \\
0 & 0 & 0 & 0 & 0 & 0 & 0 \\
0 & 0 & 0 & 0 & 0 & 0 & 0
\end{pmatrix}_{n \times 7}
$$

where N_{si} is the shape function for the ith interaction force. The **H** matrix is time dependent, i.e. it changes as the vehicle traverses the bridge and will only have non-zeros entries at the nodal rotation and displacement degrees of freedom of the specific beam elements which are in contact with the vehicle tyres.

$$
K_{bb} = \left(\begin{array}{c|c} H & H \end{array} \begin{pmatrix}
k_{s1}+k_{t1} & 0 & 0 & 0 & 0 & 0 & 0 \\
: & k_{s2}+k_{t2} & 0 & 0 & 0 & 0 & 0 \\
: & : & k_{s3}+k_{t3} & 0 & 0 & 0 & 0 \\
: & : & : & k_{s4}+k_{t4} & 0 & 0 & 0 \\
: & : & : & .. & k_{s5}+k_{t5} & 0 & 0 \\
: & .. & .. & .. & .. & k_{s6}+k_{t6} & 0 \\
symm. & .. & .. & .. & .. & .. & k_{s7}+k_{t7}
\end{pmatrix} \right)^T_{n \times n}
$$

120

_____

$$M_g = \begin{pmatrix} M_v & 0 \\ 0 & M_b \end{pmatrix}$$

$$C_g = \begin{pmatrix} C_v & 0 \\ 0 & C_b \end{pmatrix}$$

$$K_g = \begin{pmatrix} K_v & K_{vb} \\ K_{bv} & K_b + K_{bb} \end{pmatrix}$$

APPENDIX B.1

The histograms of the axle load distribution for the SA5, SA6 and BD7 vehicles are presented here.

- **BD7 vehicles axle loads:**
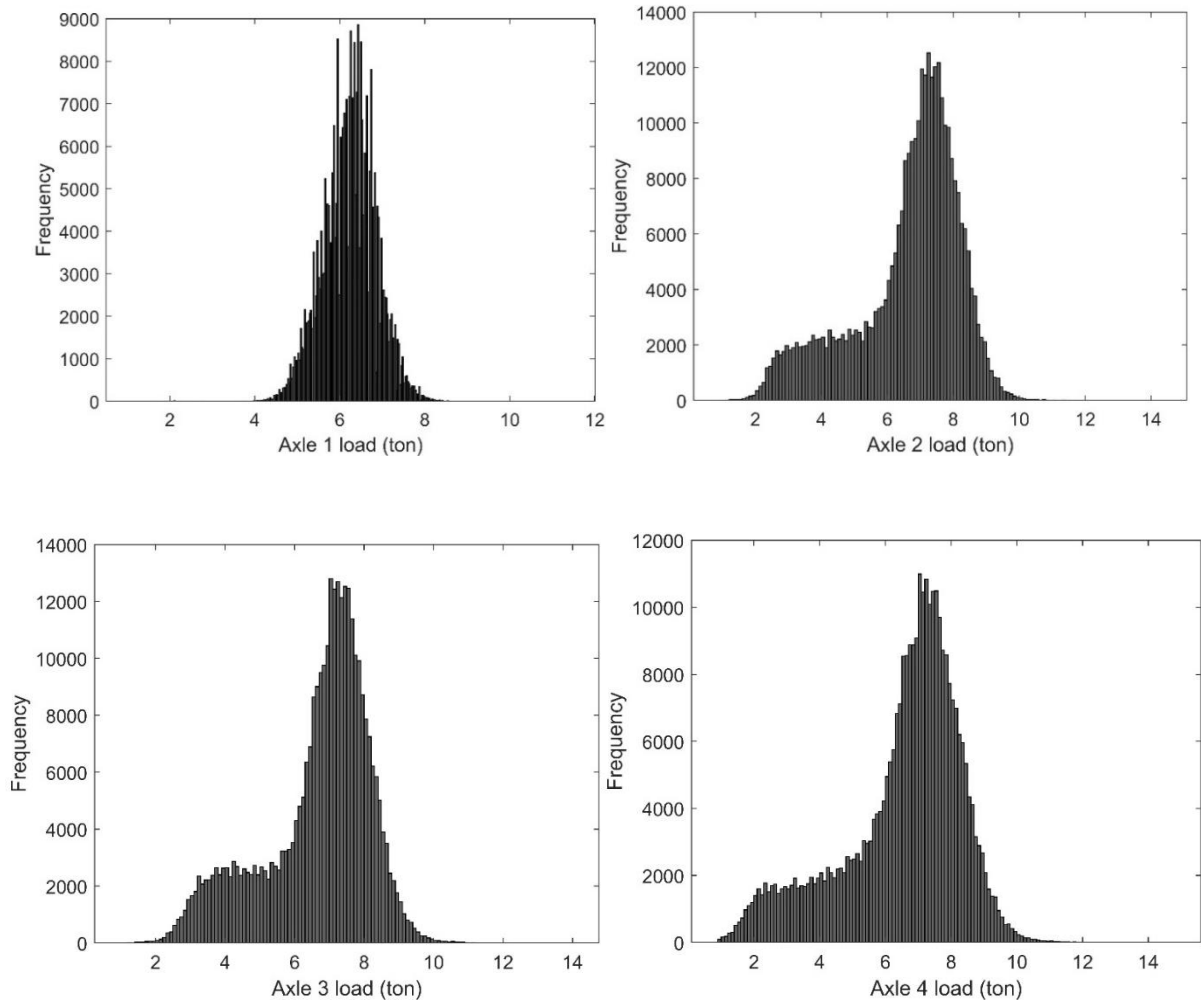
Figure B.1: Axle loads of BD7 vehicles.
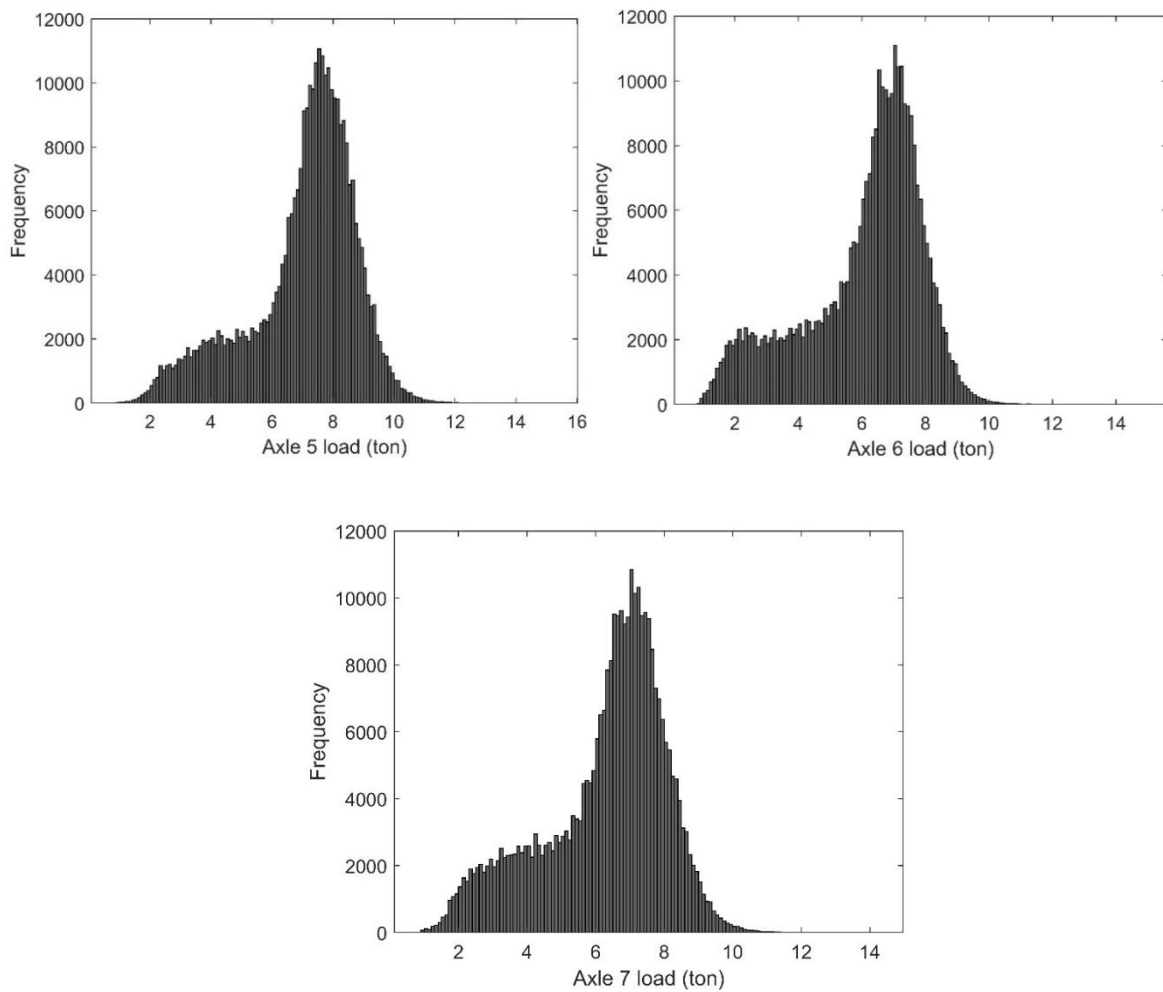
Figure B.1: Axle loads of BD7 vehicles continued.

- **SA6 vehicles axle loads:**
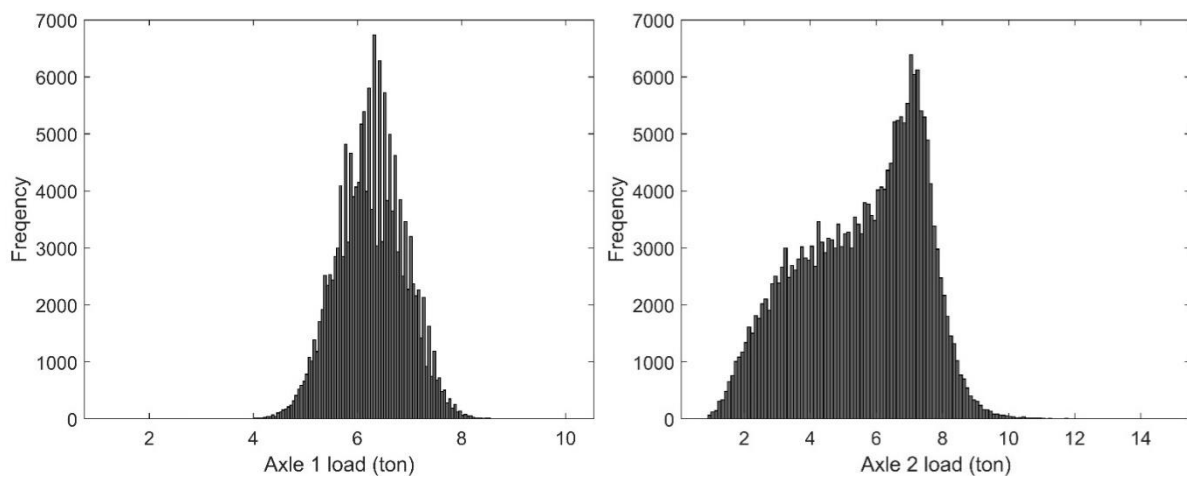
Figure B.2: Axle loads of SA6 vehicles.
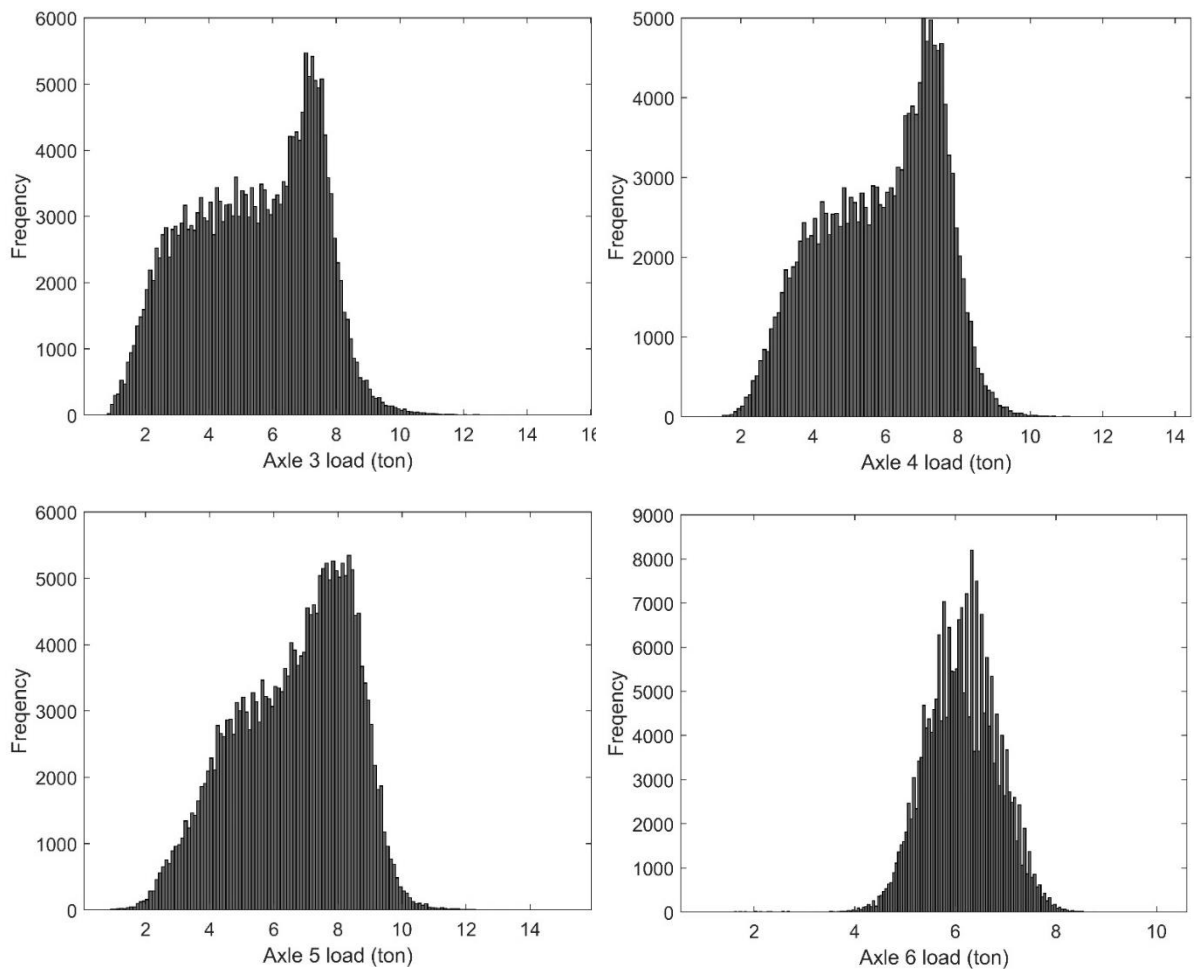
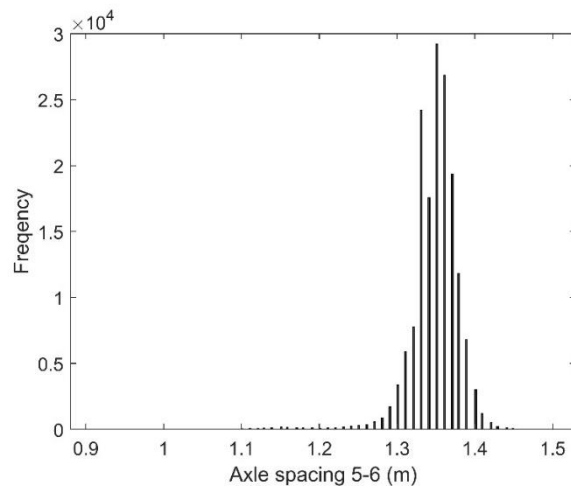Figure B.2: Axle loads of SA6 vehicles continued.

- **SA5 vehicles axle loads:**

Figure B.3: Axle loads of SA5 vehicles.

Figure B.3: Axle loads of SA5 vehicles continued.

APPENDIX B.2

The histograms presenting the axle spacing for the SA5, SA6 and BD7 vehicles are provided here:

- **BD7 vehicles axle spacing:**
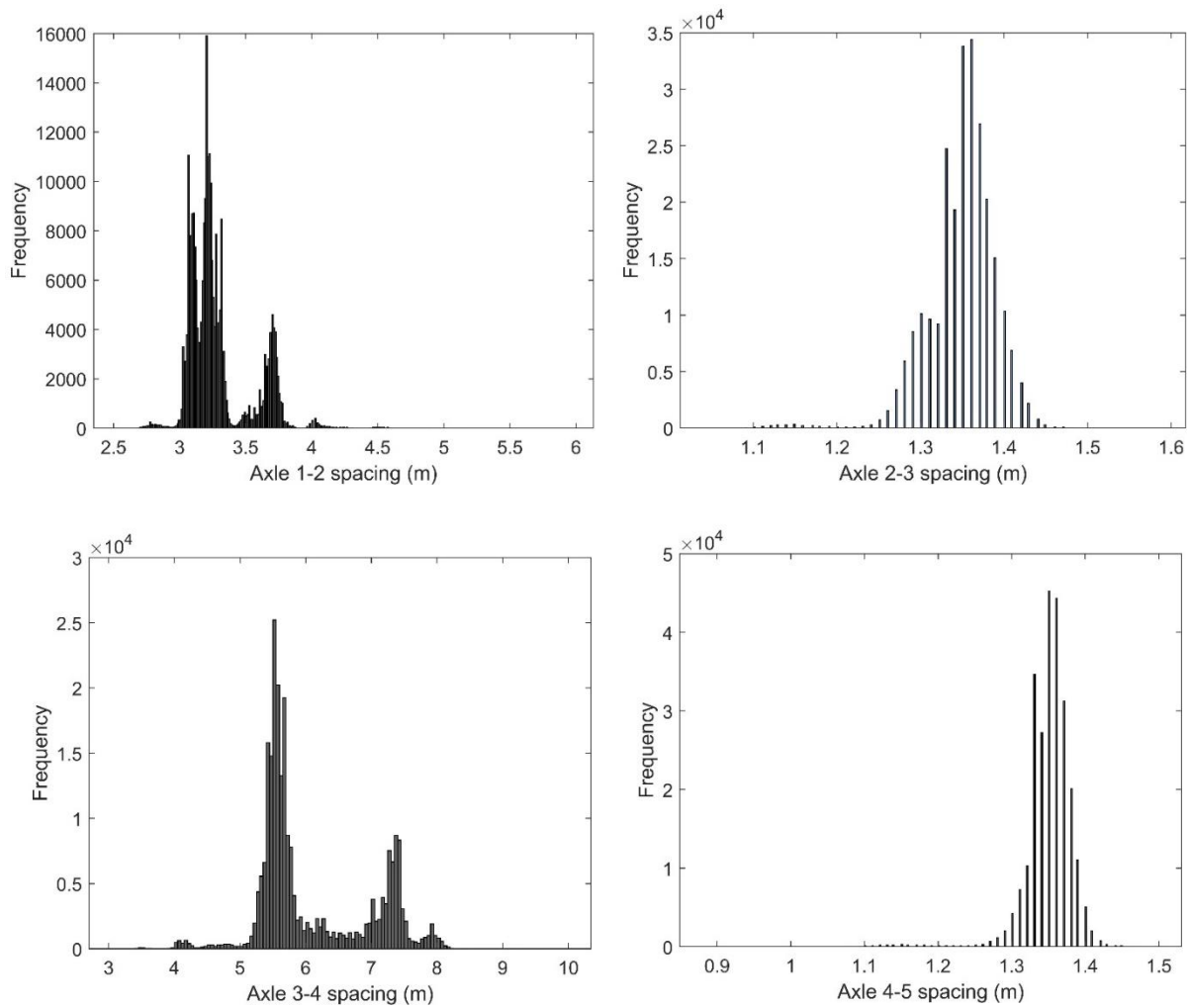
Figure B.4: Axle spacing of BD7 vehicles.
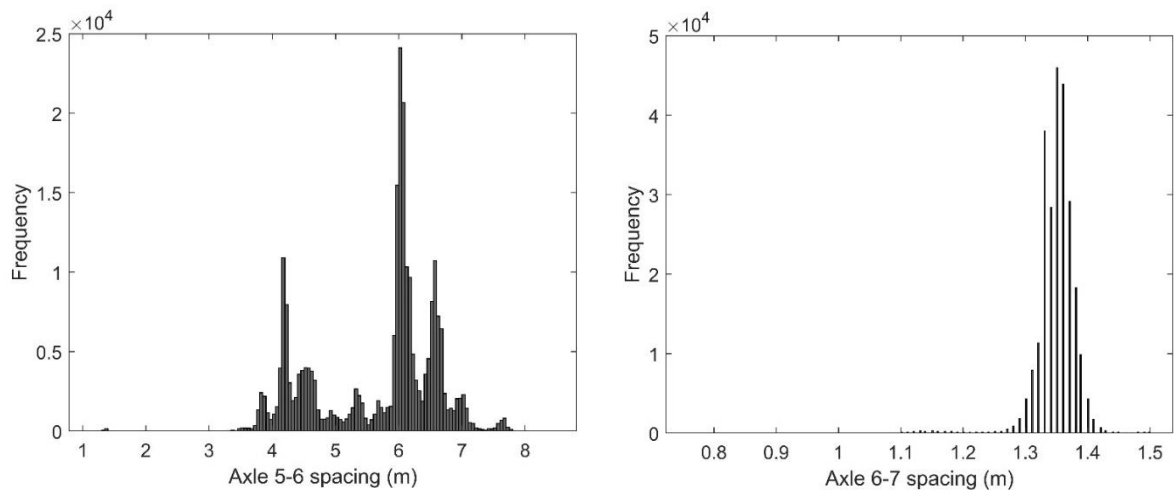
Figure B.4: Axle spacing of BD7 vehicles continued.

- **SA6 vehicles axle spacing:**
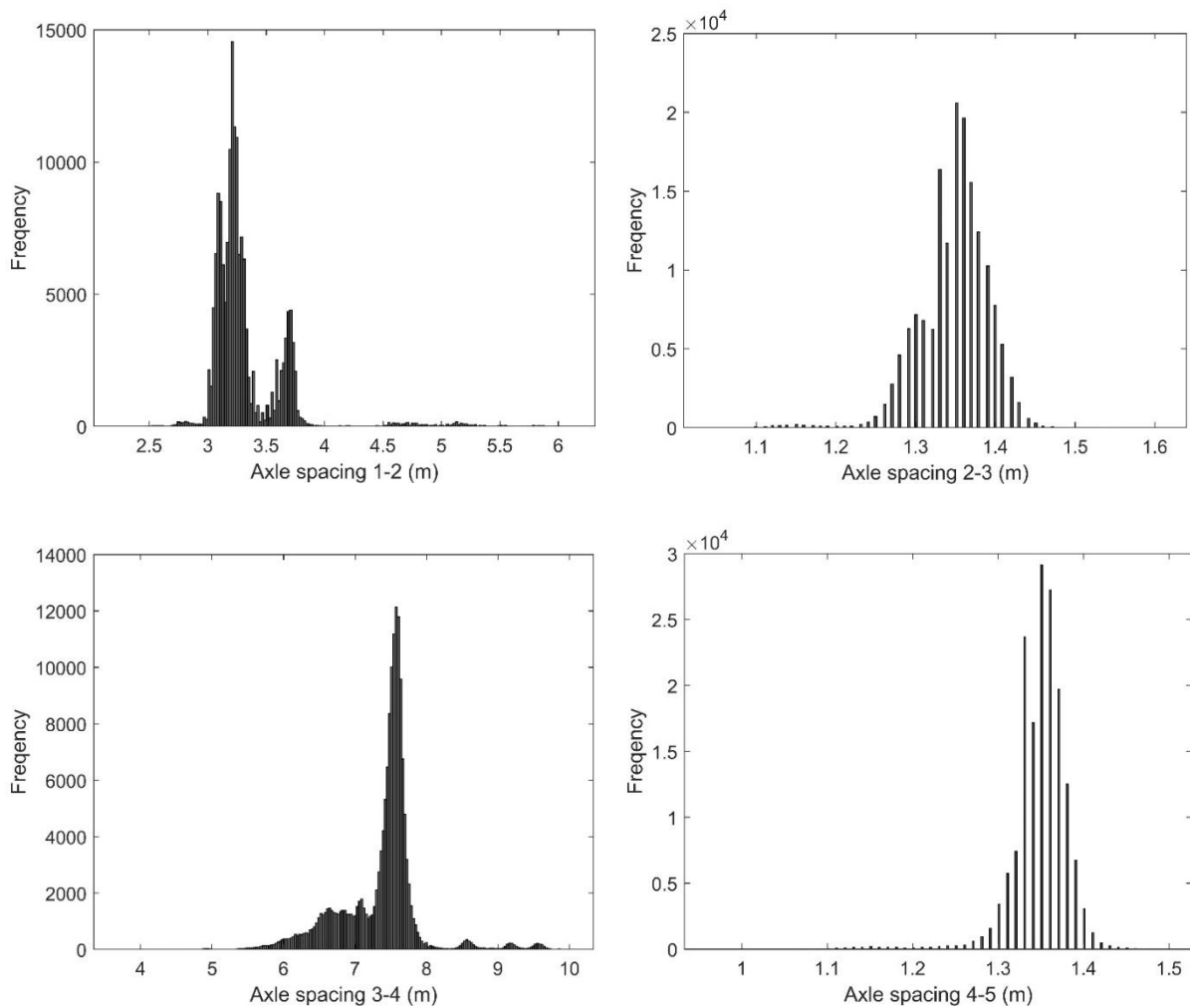
Figure B.5: Axle spacing of SA6 vehicles.

_____

Figure B.5: Axle spacing of SA6 vehicles continued.

- **SA5 vehicles axle spacing:**
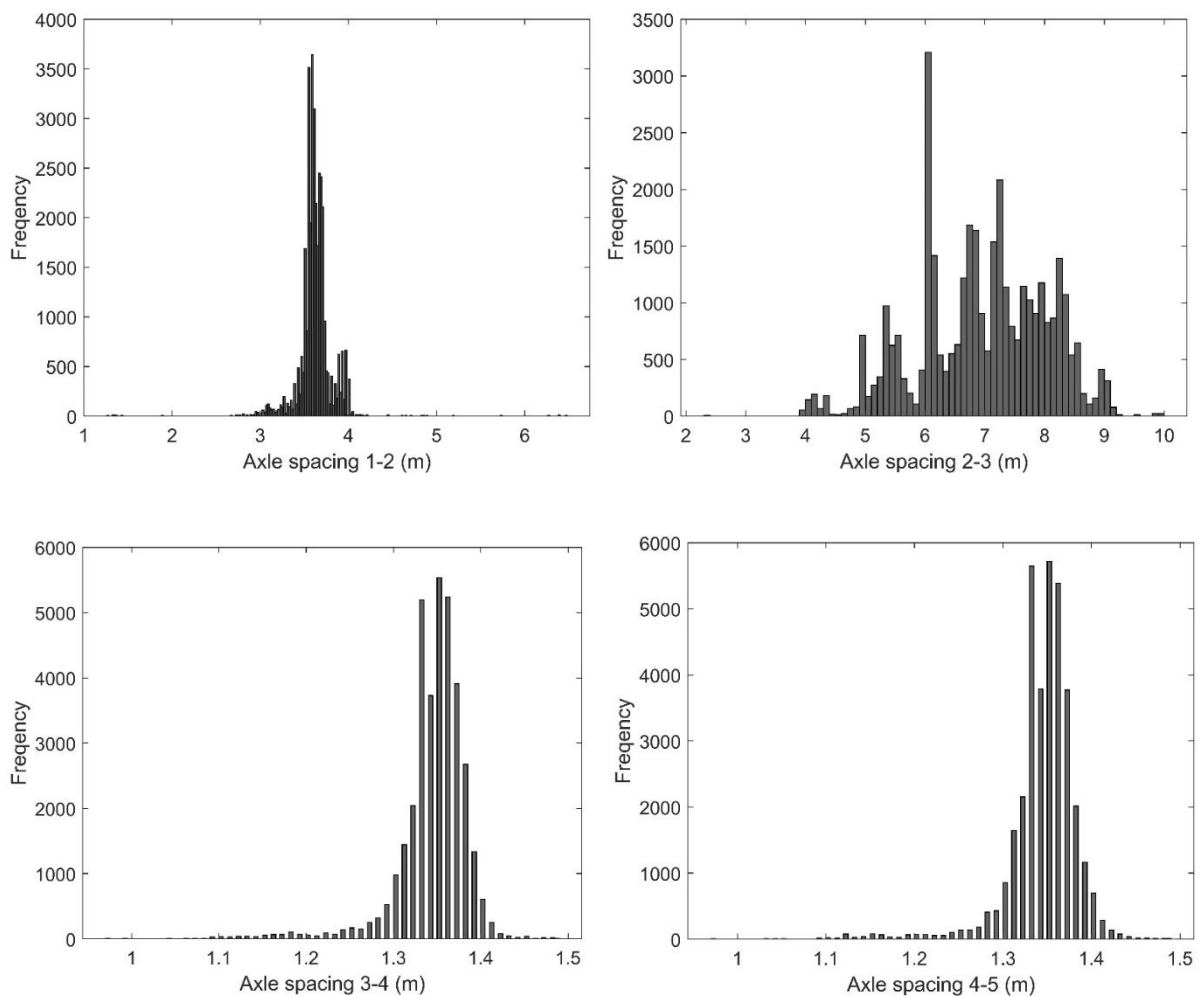
Figure B.6: Axle spacing of SA5 vehicles.

The Characterization of the Dynamic Interaction between Highway Bridges and Long, Multi-Trailer Heavy Vehicles
_____

APPENDIX C.1

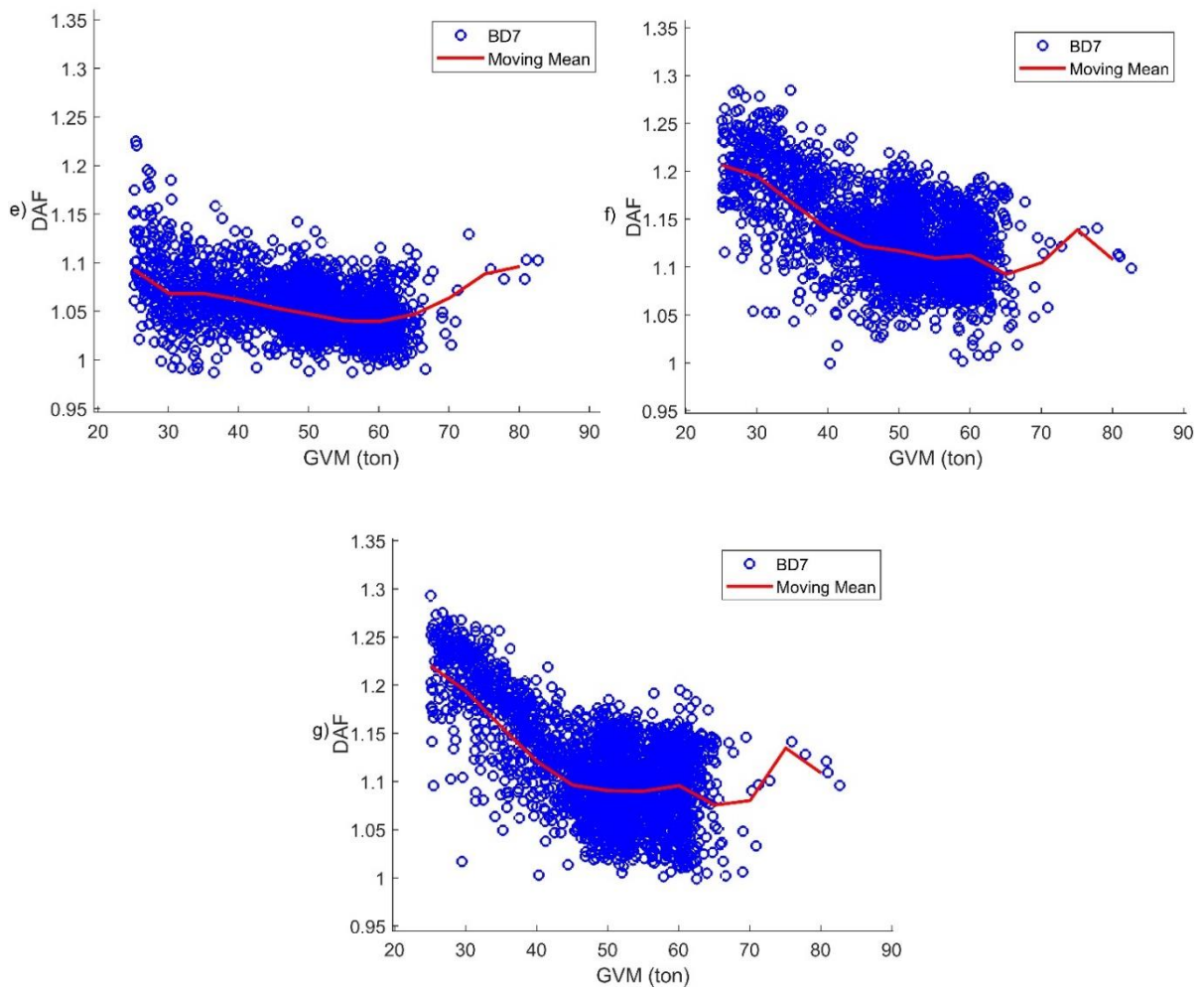The relationship between the DAF and GVM of the BD7 vehicle population is presented here for the range of bridges considered.
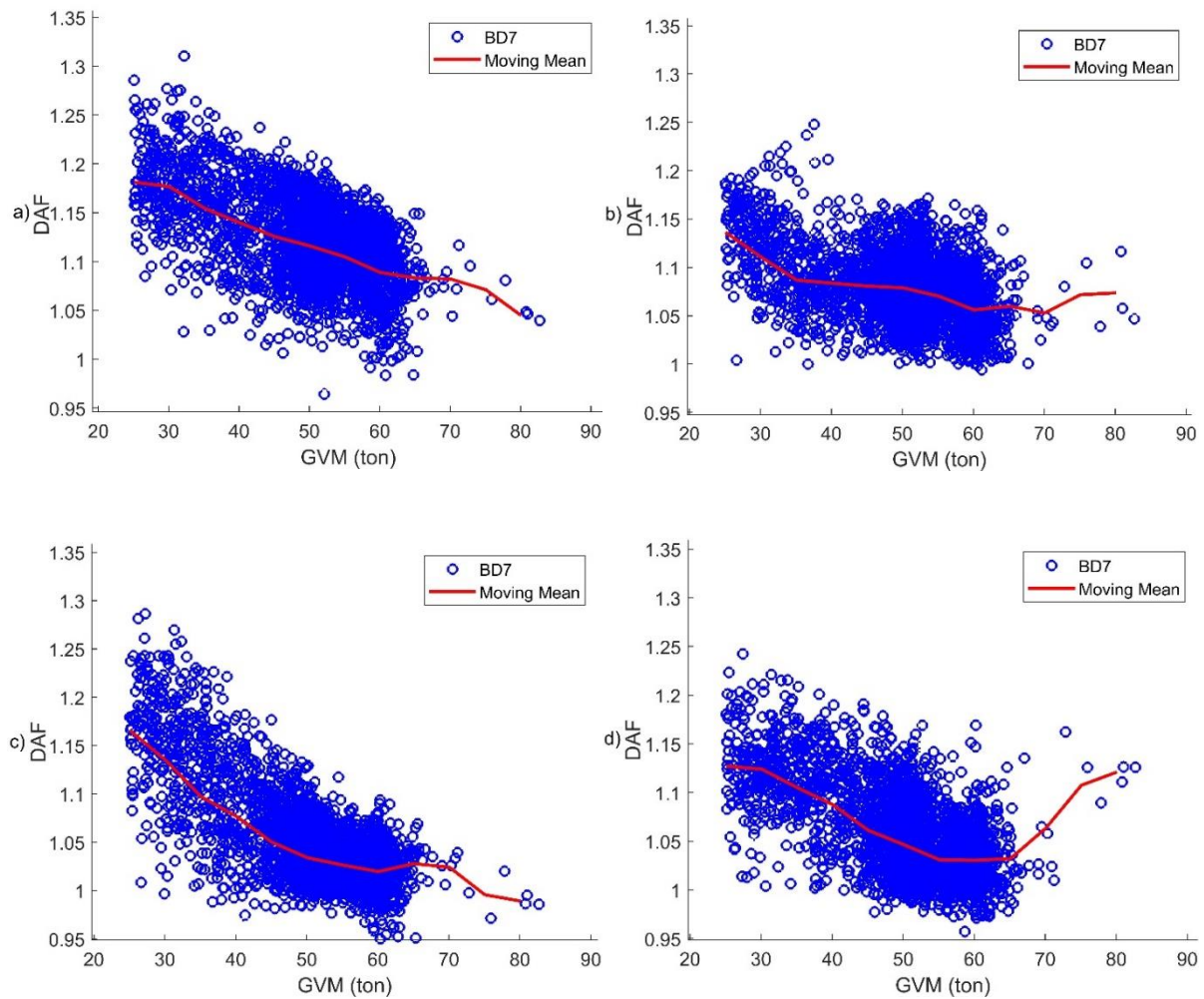
Figure C.1: DAF vs GVM for: a) 10m, b) 15m, c) 20m, d) 25m.

Figure C.1: DAF vs GVM for: e) 30m, f) 35m, g) 40m.

APPENDIX C.2

The relationship between the DAF and vehicle velocity of the BD7 vehicle population is presented here for the range of bridges considered.
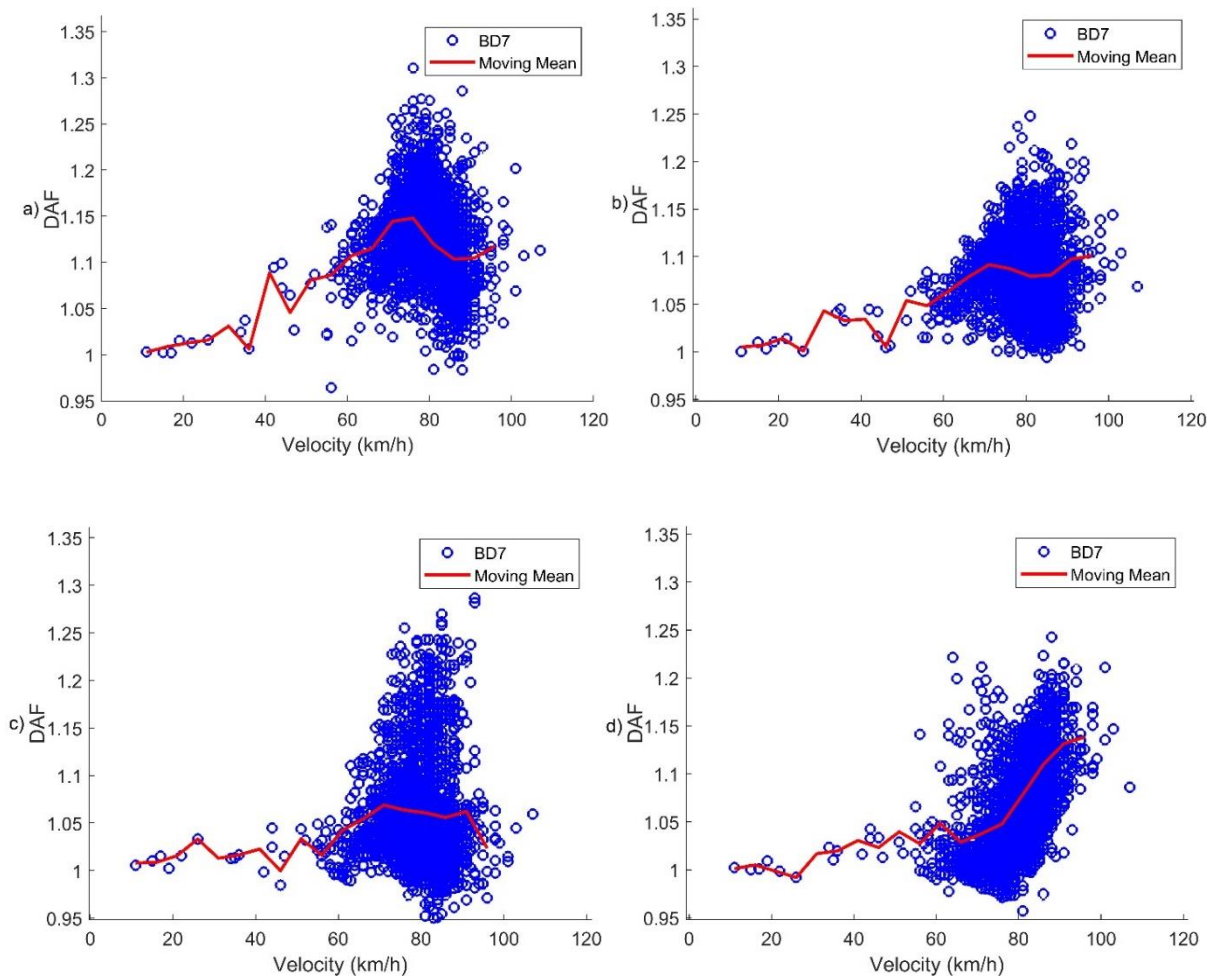

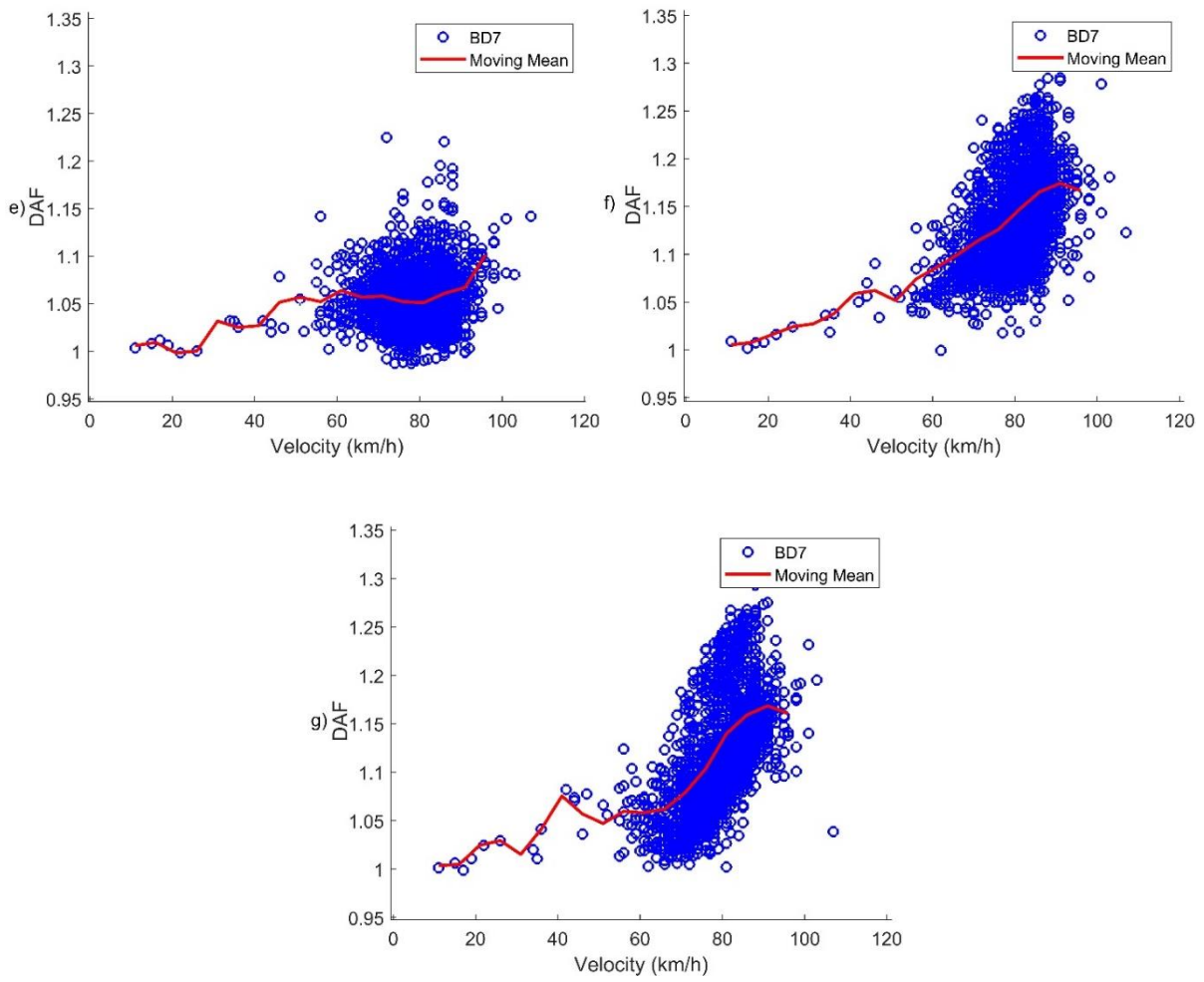Figure C.2: DAF vs velocity for: a) 10m, b) 15m, c) 20m, d) 25m, e) 30m, f) 35m, g) 40m.

Figure C.2: DAF vs velocity for: e) 30m, f) 35m, g) 40m.